LAUR-95-217

January 1995

MECHANICAL AND PHYSICAL PROPERTIES OF PERLITE FROM THE GEOPHYSICAL ARRAY FOR SMALL-SCALE EXPLOSIVE EXPERIMENTS SOCORRO, NEW MEXICO

H. N. Plannerer and D. M. Romero

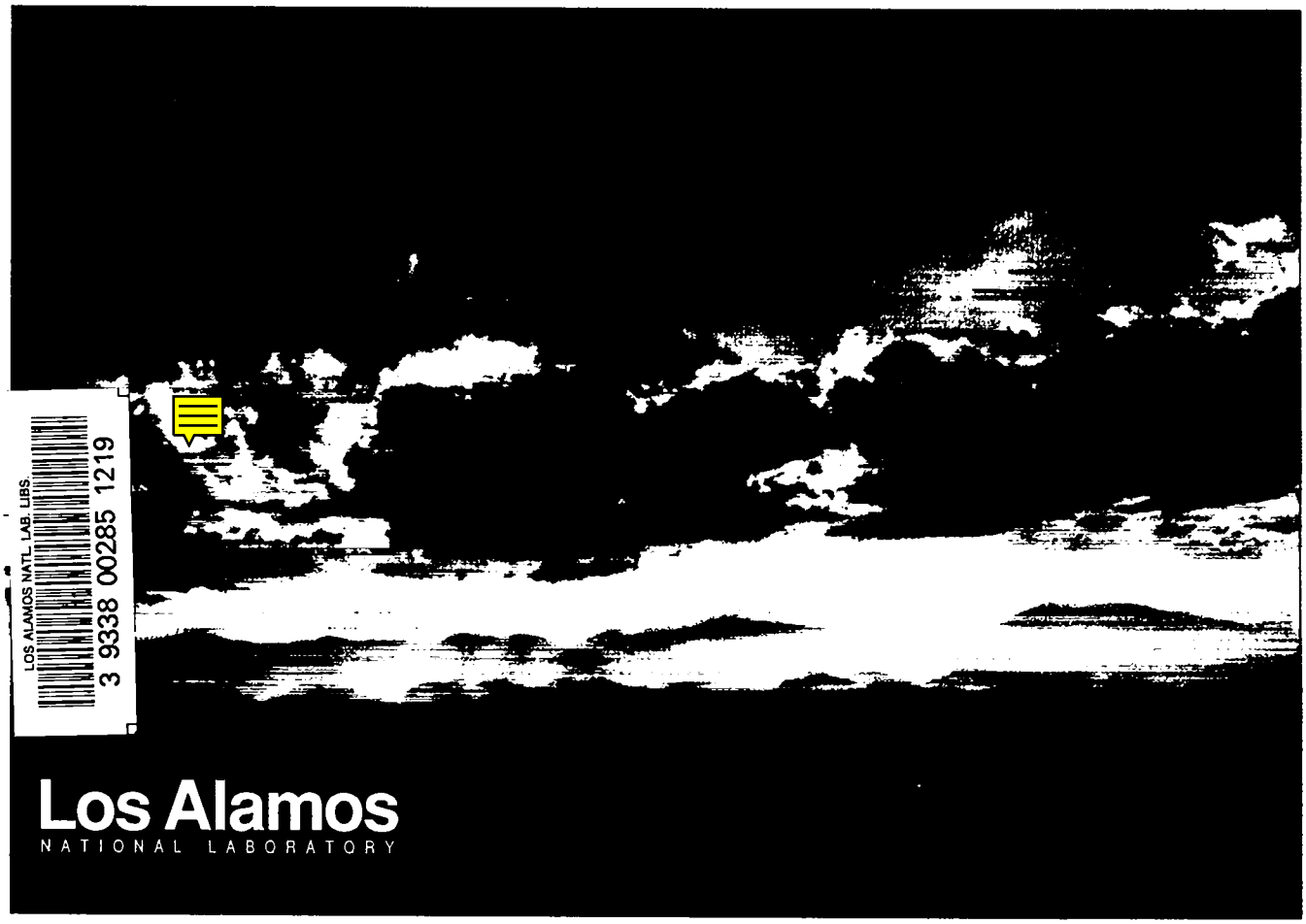

Los Alamos
NATIONAL LABORATORY

Photograph: by Chris J. Lindberg

Los Alamos National Laboratory is operated by the University of California for the United States Department of Energy under contract W-7405-ENG-36.

An Affirmative Action/Equal Opportunity Employer

DISCLAIMER

Abstract

Mechanical properties for perlite in uniaxial compression, grain density, bulk density, and moisture content were measured for a limited suite of samples collected from the Grefco Dicaperl mine south - southwest of Socorro, New Mexico. These measurements were requested as parameter input to numerical simulations and as a compilation of elastic properties for seismic characterization of fielded small - scale chemical explosive experiments. Beyond providing basic mechanical data, test results reveal a number of important findings for site characterization of perlite. These findings address the material specific topics of stress ranges for elastic and inelastic deformation, non uniformity of effective elastic moduli among specimens of the sample suite, and perlite anisotropy. Although derived from static tests, the mechanics of perlite equally influence site characterization for dynamic response.

Table of Contents

List of Tables

List of Figures

Introduction

Small - scale chemical explosive experiments were planned for and executed the summers of 1993 - 94 for a ground motion analysis fulfilling an objective of the Los Alamos National Laboratory Source Region Program. The experiments, with charges to 68 kg petrogel, were designed to measure changes in shock wave and seismic coupling as a function of burial depth and structural setting (Edwards *et al.*, 1994). The geologic setting for these experiments was the Dicaperl perlite dome south - southwest of Socorro, New Mexico, which is being quarried by Grefco for its volcanic glass. Perlite at the selected site has a depositional flow banding with prominent north - northeast strike and a steep dip angle. Superimposed on this depositional feature are two dominant joint sets, one oriented approximately N5°E and the other at N60°W. A quarry floor surface and borehole geophysical array was arranged in radial pattern about one of several detonation centers. The array consisted of accelerometers and velocity transducers.

Mechanical and physical properties for Dicaperl perlite were requested in the planning stage of experiment design, especially for parameter input to the SMC Lagrangean finite difference code (Dey and Kamm, 1993) being applied to optimize locations for transducer placement (Kamm, 1993). To that end, grain density, dry bulk density and moisture determinations were made on supplied quarry floor material (Plannerer, 1993b). A determination of incipient pore crush pressure was not possible for technical reasons. A lower limiting stress value for incipient crush was made possible from previously acquired hydrostatic data for the No Agua mine perlite, the quarry for which is located 6.9 miles due north of Tres Piedras in northern New Mexico (Plannerer, 1993a). Beyond parameter input for code applications, uniaxial compression tests were performed to provide fracture strength, Young's modulus, and Poisson's ratio (Plannerer, 1993b). Longitudinal wave velocity was measured once a seismic velocity anisotropy was recognized in the data set collected from the geophysical array (Plannerer, 1993c). Memoranda containing these data are provided in Appendix B.

Executed field experiments have yielded a wealth of single- and three- component ground motion data. Although a few preliminary conclusions are reported in the data compilation by Edwards *et al.* (1994), analysis of the data to separate geometry effects resulting from source depth-of-burial from structural effects remains to be conducted. Of particular interest to rock mechanics, a preliminary conclusion cites variability in rock properties as one contributing feature influencing azimuthal variability in spall characteristics.

This report serves two functions. It formalizes earlier reported physical properties and uniaxial stress data. These values have undergone minor adjustment reflecting completeness of interpretation. The report also serves as a descriptive characterization of perlite mechanics. This characterization may find application in the final interpretation of ground motion observations. The report reviews symmetry constraints implied from lithology and compares them with symmetry constraints implied from elastic measurements. It examines data variability as a material anisotropy and as

material non uniformity. And, it demonstrates that perlite, a glass - based material, has a mechanical response similar to brittle polymineralic rock, for which dynamic characteristics such as wave speed are well correlated to particular regions of mechanical response.

Appendix A of this report contains descriptive information for each specimen tested in uniaxial compression. The data are supplemented with various stress and strain plots, instantaneous Young's modulus and Poisson's ratio, summary tables, and a post - test photograph of the specimen.

Samples

All tests reported in this work were conducted with bulk material collected within the field test sensor array for small - scale explosive experiments in perlite or its immediate vicinity. The site is within the confines of Grefco's Dicaperl quarry operations located three miles south - southwest of Socorro, New Mexico. The suite of collected rock represents material from limited distribution and is not representative of rock exposed throughout the quarry or rock exposed across the fielded sensor array.

Bulk material was collected at three separate time intervals. Material collected April, 1993, was blocks of surface rock from the quarry floor that was not subjected to field test. This material was exposed to the elements for an unspecified amount of time and never protected from further moisture exchange prior to test or analysis. Most physical properties and, with one exception, all mechanical tests were conducted with this material. Material collected June, 1993, provided an additional perlite specimen (16s) for mechanical testing. This material was collected north - northwest of the geophysical array. It was included for analysis because of its dense glassy matrix, which is not typical of material collected earlier, and because such material cannot be excluded as existing at depth below the geophysical array. Material collected May, 1994, and used solely to supplement moisture determinations, was extracted from a post field test excavation that exposed perlite to within 4½ feet above a 30 foot deep detonation point. This material was exposed to the elements for approximately one week prior to collection but subsequently protected from further moisture exchange prior to analysis.

Physical Properties

Measurement of dry bulk density and moisture were performed to ASTM standards with deviation to procedures noted in the following paragraphs. Bulk density for "laboratory dry" perlite was obtained by geometric determination. Grain density measurement was performed according to modified manufacturer's procedure.

The various density measurements are summarized in Table 1. A helium pycnometer was used to measure grain density of dry crushed perlite. Eight measurements ranged 2.341 - 2.359 g/cm^3 with a mean value of 2.350 g/cm^3. Dry bulk

density was obtained for irregular shaped specimens using the boiling water technique of ASTM C20-83 (1985). Three specimens provide bulk density values of 1.83 - 1.93 g/cm^3. Bulk density for "laboratory dry" perlite obtained its volumetric measurement from the dimensions of a right cylindrical specimen, which was prepared for mechanical test. The mass of the specimen is that of solids plus moisture at laboratory conditions. These specimens contain up to 3.0% moisture (see Table 2). Specimens comply with dimension and shape tolerances in accordance with ASTM D4543-85 (1992). "Laboratory dry" bulk densities of 1.79 - 2.08 g/cm^3 were obtained by this method. The mean value of eleven determinations is 1.93 g/cm^3.

Table 1. Perlite density measurements.

Dry Bulk Density, (ρ_d) [1]:

Quarry floor specimens, 3 each; collected April, 1993:
Mean: 1.86 g/cm^3 Range: 1.83 - 1.93 g/cm^3

Bulk Density, laboratory dry, (ρ_{geom}) [2]:

Quarry floor specimens; test specimens; 10 each; collected April, 1993:
Mean: 1.92 g/cm^3 Range: 1.79 - 2.05 g/cm^3

Quarry specimen not from geophysical array; test specimen (16s); 1 each; collected June, 1993; dense glassy matrix:
Value: 2.08 g/cm^3

Grain Density, (ρ_g) [3]:

Quarry floor specimens, 2 each; 8 determinations; collected April, 1993:
Mean: 2.350 g/cm^3 Range: 2.341 - 2.359 g/cm^3

---

[1] Boiling water technique, ASTM C20-83 (1985); $\rho_d = M_s / V$; where M_s is mass of solids; and V is the exterior volume.

[2] Geometric determination; $\rho_{geom} = M_{s+moist} / V_{geom}$; where $M_{s+moist}$ is mass of solids and moisture, and V_{geom} is the exterior volume of test specimen measured as a right cylinder. Specimens conform to dimension and shape tolerances in accordance with ASTM D4543-85 (1992).

[3] Acquired by helium pycnometer. Determined according to modified manufacturer's procedure; $\rho_g = M_s / V_s$; where V_s is the volume occupied by solids.

Table 2. Measured moisture content of perlite.

Moisture, (w) [1]:

Quarry floor specimens; collected April, 1993; 3 each; crushed:
Mean: 0.28% Range: 0.23% - 0.30%

Quarry floor specimens; collected April, 1993; 3 each; not crushed:
Mean: 0.25% Range: 0.16% - 0.37%

Specimens recovered 4½ feet above 30 foot deep detonation site; collected May, 1994: 3 each:
Mean: 8.71% Range: 5.67% - 11.96%

Quarry floor specimens; collected April 1993; 10 each; laboratory dry; post - mechanical test:
Mean: 0.71% Range: 0.16% - 3.0%

Quarry specimen (16s) not from geophysical array; collected June, 1993; 1 each; laboratory dry; post - mechanical test; dense glassy matrix:
Value: 1.21%

[1] Determined according to ASTM D2216-90 (1992); $w = (M_W \times 100) / M_S$, where M_W is water mass and M_S is solids mass. Variations from standard method are: (1) entire bulk specimen was not used in determination; (2) specimens were not crushed to pass sieve sizes; and, (3) minimum mass of moist specimen was 20 grams.

Moisture was determined by drying perlite specimens to constant mass according to ASTM D2216-90 (1992) with adaptations. Since the current standard test method has inproportionate emphasis on soils, the following deviations in procedure were applied to rock specimens. The entire bulk specimen was not used to make a determination. The minimum representative subsample of moist rock was established as 20 grams. Moisture contents are reported to ±0.01%. Subsamples that were crushed were not crushed to uniform size nor were subsamples required to pass a standard sieve. Drying was conducted at 110°C ± 5°C in agreement with the standard. In addition to moisture determination of bulk materials, each specimen tested for mechanical properties was sampled post - test for moisture. Prior to mechanical test, specimen moisture contents were altered by sample preparation procedures. They were subsequently exposed to the atmosphere and permitted to establish a "laboratory dry" condition.

Tabulation of moisture contents in Table 2 shows that the unprotected quarry floor specimens collected in 1993 are exceedingly dry with less than 0.4% moisture. The

amount of moisture that was permitted to exchanged with the atmosphere prior to measurement is not known. The excavation in the proximity of a 1994 detonation site yielded material that was moist in comparison to quarry floor specimens. This material may be more representative of the moisture content about 25 feet below the geophysical array. Moisture content of this perlite is highly variable among three bulk samples collected in close proximity suggesting that moisture exchange with the atmosphere was in progress. Their moisture contents range 5.7 - 12.0%. Subsample analyses indicate that the three bulk samples are generally inhomogeneous with their moisture contents varying as much as 2% . Specimens used in mechanical tests have a mean moisture content of 0.7% , which is representative of quarry floor samples and not water saturated samples from depth.

Distribution of moisture content with depth was implied from a short seismic refraction survey conducted by Cogbill (1993) across a portion of the geophysical array. The survey resolved a refracting horizon 4 to 10 meters below the quarry floor separating perlite of two distinctive wave velocities. An interpretation for the refractor is that it represents perlite approaching water saturation. The moisture content required to saturate perlite may be estimated from grain density and dry bulk density values of Table 1. That moisture content based on mean values is 11.2% . This value is met among samples obtained 25 feet below the quarry floor surface at one of the detonation centers (Table 2). Interpretation of the refracting horizon as being a horizon of water saturated perlite is consistent with measured physical properties.

Total porosity may be estimated from the relationship, $\phi = 1 - (\rho_d/\rho_g)$, where ρ_d is dry bulk density and ρ_g is grain density. Based on mean density values listed in Table 1, perlite can be expected to have a total porosity of 20.9% .

Elements of the Symmetry Model

Perlite represents volcanic glass of rhyolitic composition, which incorporated water at low temperature (Carmichael *et al.*, 1974). Perlite texture from the site of the geophysical array includes a pronounced depositional flow band structure. This flow band structure is characterized by composite thin layers of glass. At the submillimeter scale, glass residing between band structure lamellae is vesicular glass. Vesicular outlines of glass have an oblate spheroid geometry with the spherical axis aligned perpendicular to the plane of banding. The glass contains less than 5 volume percent crystals and crystal clusters of feldspar and quartz(?), which rarely exceeds 5 mm diameter.

Flow banding is cut by narrow, submillimeter wide, open fractures. These fractures are discontinuous planar structures with typically 1 - 2 cm lengths and widths ≤1 mm. It is common for these open fracture segments to reside along specific horizons of flow banding. Fractures are traceable as linear extensions to adjacent bands suggesting that the open void structures were at one time contiguous. No displacement of flow banding is observed across these fractures. They are interpreted as unhealed segments of

a fracture network that was part of the original rock fabric. The relationship between these fractures and the joint pattern of *in situ* perlite is not known.

The preceding descriptive information is the basis for a symmetry model construct. Constituent elements of the rock, which control mechanical anisotropy, typically correspond with the geometry, mineralogy and distribution of physical features. For perlite, as with other geologic materials, the constituent elements are found both on the macroscopic and microscopic level. At the macroscopic level these are elements such as load bearing phases, phase orientation and porosity structure. Microscopically there exists the inherent microcrack structure.

Unlike most geologic material, which consists of mono- or polymineralic crystalline phases, the dominant phase in perlite is glass, an isotropic material. The few crystals found in the glass will have no significant contribution to the model. The other macroscopic feature of particular significance to symmetry is the influence of the porosity structure. This porosity structure is the combined contribution of vesicle void structure and the void structure associated with fracture segments as observed cutting across band lamellae. An asymmetric porosity structure implies a symmetry less than isotropic. Depending on the significance of void structure due to fractures, perlite petrofabric is suggestive of either a transverse isotropic or orthorhombic symmetry. Not included here is the possibility of creating symmetry constraints by eliminating void structure through crushing or shape modification. There is no evidence from test results (Appendix A) suggesting that a mechanism for pore crush was operative in uniaxial compression.

Microcrack structure contributes a significant influence to the symmetry model of nearly every geologic material. This investigation provides no direct observation of microcracks and their distribution through optical or scanning electron microscopy. Although it may be inferred that the geometry of the glass petrofabric effectively controls microcrack distribution along various planar orientations, microcrack characteristics are generally deduced from mechanical response. Microcrack structure and its influence on symmetry are explored in various sections pertaining to elastic and inelastic mechanical response.

Mechanical Behavior

A suite of eleven perlite specimens was tested in uniaxial compression to determine mechanical behavior. The operating procedure for these tests was ASTM D3148-86 (1992). Unconfined specimens were monotonically loaded to failure at strain rates of 0.9×10^{-6} sec^{-1} to 4.4×10^{-6} sec^{-1}. Tests were performed in load control mode versus one of displacement control. Axial and circumferential displacements were monitored with electrical extensometers. Right cylindrical specimens of two inch diameter perlite were prepared for test. Perlite was tested in one of two orientations; maximum principal stress applied perpendicular or parallel to flow banding.

In uniaxial compression and with low applied differential stress, perlite has the characteristics of a linear elastic material. The strain relationship with applied stress may be adequately represented as linear. Young's modulus and Poisson's ratio are nearly constant and specimen volume decreases linearly with compression. With greater applied stress volumetric strain deviates from elastic linearity. This deviation is reflected in a volume increase relative to the behavior of a linear elastic material. Perlite deformation becomes nonlinear, moduli continually change and void space is created in the rock. This response to applied stress is known as dilatancy (Jaeger and Cook, 1979). Dilatancy increases with stress until perlite fails macroscopically.

The mechanical behavior of glass-based perlite is consistent with the behavior of brittle polymineralic crystalline geologic materials. Brace *et al.* (1966) categorized stages of mechanical behavior for brittle polymineralic crystalline rock and correlated them with the mechanics. The mechanical stages are distinguished by the relationship of total volumetric strain, ε_v^{tot} , to the volumetric strain of the elastic reference line for the material at applied differential stress, $\Delta\sigma$. The elastic reference line is the line segment with slope, $d\varepsilon_v/d\sigma$, coincident with linear elastic deformation, extended beyond the elastic range. Volumetric strain in excess of the elastic reference line is taken as open crack volume. Observed volume strain is thus the total of two component strains, that of the elastic matrix and of crack volume. Observations of brittle crystalline materials generally show deviations of volume strain from the elastic reference line above and below the stress range characterized by elasticity. Both are attributed to measurable crack volume. The categories of mechanical behavior are, in order of increasing applied stress, crack closure, linear elastic deformation, and microcracking. Microcracking in its various modes continues unto mechanical failure.

The order of presentation of mechanical categories for perlite starts with linear elastic deformation. The elastic range and, consequently, the adjacent non linear mechanics are formulated based on establishing the elastic reference line. The elastic reference line and the elastic constants create a framework of parameters relevant to crack closure and microcracking. Therefore, non linear mechanics are presented following a discussion of the elastic range.

Linear Elastic Deformation

Each of the perlite specimens tested has a stress range for which the mechanical response is adequately represented by the linear elastic law, $\sigma = E\varepsilon$; where σ is applied stress; E is Young's modulus; and, ε is strain in the direction of the applied stress. Young's modulus, Poisson's ratio and the elastic reference line were determined for the elastic range of each specimen. These values are compiled in Table 3. The elastic reference line is represented by its slope, $d\varepsilon_v/d\sigma$. The applicable stress range for elastic behavior is given by its maximum stress value, σ_{Ia} . The compilation segregates individual test specimens based on stress orientation to flow banding in order to address the role of symmetry in mechanical response.

Table 3. Mechanics of linear elastic deformation.

Perlite Specimen	$d\varepsilon_v / d\sigma$	Young's Modulus	Poisson's Ratio (1)	σ_{Ia} (2)
	(10^{-3} kbars^{-1})	(kbars)		(bars)
	Principal stress **perpendicular** to flow banding.			
1s	3.467	166.5	0.211	150
2s	3.529	168.2	0.203	180
4s	7.153	117.4	0.080	215
6s	7.082	116.0	0.089	240(?)
16s	3.299	224.0	0.131	235(?)
	Principal stress **parallel** to flow banding.			
3s	0.678	238.1	0.419	180
5s (3)	1.693	280.3	0.263	n/d
5s2 (3)	1.156	273.5	0.342	415
7s (4)	n/d	n/d	n/d	n/d
13s (5)	1.423	377.1	0.232	410
14s (5)	1.056	459.2	0.257	655
15s (5)	0.879	465.1	0.296	490

(1) for a transversely isotropic material with axis of symmetry in the 3-direction, the static Poisson's ratio listed for stress normal to flow banding is equivalent to ν_3 , in agreement with the nomenclature of King (1970). Uniaxial compression applied perpendicular to the axis of symmetry results in two additional Poisson's ratios, ν_1 and ν_2 , which are defined in the text. Because transverse strain measurement was made with a single circumferential extensometer, individual in-plane and symmetry axis strain components were not distinguished for this test configuration. Poisson's ratio listed under the heading of stress parallel to flow banding is not an expression of either the ratio ν_1 or ν_2 .

(2) differential stress at initiation of microcrack growth. This stress is the maximum stress corresponding to elastic deformation.

(3) specimen **5s** was loaded to the maximum force transducer setting without failing. The load rate was then reversed and the specimen was unloaded. A second test (**5s2**) was performed on the same specimen to reach fracture failure. Discussions and plots referring to elastic deformation use data from test **5s** whenever possible.

(4) the uniaxial compression test **7s** provided only limited data recovery and most mechanical properties were *not determined.*

(5) specimens **13s, 14s** and **15s** were prepared from the same bulk sample. Each was cored with cylindrical axis parallel to flow banding. The cylindrical axis for **15s** was oriented at a right angle to both **13s** and **14s**.

The compilation of elastic measurements in Table 3 shows considerable variability. This variability exceeds that which can be attributed to noise in data acquisition or from analytic technique. The elastic measurements, therefore, reflect variability in rock properties. Distribution of mechanical parameters may be visualized with the aid of two plots. Figure 1 is the three dimensional projection of σ_{Ia} , maximum stress for observed elasticity; $d\varepsilon_v/d\sigma$, slope of the elastic reference line; and, Young's modulus. Figure 2 is the base plane of Fig. 1 with interpretive detail. Setting aside crack closure, which occurs at the low end of the stress range, the stress σ_{Ia} is used in Fig. 1 to bracket the elastic range from zero applied stress to its maximum observed limit. Nonlinear, irreversible behavior develops above σ_{Ia} . The slope, $d\varepsilon_v/d\sigma$, expresses sensitivity of the material to deform volumetrically under applied differential stress. The greater the value of $d\varepsilon_v/d\sigma$ the greater the volumetric deformation for an applied stress. Projected in the third dimension is Young's modulus. This modulus is the effective Young's modulus for the particular test specimen. It is not the intrinsic modulus for perlite or the intrinsic modulus for that particular specimen. Poisson's ratio could replace Young's modulus in Fig. 1, however, the effective Poisson's ratio has a more complex relationship with its intrinsic value than does Young's modulus (Walsh, 1965b and 1965c). Intrinsic implies an elastic medium with no cracks. Therefore, the effective elastic modulus in Fig. 1, whether Young's modulus or Poisson's ratio, is a statement of inherent microcrack structure.

Figure 1 shows that each of the three parameters has a range of values. This variability is neither random nor a single linear relationship in multidimensional space. The distribution of three parameters tends to identify two trends. Young's modulus correlates well with $d\varepsilon_v/d\sigma$ for part of the distribution (Fig. 3) and with σ_{Ia} for the remaining distribution (Fig. 4). There may be one data point that satisfies both trends. Also identified in Fig. 1 is one additional characteristic, orientation of applied stress to flow banding. It is noted that with stress normal to flow banding, Young's modulus correlates with $d\varepsilon_v/d\sigma$. The second trend holds for stress applied parallel to flow banding. Therefore, orientation is reflected in parameter trends, and there is justification for the segregation of data by orientation in Table 3.

Perlite cannot be considered an isotropic material based on recognition of the two parameter relationships in Fig. 1, and correlation of these relationships with orientation to applied stress. Something other than an isotropic glass petrofabric has design on the symmetry of this material. The macroscopic petrofabric suggests a symmetry form that is either transverse isotropic, with a single axis of symmetry normal to flow banding, or orthorhombic, with three mutually perpendicular planes of symmetry. Transverse isotropy requires elastic properties in all directions at right angles to the symmetry axis to be identical (Jaeger and Cook, 1979). This is not observed in the data of Table 3 nor displayed in Fig. 1. The data should cluster about two values instead of forming two linear relationships. Perlite as interpreted from these data is not transversely isotropic. This conclusion leaves three choices for constraining elastic symmetry. First, perlite is transversely isotropic but the choice of symmetry axis is incorrect. Second, perlite is transversely isotropic but on the scale of the two inch diameter test specimen the elastic

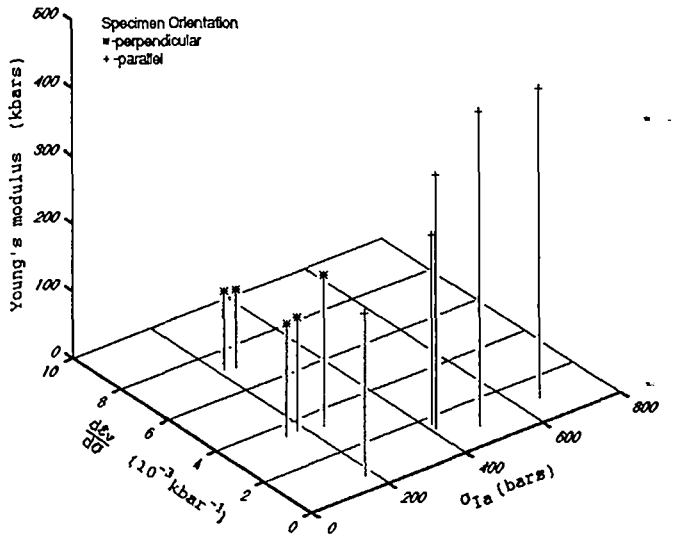

Fig. 1. Multidimensional projection of linear elastic parameters. Projection demonstrates dependency of Young's modulus on stress orientation to perlite flow banding. Base of projection is the transition stress, σ_{Ia} , from elastic to inelastic behavior plotted against slope of the elastic reference line, $d\varepsilon_v/d\sigma$.

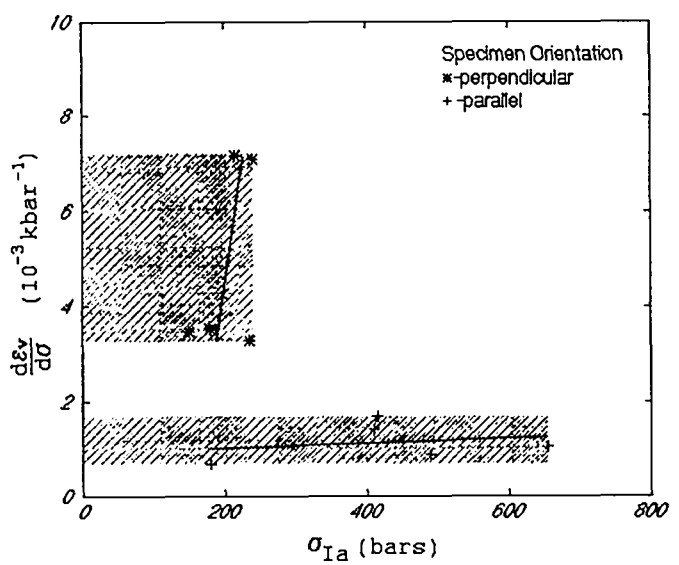

Fig. 2. Maximum stress range for linear elastic behavior as a function of stress orientation. Axes are the same as base plane of Fig. 1. Symbols represent individual test determinations of the transition stress from elastic to inelastic behavior. Shaded areas show maximum extent of elastic deformation among all test specimens of a particular stress orientation to flow banding. Straight lines are least squares fit of transition stress level, σ_{Ia} , to the slope of the elastic reference line, $d\varepsilon_v/d\sigma$.

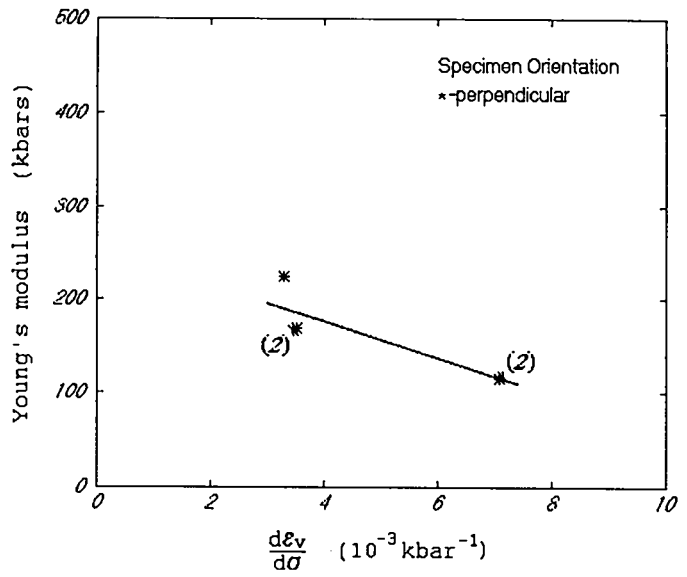

Fig. 3. Young's modulus as a function of the elastic reference line slope, $d\varepsilon_v/d\sigma$. Plot pertains to specimens with maximum principal stress oriented perpendicular to flow banding. Straight line is least squares fit to experimental data. The symbol, (2), indicates the presence of two overlapping data points.

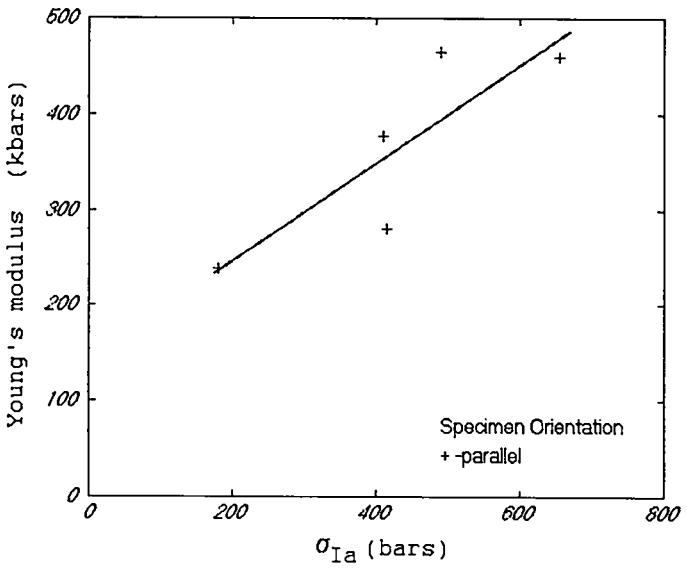

Fig. 4. Young's modulus as a function of the transition stress, σ_{Ia} . Plot pertains to specimens with maximum principal stress oriented parallel to flow banding. Straight line is least squares fit to experimental data.

properties are not uniform from specimen to specimen. Third, perlite is actually of lower symmetry form. The symmetry representation of perlite elasticity is not resolved with available test results and, therefore, remains problematic.

Mechanical testing of perlite for the Source Region Program was never designed to provide a matrix of stiffness constants or compliances for anisotropic perlite. Interpretation of wave propagation from field observation should properly be modeled with the matrix of constants consistent with mechanical symmetry. Should perlite be of low symmetry form, determination of appropriate constants becomes difficult. Rarely are stiffness constants for low symmetry forms so fully determined to reasonably interpret elastic behavior. In this situation it is customary to assume transverse isotropy. Determination of the five independent stiffness constants required of a transversely isotropic material is reasonable and should be considered to model elastic wave propagation through Dicaperl mine perlite.

For the purpose of modeling wave propagation from field observation and assuming for interpretive purposes that perlite is transversely isotropic with symmetry axis normal to flow banding, then there are salient characteristics to the data in Table 3 that should be reflected in the model. Depending on stress orientation there are limits to ranges of elasticity. The shaded areas in Fig. 2 represent the maximum range of stress for which perlite is elastic in a particular stress orientation. The two stress configurations provide significantly different ranges. Normal to flow banding, every test specimen has passed through the elastic range into inelastic behavior by 240 bars differential stress. The range at which the transition occurs is relatively well defined from 150 bars to 240 bars. This is not the behavior when stress is applied parallel to banding. In that case every specimen has passed through the elastic range by 655 bars of stress and the transition stress range may be as great as 475 bars. This distinction in elastic behavior should be expected to preferentially influence longitudinal wave velocity.

Longitudinal wave velocity through rock in uniaxial compression was described by Tocher (1957) and Thill (1973). These investigations are informative for two reasons. First, they describe changes in wave velocity in association with mechanics of brittle rock. In each of the mechanical regions of crack closure, linear elastic deformation and microcracking, longitudinal wave velocity follows predictable patterns. These patterns are related to microcrack behavior under stress. Second, they describe propagation velocity both normal and parallel to applied stress. These differences result from preferential closure of some microcracks under the influence of a non hydrostatic stress. In the elastic range, longitudinal wave velocity is increasing at a low and constant rate. It is near or at its maximum velocity for any load condition. In the inelastic region above linear elastic deformation, wave velocity in the direction of applied stress will first slowly increase, however, a mode change in microcrack extension or growth will reverse this trend. In the direction perpendicular to applied stress, longitudinal velocity starts decreasing once the transition to inelastic behavior occurs. Thus, the character of wave propagation will not only be a function of stiffness constants but also other mechanical characteristics, such as, the applicable transition stresses from elastic to inelastic behavior.

The elastic constants of Young's modulus and Poisson's ratio listed in Table 3 were acquired from static stress and strain measurements with little regard to symmetry restrictions. These data have been useful for demonstrating perlite anisotropy. Unfortunately, there was insufficient foresight to instrument directional strain measurements to take advantage of perlite being modeled as transversely isotropic. With a single axis of symmetry there are three Poisson's ratios. One Poisson's ratio corresponds correctly to the Table 3 listing for maximum principal compressive stress normal to flow banding. It is the negative ratio of the strain perpendicular to the symmetry axis divided by strain parallel to the axis. This Poisson's ratio is ν_3 , in agreement with nomenclature of King (1970). The other two Poisson's ratios come about from compressive stress applied normal to the axis of symmetry. Poisson's ratio, ν_1 , is the negative ratio of the strain perpendicular to both the direction of compression and the axis of symmetry divided by the strain parallel to the direction of compression. Poisson's ratio, ν_2 , is the negative ratio of the strain parallel to the axis of symmetry divided by the strain parallel to the direction of compression. Because of the technique used to measure transverse strain for test specimens of this orientation, Poisson's ratio in Table 3 for specimens oriented parallel to flow banding corresponds to neither ν_1 nor ν_2. There are no static measurements for these Poisson's ratios.

Elements of perlite symmetry at the microscopic level are implied through observations of one or more elastic constants. The discussion shall rely on measured values for Young's modulus. These structural elements are the microcrack structure. The microcrack structure throughout all stress levels of linear elastic deformation, and for that fact the crack closure region at low end stress levels, is an inherent crack structure that is not activated to grow or change in orientation.

Variability of elastic moduli with stress and orientation has been recognized and studied for considerable time. In the geologic community, Birch (1961) reviewed a collection of compressional wave velocity data for a broad spectrum of rock types and concluded that elastic constants were influenced by an external stress acting to close open porosity. Walsh (1965a), using analytical models for dilute concentrations of spherical pores and narrow cracks with supporting test data, states that hydrostatic stresses acting on cracks in rock were responsible for influencing elastic moduli without causing significant consequence to the porosity of the rock. With an analytical extension to non hydrostatic stress conditions, Walsh (1965b) specifically cites microcracks for influencing the relative value of Young's modulus. These broad based studies of elastic solids are compelling evidence that variability in Young's modulus with stress is attributed to an overprint of microcracks on the petrofabric.

The theoretical expressions developed by Walsh (1965a and 1965b) were meant for a low concentration of randomly oriented cracks in plane stress or plane strain. This constraint assumed cracks were sufficiently separated as to render elastic interactions negligible. An analytic technique developed for composite materials by Hill (1965) and independently by Budiansky (1975) was found applicable to investigate effective properties of a cracked material without limitation to a dilute crack concentration. The technique is known as the self - consistent method or approximation.

Budiansky and O'Connell (1976) used the self-consistent method to analytically estimate effective elastic moduli for a homogeneous, isotropic body permeated with many flat cracks. The method develops with consideration for the change in potential energy between uncracked body and crack included counterpart. Potential energy terms for pre- and post-crack material are formulated as a function of crack energy, which is released through incorporation of a sufficiently random and uncorrelated crack distribution. Elastic moduli, which are mathematical components of potential energy terms, are isolated to form a ratio of effective to intrinsic moduli and made a function of crack energy for an individual crack times a crack density parameter. The form of the crack density parameter was selected to be consistent with elliptical crack geometry. The resultant crack density parameter and an expression for fluid saturation were found to be directly responsible for variations in effective moduli. These dependencies were demonstrated by comparing theory with wave velocities measured in laboratory rock samples (O'Connell and Budiansky, 1974).

Hoenig (1979) extended the analysis of Budiansky and O'Connell (1976) by introducing certain non-random crack distributions into an isotropic homogeneous material. The purpose was to gain knowledge of the role anisotropic crack distributions have on varying elastic compliances and elastic wave speeds. Introduction of symmetrically constrained cracks renders an otherwise homogeneous material macroscopically transversely isotropic. The analysis again found that effective elastic moduli depend on the crack density parameter of Budiansky and O'Connell and a saturation parameter.

Theory of self - consistent approximations for elastic moduli of cracked solids recognizes that the ratio of effective to intrinsic Young's modulus for dry, saturated, and partially saturated cracks decreases with increasing magnitude of crack density parameter. This parameter depends only on crack area and perimeter, and is independent of crack or pore volume (O'Connell and Budiansky, 1974). The mathematical form of the parameter indicates that large cracks are more effective at reducing moduli than are a greater number of small cracks with the same total crack area. Coalescence of small cracks into a fewer number of large cracks results in a substantial reduction of the effective Young's modulus.

These theoretical and applied studies of the relationship between effective moduli and microcracks is convincing evidence that the variability in measured Young's modulus for perlite is directly linked to its microcrack structure. Detailed analysis of this structure is not possible from the suite of mechanical tests. Analysis of microcracks generally evolves through measurement of longitudinal and shear wave velocities. Trends among the data set of static Young's modulus do, however, offer generalized conclusions about relative crack areas responding to uniaxial compression, and about microcrack influence on elastic symmetry.

Analysis of microcracks from static data rely on determination of the intrinsic elastic constant. For this analysis it would require knowledge of the intrinsic Young's modulus, a value that was not experimentally sought but according to Walsh (1965b) is

obtainable. Without direct measurement of the value the discussion of microcrack structure may continue with the assumption that the intrinsic Young's modulus is independent of uniaxial stress orientation. This assumption has some basis of validity. Birch (1961) found that even among strongly anisotropic igneous and schistose rock, velocity anisotropy resulting from open cracks at low pressure transforms to velocity isotropy at high pressure to within a few percent. This implies that the petrofabric for most geologic materials is statistically isotropic when crack structure is closed. Applied to perlite, the assumption presupposes that the porosity structure due to vesicles and fracture segments is insignificant to the symmetry model. Then, the magnitude of intrinsic moduli should be nearly independent of stress orientation to flow banding. The significance of the assumption is founded in a conclusion from Walsh (1965b) that the intrinsic Young's modulus is of magnitude greater than any measured value obtained from the elastic region. The minimum magnitude of the intrinsic value for perlite is, therefore, greater than the maximum effective modulus, measured to be 465.1 kbar (Table 3). The intrinsic elastic constant shall be assumed to be of magnitude 470 kbars for microcrack discussion.

Effective Young's modulus for perlite oriented with principal stress perpendicular to flow banding is 116.0 kbars to 224.0 kbars. These values are consistently low and narrower in range than moduli for stress applied parallel to flow banding. Those values range from 238.1 kbars to 465.1 kbars. Relative to the intrinsic value, the low magnitude moduli perpendicular to banding implies that the average crack radius per unit volume of perlite is greater in that orientation than that responding to stress directed parallel to banding. These relative magnitudes can be bounded assuming applicability of O'Connell and Budiansky's (1974) model as shown in their Fig. 1. Their figure displays effective to intrinsic Young's modulus as a function of crack density parameter for a Poisson's ratio of 0.33. The effect of varying Poisson's ratio from this value is small. The range in ratio of effective to intrinsic Young's modulus (0.25 to 0.48) for stress oriented normal to perlite flow banding is equivalent to crack density parameters of 0.41 to 0.29. The range in ratios (0.51 to 0.99) for stress applied parallel to flow banding is equivalent to a range in crack density parameter of 0.27 to 0.0. A zero crack density parameter is material with no cracks and a parameter of $9/16$ or 0.56 implies a loss of coherence of the material that is produced by an intersecting crack network. Assuming similar number of microcracks in either orientation, the interpretation for perlite is that crack area responsible for reducing Young's modulus in a direction normal to flow banding is significantly large, but not so large as to render it noncoherent. That crack area is also large compared to crack area normal to the symmetry axis. This finding is contrary to macroscopic observation that open crack segments are oriented perpendicular to flow bands. It implies that participation of macroscopic open fractures is relatively insignificant to the mechanics of the symmetry model.

Crack Closure

Loading perlite from ambient stress by uniaxial compression preferentially closes inherent microcracks permeating the elastic matrix. Crack closure is sensitive to both the direction of principal stress and the thickness asperity ratio (thickness to width) of the crack (Berg, 1965; Nur and Simmons, 1969). Cracks with smallest asperity ratio require the least stress for conjugate boundary closure. For a fixed asperity ratio, cracks with normals within a defined angle to the principal stress will be closed given that the stress component normal to the crack exceeds that required for closure. The result is an elastic material with cracks closed in some directions and open in others. The process of crack closure is detected in the initial deformation response to stress by nonlinear elimination of rock volume. Cracks of preferential orientation are closed and the closure process is complete when the deformation response becomes essentially linear.

Table 4. Crack closure stresses.

Principal stress **perpendicular** to flow banding.		Principal stress **parallel** to flow banding.	
Perlite Specimen	σ_C ([1])	Perlite Specimen	σ_C
	(bars)		(bars)
1s	30	3s	60
2s	35	5s ([2])	50
4s	10	5s2 ([2])	40
6s	0	7s	n/d ([3])
16s	35	13s ([4])	80
		14s ([4])	0
		15s ([4])	90

([1]) Crack closure stress.

([2]) specimen **5s** was loaded to the maximum force transducer setting without failing. The load rate was then reversed and the specimen was unloaded. A second test (**5s2**) was performed on the same specimen to reach fracture failure. Discussions and plots referring to elastic deformation use data from test **5s** whenever possible.

([3]) the uniaxial compression test **7s** provided only limited data recovery and most mechanical properties were *not determined.*

([4]) specimens **13s, 14s** and **15s** were prepared from the same bulk sample. Each was cored with cylindrical axis parallel to flow banding. The cylindrical axis for **15s** was oriented at a right angle to both **13s** and **14s.**

Stress transition from the region of crack closure to that of linear elastic deformation is compiled in Table 4 as the parameter σ_C . The transition stress is segregated by stress orientation to flow banding in keeping with the segregation of elastic parameters. Closure stresses for principal stress normal to flow banding are 0 bars to 35 bars. Parallel to banding these stresses are 0 bars to 90 bars. Closure stresses in each of the two groups of data have a flat distribution.

The flat distribution of closure stresses suggests that either the average thickness asperity ratio is not uniform among test specimens or microcracks have an orientation dependence in addition to the orientation grouping of Table 4. These assumptions can be examined with closure stresses observed for three specimens from the same bulk sample that also were cored with known angular relationships. Each of specimens 13s, 14s and 15s were cored with cylindrical axis in the plane of banding. Specimens 13s and 14s were cored as adjacent specimens with cylindrical axes parallel to each other. These two specimens have closure stresses of 80 bars and 0 bars, respectively. The third specimen was cored perpendicular to the previous two, also in the plane of banding. This specimen, 15s, has a closure stress of 90 bars. Among the three specimens there is as much variation in closure stress between adjacent and parallel specimens as there is between adjacent and perpendicular specimens. Normal to the symmetry axis the flat distribution of closure stresses appears to be the result of a non uniform distribution of crack asperity ratio rather than a preferred orientation of microcracks.

Thickness asperity ratio can be estimated from crack closure stress based on the mathematical relation developed by Berg (Eq. 17; 1965), which relates normal compressive stress at infinity to the physical feature of just closing a crack. Assuming a rigidity modulus of 180 kbars for perlite, a Poisson's ratio of 0.34, and the closure stress maxima for each specimen orientation (Table 4), the greatest crack asperity ratios closed in uniaxial compression are of the magnitude 1×10^{-4} for principal stress normal to banding and 3×10^{-4} parallel to banding. These values testify to the fact that cracks participating in the crack closure process, which are the same as those reducing the magnitude of the effective elastic moduli (Walsh, 1965b; Thill, 1973), are extremely fine.

Dilatancy

Dilatancy, or the inelastic increase in volume of rock with applied stress (Paterson, 1978), was observed for all perlite specimens subjected to uniaxial compression. Volume increase over that attributed to linear elastic deformation is caused by microcrack extension (growth) and creation of new cracks. The stress induced volume increase is an open volume or porosity often given the name crack porosity or crack volume. The stress region for observed dilatant effects incorporates both stable crack growth and ultimately a mechanical instability in crack development that results in macroscopic failure (Brace *et al.*, 1966). Microscopic studies, such as those by Brace and Bombolakis (1963) and Tapponnier and Brace (1976), and computations from elastic velocity data by Hadley (1976) suggest that dilatant crack growth is initiated with

extension and widening of preexisting crack-like, low aspect ratio cavities. New crack development occurs with appreciably greater applied stress.

The onset of dilatancy is recognized from the first measurable and continuous strain deviation from the elastic reference line. Although activation of crack growth is likely initiated prior to macroscopic detection of the process (Tapponnier and Brace, 1976), the stress designated as σ_{Ia} is used in this report for the detected transition from linear elastic deformation to dilatancy. This is the often quoted stress *C'* used by Brace *et al.* (1966). Table 3 lists the transition stress σ_{Ia} observed for perlite specimens.

Dilatancy culminates with specimen failure. For laboratory specimens of perlite, failure is manifested as shear fracture and subsequent tensile splitting. The tensile splitting is likely the result of uncontrolled post - failure response of the test machine to the loss of material strength between platens. Fracture strengths for perlite are listed in Table 5 and designated σ_F .

Between the two stresses σ_{Ia} and σ_F perlite creates crack porosity in response to applied stress. This stress range is referred to as the microcrack region. The response of creating porosity with increased stress intensity is not linear and portions of the process show exponential increases. Crack porosity is shown in Figs. 5 and 6 as a function of the reduced stress, $(\sigma - \sigma_{Ia})$. Both figures consist of panels, each panel representing a different specimen. Figure 5 is for specimens with uniaxial stress directed normal to flow banding and Fig. 6 for specimens with stress applied parallel to flow banding. Traces of crack porosity with stress in these figures show generally similar characteristics. Crack porosity is initially slow to develop. A pronounced increase in porosity starts at about half the total reduced stress range. The traces typically show abrupt changes in slope or form, which imply mode changes in microcrack development. And, a rapid increase in porosity often but not always precedes macroscopic failure. The specifics of each trace in Figs. 5 and 6, however, are not reproducible even among specimens similarly grouped according to stress orientation. Values for the stresses σ_{Ia} , σ_F , and $(\sigma - \sigma_{Ia})$, and crack porosity each must be expressed with ranges of values. The relationship among stress parameters is best depicted with a diagram.

Figure 7 is a summary diagram developed from the base plane of Fig. 1 to include observations for dilatant effects and fracture failure. The diagram is shown with differential stress on the abscissa and the elastic reference line parameter $d\varepsilon_v/d\sigma$ on the ordinate. The latter segregates perlite specimens by stress orientation. The shaded regions correspond to the shaded regions of Fig. 2. They represent maximum differential stresses for each of the two stress orientations that are the maximum extent of linear elastic deformation. The mechanics of the microcrack region are provided as boxed outlines, again one for each stress orientation, and horizontal bars with symbols to represent individual test results.

Table 5. Fracture failure stresses.

Principal stress **perpendicular** to flow banding.		Principal stress **parallel** to flow banding.	
Perlite Specimen	σ_F [1]	Perlite Specimen	σ_F
	(bars)		(bars)
1s	249	3s	310
2s	280	5s [2]	--
4s	280	5s2 [2]	532
6s	247	7s	369
16s	319	13s [3]	726
		14s [3]	963
		15s [3]	904

[1] Fracture failure stress.

[2] specimen **5s** was loaded to the maximum force transducer setting without failing. The load rate was then reversed and the specimen was unloaded. A second test (**5s2**) was performed on the same specimen to reach fracture failure.

[3] specimens **13s**, **14s** and **15s** were prepared from the same bulk sample. Each was cored with cylindrical axis parallel to flow banding. The cylindrical axis for **15s** was oriented at a right angle to both **13s** and **14s**.

Stresses required to activate crack growth are shown as the shaded regions within the boxed outlines of Fig. 7. Activation stress for each specimen is the lowest (left most) stress indicated by individual horizontal lines. The range of activation stresses are different for the two stress orientations. Normal to flow banding non elastic behavior is consistently activated in the relatively narrow range of 150 bars to 240 bars. In comparison, this range is 180 bars to 655 bars differential stress for stress applied parallel to flow banding. The overlap of shaded and boxed outline regions in the figure indicates that the mechanical response of perlite to stress is not harmonious. That is, some specimens in close spatial relationship may proceed with inelastic behavior while others remain soundly linear elastic.

Fracture strength is represented in Fig. 7 with the symbol attached to the high stress end of horizontal lines. Again the disparity in mechanical response of perlite to orientation of applied stress follows previously recognized trends. With stress applied normal to flow banding, fracture strength is a narrow consistent stress range and that stress range is low compared with the range of fracture strengths observed for a stress oriented parallel to flow banding. Changing the perspective, all stresses to the right of the boxed outlines are unstable stresses in that no test specimen exists without being subjected to macroscopic failure. All specimens with stress applied normal to flow banding reside in the unstable stress field at stresses above 319 bars. This is not the case for perlite with applied stress parallel to flow banding for which some specimens in close spatial relationship may separately exhibit linear elastic behavior, dilatancy, or themselves may have failed. Damage models, therefore, should consider both the orientation dependence of the unstable stress field and homogeneity of damage.

Summary

Moisture determinations of perlite from surface sampling and from sampling an excavated detonation center lend physical evidence that the velocity stratification observed by Cogbill (1993) in a refraction survey at the geophysical array may be due to increased water content with depth. Measurements indicate moisture contents of 5.2% to 12.7% about 25 feet below the quarry floor. This compares with moisture contents of $\leq$ 0.4% for quarry floor specimens. Results of mechanical tests are most appropriate for the rock medium at or just below the quarry floor since they were conducted with a low moisture content.

The interpretation of data collected from uniaxial compressive stress tests conducted on laboratory dry specimens of perlite has been developed through consideration of an elastic symmetry model, and from observations of elastic and inelastic behavior. Although derived from static testing, the interpretation should be both informative and influential to establishing site characterization for perlite responding to dynamic stress conditions.

Perlite, a glassy volcanic rock, has the mechanical characteristics of a brittle polymineralic crystalline geologic material. This mechanical response includes stress regions for crack closure, linear elastic deformation and microcracking. Activation of microcrack growth in a process known as dilatancy restricts the stress range for linear elastic behavior. Transition from linear elastic behavior to microcracking occurs over a range of stresses and is a function of stress orientation to flow banding. Longitudinal wave velocity for material undergoing dilatancy may slowly increase from the near maximum velocity achieved in the linear elastic region, however, a mode change in microcrack extension or creation of new cracks would be expected to reverse this trend.

Perlite has an inherent microcrack structure that is largely responsible for its elastic symmetry. The thickness asperity ratio for these cracks is of magnitude 10^{-4}. Microcracks appear to be more extensive in area parallel to the plane of flow banding

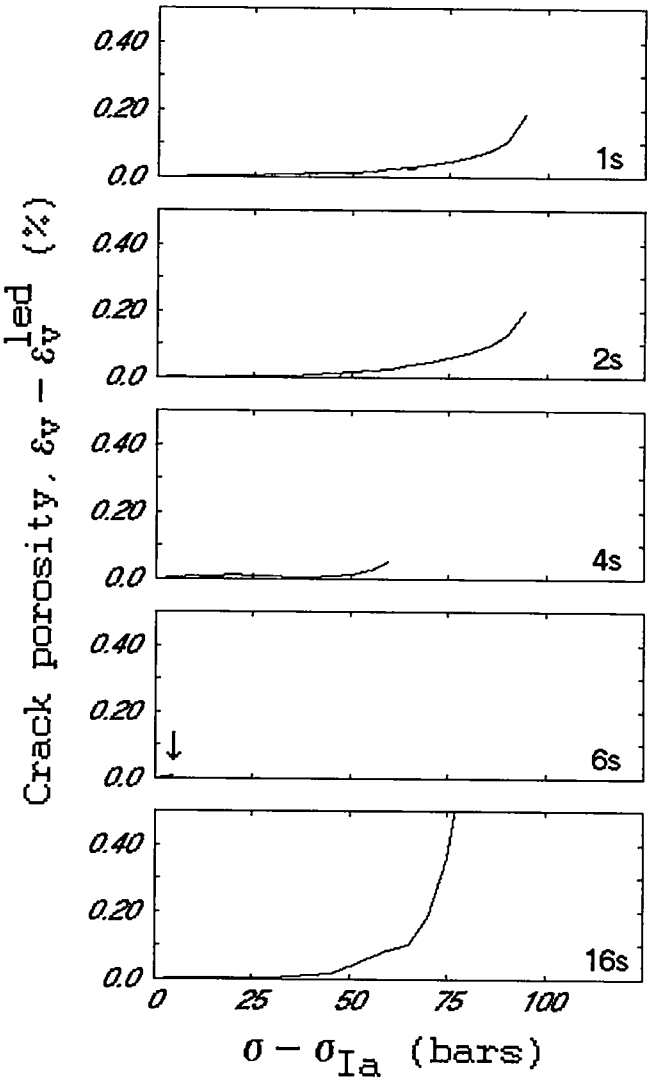

Fig 5. Crack porosity as a function of reduced stress (σ - σ_{Ia}) for specimens with principal stress oriented normal to flow banding. Symbols ε_v^{led} and σ_{Ia} refer to linear elastic volumetric strain at stress, and stress level of initiated crack growth, respectively. Specimen 16s reaches 0.69% crack porosity at (σ - σ_{Ia}) = 80 bars.

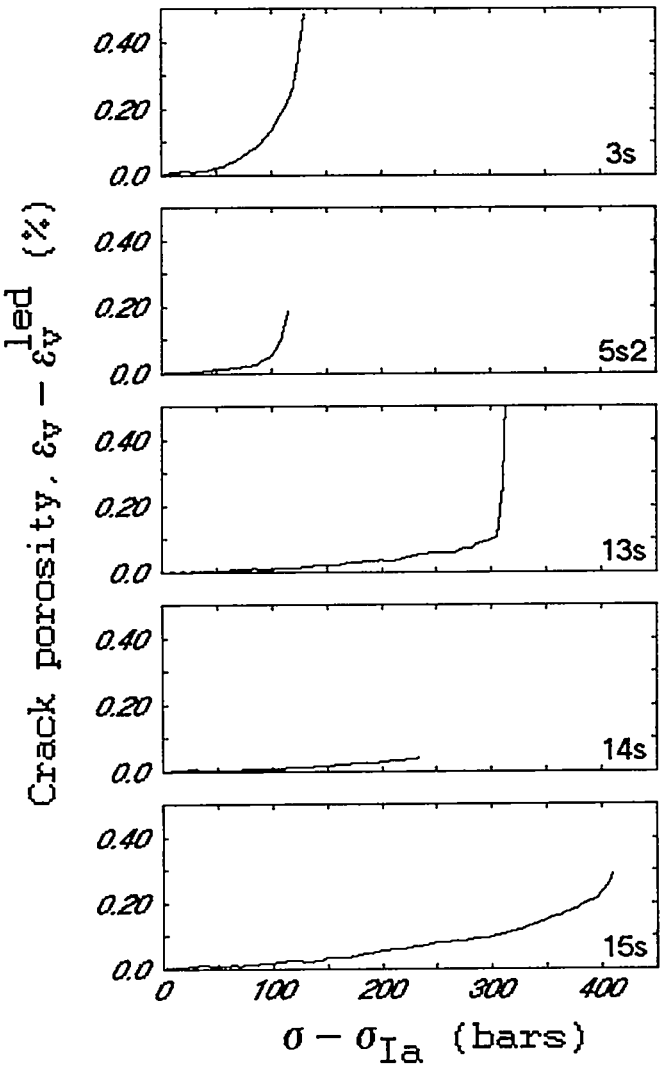

Fig 6. Crack porosity as a function of reduced stress (σ - σ_{Ia}) for specimens with principal stress oriented parallel to flow banding. Symbols ε_v^{led} and σ_{Ia} refer to linear elastic volumetric strain at stress, and stress level of initiated crack growth, respectively. Specimen 13s reaches 0.66% crack porosity at (σ - σ_{Ia}) = 315 bars.

than perpendicular to it. Variability in crack closure stress among specimens cored with cylindrical axis parallel to flow banding suggest a non uniform distribution of cracks rather than an application of stress at various angles to preferred crack orientations.

Macroscopic textural features suggest a mechanical symmetry model for perlite that is transversely isotropic. That model is not satisfied by the mechanical response of perlite to uniaxial stress. Alternatively, the elastic symmetry of perlite may: (1) be transversely isotropic but the symmetry axis is not coincident with the direction normal to flow banding; (2) be transversely isotropic but the microcrack structure is not uniform in crack area or crack number over short distances; or (3) actually be of lower symmetry form. Symmetry restrictions require the use of at least five independent elastic coefficients to describe properly the behavior of elastic waves in perlite.

Fracture strength, like the transition stress from linear elastic deformation to microcracking, occurs over a range of stresses and is orientation dependent. All specimens, in which stress was applied normal to flow banding, failed macroscopically at or before reaching a stress level of 319 bars. This behavior is not observed among specimens with applied stress oriented parallel to flow banding. Above 319 bars stress, while all specimens of the one orientation have failed, specimens with principal stress parallel to flow banding can be responding to any one of three mechanical characteristics. These are linear elastic deformation, microcracking or themselves have failed. Not until a stress level of 963 bars is the unstable stress region reached by all perlite specimens.

Acknowledgment.

H. Plannerer wishes to thank Dr. Edward Van Eeckhout for review of the report and comments on this work.

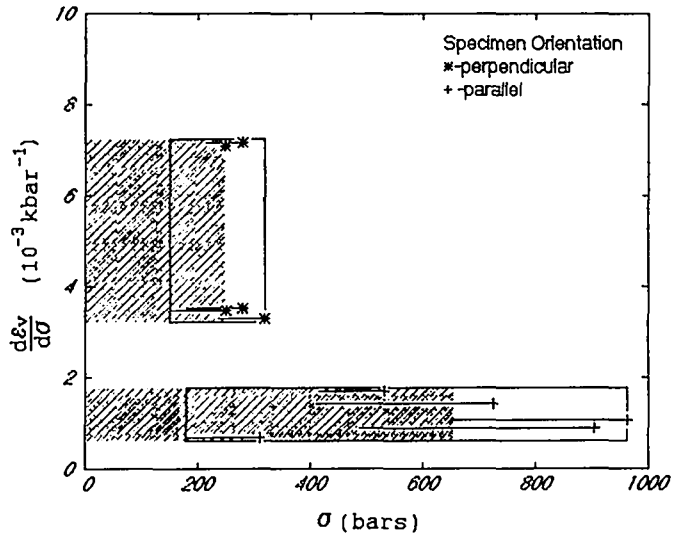

Fig. 7. Stress limits for microcrack initiation and growth. Test specimens are segregated by orientation of principal stress to flow banding based on the slope of elastic reference lines, $d\varepsilon_v/d\sigma$. The symbol σ refers to differential stress for static uniaxial compression. Stress range of microcracking and the fracture strength for each specimen are indicated with a horizontal line followed with a symbol, respectively. Shaded regions between σ = 0 bars and lower stress boundary of boxed outlines represents stress regions for which specimens deform elastically and there is no evidence for crack initiation or growth (Table 6, Stress region A). Shaded regions within the boxed outlines represents the stress ranges for which all specimens initiate crack growth (Table 6, Stress region B). All microcrack growth ceases with macroscopic failure prior to stress levels indicated by right-most boxed outline (Table 6, Stress C). Unstable stresses lie to the right of the boxed outlines.

Table 6. Stress limits for microcrack initiation and growth. Refer to Fig. 7 caption for explanation of stress regions.

Orientation of principal stress to flow banding	Stress region A	Stress region B	Stress C
perpendicular	0 - 150 bars	150 -240 bars	319 bars
parallel	0 - 180 bars	180 - 655 bars	963 bars

References

ASTM C20-83, Standard test methods for apparent porosity, water absorption, apparent specific gravity, and bulk density of burned refractory brick and shapes by boiling water. American Society for Testing and Materials, Philadelphia, *15.01*, Refractories; Carbon and Graphite Products; Activated Carbon, 7-9, 1985.

ASTM 2216-90, Standard test method for laboratory determination of water (moisture) content of soil and rock. American Society for Testing and Materials, *4.08*, Soil and Rock; Dimension Stone; Geosynthetics, 295-298, 1992.

ASTM 3148-86, Standard test method for elastic moduli of intact rock core specimens in uniaxial compression. American Society for Testing and Materials, Philadelphia, Volume *4.08*, Soil and Rock; Dimension Stone; Geosynthetics, 427-430, 1992.

ASTM 4543-85, Standard practice for preparing rock core specimens and determining dimensional and shape tolerances. American Society for Testing and Materials, Philadelphia, Volume *4.08*, Soil and Rock; Dimension Stone; Geosynthetics, 837-840, 1992.

Berg, C. A., Deformation of fine cracks under high pressure and shear. *J. Geophys. Res.*, *70*, 3447-3452, 1965.

Birch, F., The velocity of compressional waves in rocks to 10 kilobars, part 2. *J. Geophys. Res.*, *66*, 2199-2224, 1961.

Brace, W. F., and E. G. Bombolakis, A note on brittle crack growth in compression., *J. Geophys. Res.*, *68*, 3709-3713, 1963.

Brace, W. F., B. W. Paulding, Jr., and C. Scholz, Dilatancy in the fracture of crystalline rocks. *J. Geophys. Res.*, *71*, 3939-3953, 1966.

Budiansky, B, On the elastic moduli of some heterogeneous materials. *J. Mech. Phys. Solids, 13,* 223-227, 1965.

Budiansky, B., and R. J. O'Connell, Elastic moduli of a cracked solid. *Int. J. Solids Structures*, *12*, 81-97, 1976.

Carmichael, I. S. E., F. J. Turner, and J. Verhoogen, Igneous Petrology. McGraw - Hill, New York, 1974.

Cogbill, A. H., Results of seismic refraction survey in perlite mine. Los Alamos National Laboratory Memorandum EES3-93-235, 1993.

Dey, T. N., and J. R. Kamm, User's guide to SMC-1, 2, 3. Los Alamos National Laboratory, preprint, 1993.

Edwards, C. L., D. C. Pearson, and D. F. Baker, Ground motion data from the small - scale explosive experiments conducted at the Grefco perlite mine near Socorro, New Mexico. Los Alamos National Laboratory Report LAUR-94-1003, 1994.

Hadley, K., Comparison of calculated and observed crack densities and seismic velocities in Westerly granite. *J. Geophys. Res., 81*, 3484-3494.

Hill, R., A self - consistent mechanics of composite materials. *J. Mech. Phys. Solids, 13,* 213-222, 1965.

Hoenig, A., Elastic moduli of a non-randomly cracked body. *Int. J. Solids Structures, 15*,137-154, 1979.

Jaeger, J. C., and N. G. W. Cook, Fundamentals of rock mechanics, Chapman and Hall Ltd, London, 1979.

Kamm, J. R., 2 - D calculations for intermediate scale source experiments I. Los Alamos National Laboratory Memorandum EES3, 1993.

King, M. S., Static and dynamic elastic moduli of rocks under pressure. Proc. Eleventh Symposium on Rock Mechanics, Soc. Mining Engineers, New York, 329 - 351, 1970.

Nur, A., and G. Simmons, Stress - induced velocity anisotropy in rock: an experimental study. *J. Geophys. Res., 74*, 6667-6674, 1969.

O'Connell, R. J., and B. Budiansky, Seismic velocities in dry and saturated cracked solids. *J. Geophys. Res., 79*, 5412-5426, 1974.

Paterson, M. S., Experimental rock deformation - the brittle field. Springer-Verlag, Berlin, 1978.

Plannerer, H. N., Perlite mechanical properties. Los Alamos National Laboratory Memorandum EES3-93-208, 1993a.

Plannerer, H. N., Perlite mechanical properties. Los Alamos National Laboratory Memorandum EES3-93-261, 1993b.

Plannerer, H. N., Perlite compressional wave velocities. Los Alamos National Laboratory Memorandum EES3-93-432, 1993c.

Tapponnier, P., and W. F. Brace, Development of stress - induced microcracks in Westerly granite. *Int. J. Rock Mech. Min. Sci. & Geomech. Abstr., 13,* 103-112, 1976.

Thill, R. E., Acoustic methods for monitoring failure in rock. Proc. Fourteenth Symposium on Rock Mechanics, Amer. Soc. Civil Engineers, New York, 649 - 687, 1973.

Tocher, D., Anisotropy in rocks under simple compression. *Trans. Amer. Geophys. Union, 38,* 89 - 94, 1957.

Walsh, J. B., The effect of cracks on the compressibility of rock. *J. Geophys. Res., 70,* 381-389, 1965a.

Walsh, J. B., The effect of cracks on the uniaxial elastic compression of rocks. *J. Geophys. Res., 70,* 399-411, 1965b.

Walsh, J. B., The effect of cracks in rocks on Poisson's ratio. *J. Geophys. Res., 70,* 5249-5257, 1965c.

Appendix A. Catalog of Mechanical Tests

Static uniaxial compression tests for Dicaperl mine perlite are described in detail in this appendix. The appendix contains the following entries for test specimens:

Text

Specimen source.
Specimen description.
Characteristics of the failed specimen.

Tables

-1. Summary of physical and mechanical properties.
-2. Test conditions.
-3. Mechanical response at selected values of stress difference.

Figures

-1. Mechanical response of specimen to uniaxial compression.
-2. Post-test photograph of specimen.
-3. Volumetric strain resulting from uniaxial compression.
[*] -4. Relationship between volumetric strain and axial strain measurements.
[*] -5. Young's modulus as a function of stress difference.
[*] -6. Poisson's ratio as a function of stress difference.
[*] -7. Volumetric crack strain or "crack porosity" as a function of stress difference in uniaxial compression.

Figures utilizing a solid line for data presentation represent actual test data reduced to engineering units. Figures containing dashed or dotted lines, and indicated above with the leader [*], are data that have been smoothed and interpolated at 5 bar stress intervals. Some trends in these figures, especially those of a 10 bar stress magnitude may be an artifact of numerical processing or of noise from the original data set.

The linear elastic region, which must be identified for consistent derivation of elastic constants, is interpreted from the relationship between volumetric strain and stress difference (Fig. -3) following the interpretation of Brace et al. (1966). The linear portion of that relationship identifies elastic behavior for a particular specimen. Elastic constants reported in Table -1 are derived from appropriate stress and strain relationships (Fig. -1) for the stress range identified as linear elastic. These effective constants are obtained by least squares fit as is the slope of the linear elastic reference line, $(d\varepsilon_v/d\sigma)_{led}$, that is reported in Table -3. Instantaneous moduli plotted in Figs. -5 and -6 are derived from appropriate stress and strain relationships interpolated every 5 bars differential stress and represent a determination point by point at that stress interval.

The letters 'C', 'Ia', and 'F' appearing in most figures identify stress levels for crack closure, initiation of crack growth, and fracture failure, respectively. The transition stress 'C' separates crack closure from linear elastic behavior, and the transition stress 'Ia' separates linear elastic behavior from microcracking (dilatancy).

Perlite 1s

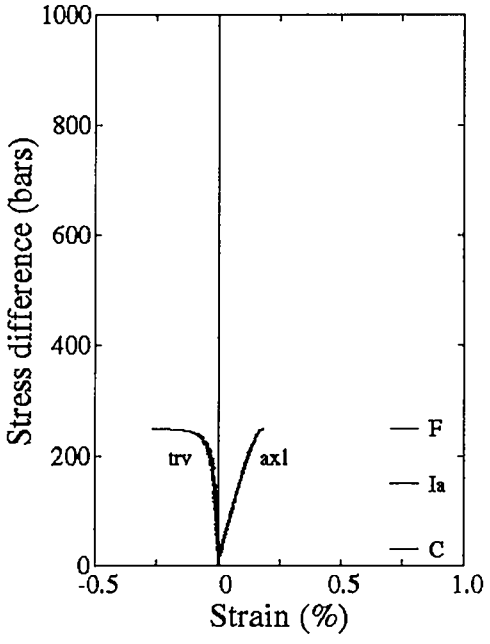

Fig. A1s-1. Mechanical response of specimen to uniaxial compression. Transition stress levels '*C*' and '*Ia*', and the fracture stress '*F*' are defined in Table A1s-3. Axial and transverse strains are identified as 'axl' and 'trv', respectively.

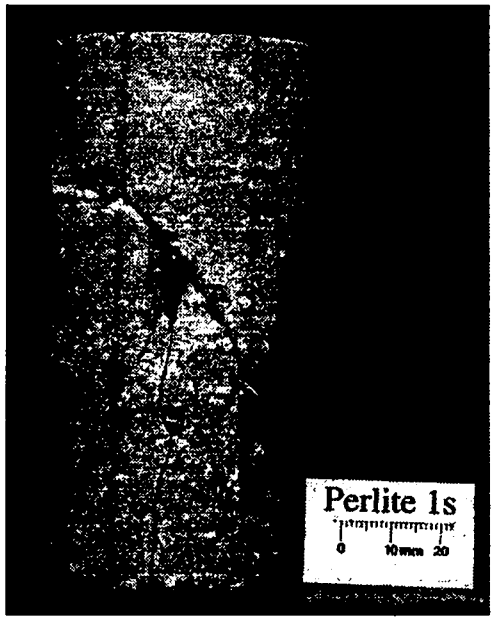

Fig. A1s-2. Post-test photograph of specimen.

Table A1s-1. Summary of physical and mechanical properties.

Specimen type	Perlite
Density, bulk (geometric determination)	1.88 g/cm^3
Density, grain	not determined
Moisture (ASTM D2216)	0.19%
Elastic constants:	
Young's modulus	166.5 kbars
Poisson's ratio	0.211
Mechanical behavior stress levels:	
Closure of pre-existing cracks	0 - 30 bars
Linear elastic deformation	30 - 150 bars
Microcracking	150 - 249 bars
Fracture strength	249 bars
Fracture angles (shear)	50°

Perlite 1s

Specimen Source. Specimen **Perlite 1s** was cored from bulk material retrieved from Grefco's perlite mine operations located off US Highway 60, 3 miles south of Socorro, Socorro County, New Mexico. The quarry is located at coordinates 34°01'32" north latitude and 106°56'14" west longitude. The sample was recovered from the quarry floor in the vicinity of the geophysical array for small - scale explosive experiments. The bulk material was retrieved April, 1993 and not protected from moisture loss. The specimen was tested May, 1993 as a laboratory dry specimen.

Table A1s-2. Test conditions.

Operating procedure	ASTM D3148
Specimen preparation	ASTM D4543
Specimen geometry:	
Shape	cylindrical
Diameter	2.10 inches
Length to diameter ratio	2.15
Specimen orientation (angle between flow banding and plane normal to cylindrical axis)	0° [$\sigma_{1\perp}$]
Strain rate; average	9.2×10^{-7} sec^{-1}

Specimen Description. The test specimen is perlite, a volcanic rock, gray in color with a distinctive "flow banding" structure. The perlite, consisting of highly porous volcanic glass, contains less than 5 volume percent crystals and crystal clusters of feldspar and quartz (?) that are ≤5 mm diameter. Pores of the glassy matrix are submillimeter in size, and have elongate, flat outlines parallel to the banding structure of the rock. The test specimen was cored such that banding is perpendicular to the cylindrical axis of the specimen. Narrow, submillimeter wide, open fractures to a length of 1.6 cm are observed on the test specimen surface but are not abundant. One such fracture, open to a width of 2 mm, is considerably wider than the others. The fractures form discontinuous linear features oriented at a high angle to the flow banding and are prevalent at specific horizons. No displacement is observed across these fractures. They are interpreted as unhealed segments of fractures that originally passed through the specimen.

Characteristics of the Failed Specimen. The failed specimen has both shear and tensile fractures. Geometric relationships between fractures suggests that shear failure preceded tensile splitting and was responsible for specimen failure. Shear failure created a single steeply inclined fracture passing entirely through the specimen. The surface of this planar feature consists of closely spaced, narrow step-like structures, which are controlled by the flow banding. The measured angle for this fracture is 50° to a plane normal to the cylindrical axis. Tensile splitting formed an abundance of splintered pieces, which are concentrated along the periphery of the specimen in close proximity to the shear plane.. Fracture surfaces resulting from tensile splitting are nearly vertical. Tensile fractures intersect the shear fracture but do not project into the facing wall.

Perlite 1s

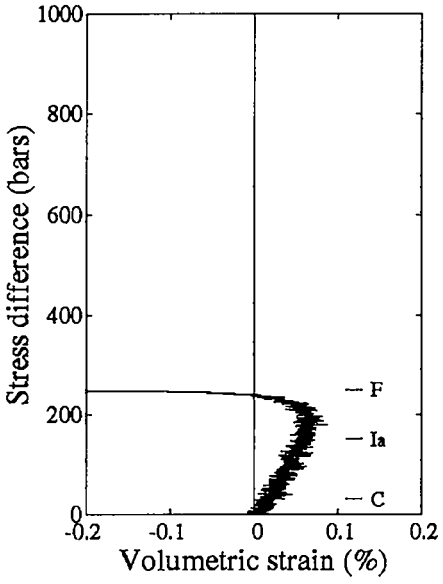

Fig. A1s-3. Volumetric strain resulting from uniaxial compression.

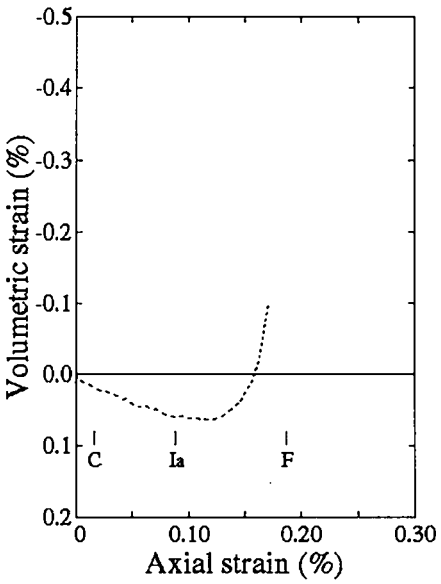

Fig. A1s-4. Relationship between volumetric and axial strain measurements.

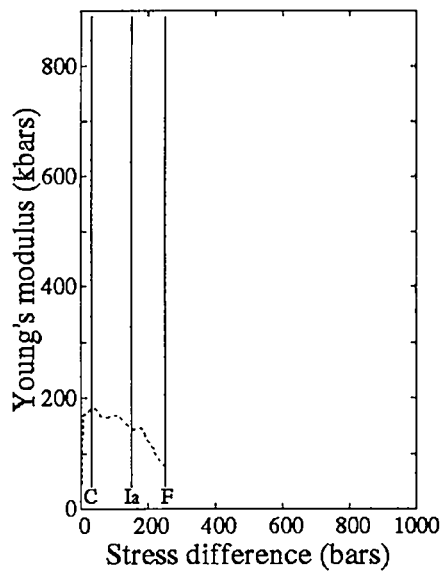

Fig. A1s-5. Young's modulus or, as appropriate, the parameter ($\Delta\sigma_{axl}$ / $\Delta\varepsilon_{axl}$) as a function of stress difference.

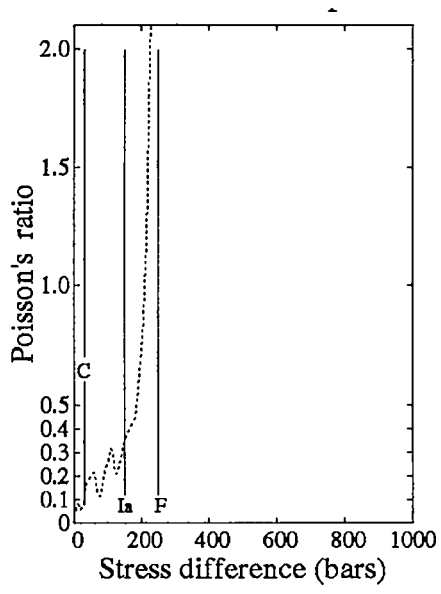

Fig. A1s-6. Poisson's ratio or, as appropriate, the parameter ($-\Delta\varepsilon_{trv}$ / $\Delta\varepsilon_{axl}$) as a function of stress difference.

Note: Transition stress levels '*C*', and '*Ia*', and the fracture stress '*F*' are defined in Table A1s-3. Axial and transverse strains are identified as 'axl' and 'trv', respectively.

Perlite 1s

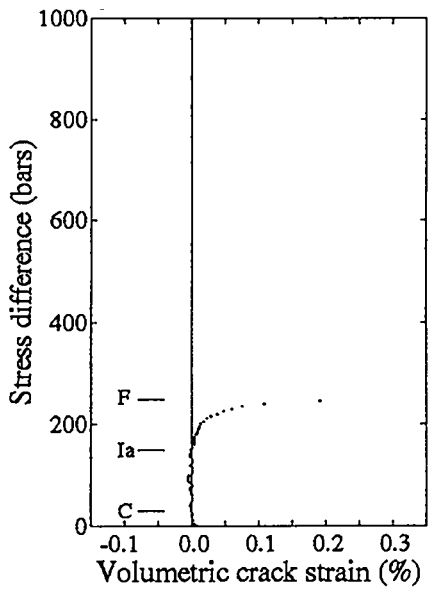

Fig. A1s-7. Volumetric crack strain or "crack porosity" as a function of stress difference in uniaxial compression. Transition stress levels '*C*', and '*Ia*', and the fracture stress '*F*' are defined in Table A1s-3.

Table A1s-3. Mechanical response of **Perlite 1s** at selected values of stress difference.

$\Delta\sigma$ (bars)	σ_3 (bars)	ε_a (%)	ε_t (%)	Mechanical behavior	Notes
30	0	0.02	0.0	c→led	Transition stress level '*C*'.
50	0	0.03	0.0	led	
100	0	0.06	-0.01	led	$[(d\varepsilon_v/d\sigma)_{led} = 3.47\times10^{-3}$ kb$^{-1}]$
150	0	0.09	-0.01	led→mc	Transition stress level '*Ia*'.
185	0	0.11	-0.02	mc	Const. volume deformation.
200	0	0.12	-0.03	mc	
249	0	0.19	-0.27	mc	Fracture stress level '*F*'.

$\Delta\sigma$ - Stress difference.
σ_3 - Confining stress.
ε_a - Axial strain.
ε_t - Transverse strain.
ε_v - Volume strain.

Mechanical behavior categories:
c - Closure of pre-existing cracks.
led - Linear elastic deformation.
mc - Microcracking.

Perlite 2s

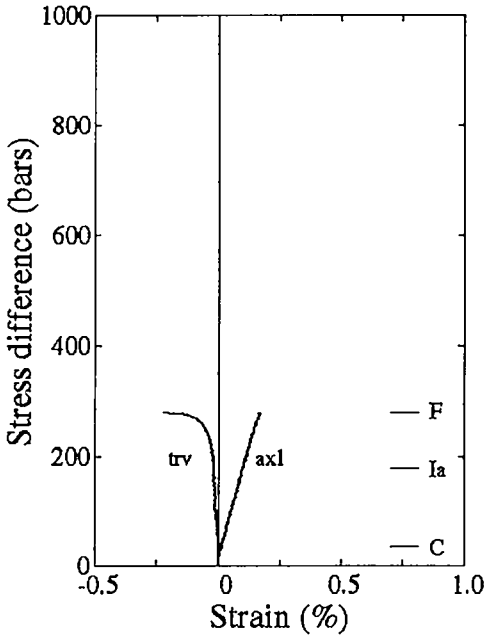

Fig. A2s-1. Mechanical response of specimen to uniaxial compression. Transition stress levels '*C*' and '*Ia*', and the fracture stress '*F*' are defined in Table A2s-3. Axial and transverse strains are identified as 'axl' and 'trv', respectively.

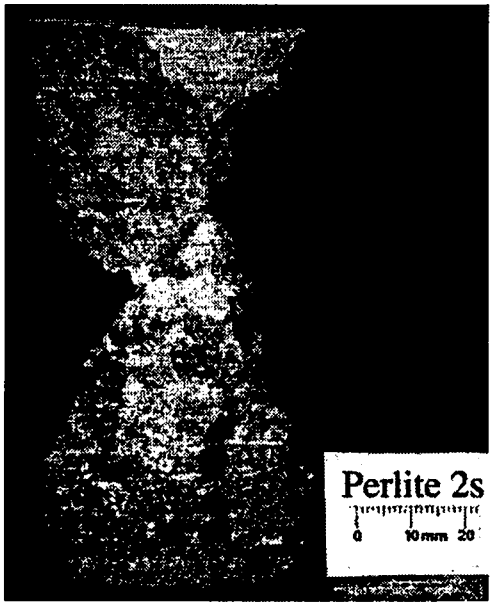

Fig. A2s-2. Post-test photograph of specimen.

Table A2s-1. Summary of physical and mechanical properties.

Specimen type	Perlite
Density, bulk (geometric determination)	1.88 g/cm^3
Density, grain	not determined
Moisture (ASTM D2216)	0.16%
Elastic constants:	
Young's modulus	168.2 kbars
Poisson's ratio	0.203
Mechanical behavior stress levels:	
Closure of pre-existing cracks	0 - 35 bars
Linear elastic deformation	35 - 180 bars
Microcracking	180 - 280 bars
Fracture strength	280 bars
Fracture angle (shear)	58°

Perlite 2s

Specimen Source. Specimen **Perlite 2s** was cored from bulk material retrieved from Grefco's perlite mine operations located off US Highway 60, 3 miles south of Socorro, Socorro County, New Mexico. The quarry is located at coordinates 34°01'32" north latitude and 106°56'14" west longitude. The sample was recovered from the quarry floor in the vicinity of the geophysical array for small - scale explosive experiments. The bulk material was retrieved April, 1993 and not protected from moisture loss. The specimen was tested June, 1993 as a laboratory dry specimen.

Table A2s-2. Test conditions.

Operating procedure	ASTM D3148
Specimen preparation	ASTM D4543
Specimen geometry:	
Shape	cylindrical
Diameter	2.11 inches
Length to diameter ratio	2.08
Specimen orientation (angle between flow banding and plane normal to cylindrical axis)	0° [$\sigma_{1\perp}$]
Strain rate; average	2.4 x 10^{-6} sec^{-1}

Specimen Description. The test specimen is perlite, a volcanic rock, gray in color with a distinctive "flow banding" structure. The perlite, consisting of highly porous volcanic glass, contains less than 5 volume percent crystals and crystal clusters of feldspar and quartz (?) that are ≤3 mm diameter. Pores of the glassy matrix are sub millimeter in size, and have elongate, flat outlines parallel to the banding structure of the rock. The test specimen was cored such that banding is perpendicular to the cylindrical axis of the specimen. Narrow, submillimeter wide, open fractures to a length of 1 cm are observed on the test specimen surface but are not abundant. These open fractures are perpendicular to the banding and are prevalent at specific horizons. No displacement is observed across these fractures. They are interpreted as unhealed segments of fractures that originally passed through the specimen.

Characteristics of the Failed Specimen. The failed specimen has both shear and tensile fractures. Geometric relationships between fractures suggests that shear failure preceded tensile splitting and was responsible for specimen failure. Shear failure created a single steeply inclined fracture passing entirely through the specimen. This surface has an average angle of 58° to a plane normal to the cylindrical axis. It is a planar feature modified by step-like structures, which are controlled by the flow banding of the rock. Tensile splitting is responsible for more vertical fractures. The overall shape for these surfaces is sub-conchoidal, modified by step-like structures. It was noted that fracture surfaces often were coated with fine glassy particles, which were locally of sufficient quantity to obscure details on the surface. It was not determined whether the glassy particles were confined to a specific fracture type.

Perlite 2s

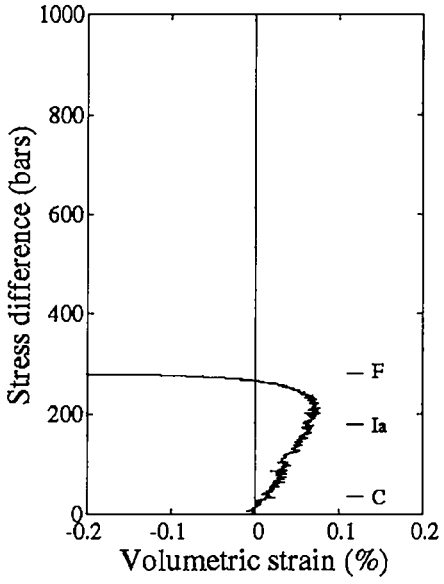

Fig. A2s-3. Volumetric strain resulting from uniaxial compression.

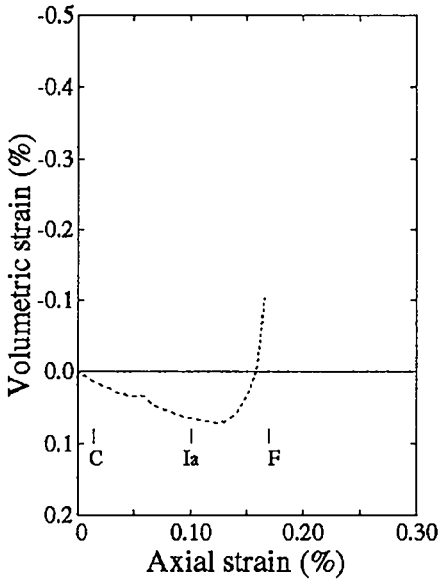

Fig. A2s-4. Relationship between volumetric and axial strain measurements.

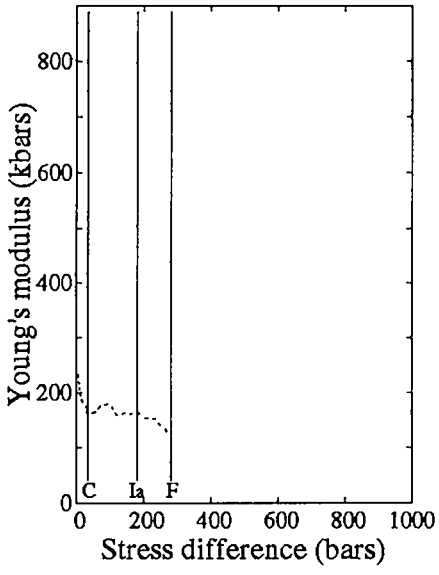

Fig. A2s-5. Young's modulus or, as appropriate, the parameter ($\Delta\sigma_{axl}$ / $\Delta\varepsilon_{axl}$) as a function of stress difference.

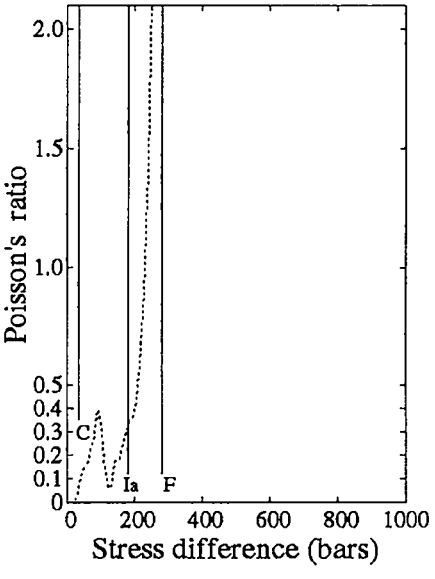

Fig. A2s-6. Poisson's ratio or, as appropriate, the parameter ($-\Delta\varepsilon_{trv}$ / $\Delta\varepsilon_{axl}$) as a function of stress difference.

Note: Transition stress levels '*C*', and '*Ia*', and the fracture stress '*F*' are defined in Table A2s-3. Axial and transverse strains are identified as 'axl' and 'trv', respectively.

Perlite 2s

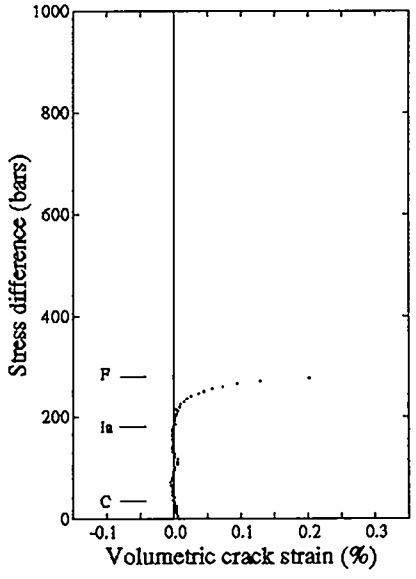

Fig. A2s-7. Volumetric crack strain or "crack porosity" as a function of stress difference in uniaxial compression. Transition stress levels '*C*', and '*Ia*', and the fracture stress '*F*' are defined in Table A2s-3.

Table A1s-3. Mechanical response of **Perlite 2s** at selected values of stress difference.

$\Delta\sigma$ (bars)	σ_3 (bars)	ε_a (%)	ε_t (%)	Mechanical behavior	Notes
35	0	0.01	0.0	c→led	Transition stress level '*C*'.
50	0	0.02	0.0	led	
100	0	0.05	-0.01	led	$[(d\varepsilon_v/d\sigma)_{led} = 3.53\times10^{-3}$ kb$^{-1}]$
150	0	0.08	-0.01	led	
180	0	0.10	-0.02	led→mc	Transition stress level '*Ia*'.
200	0	0.11	-0.02	mc	
210	0	0.12	-0.03	mc	Const. volume deformation.
250	0	0.15	-0.05	mc	
280	0	0.17	-0.23	mc	Fracture stress level '*F*'.

$\Delta\sigma$ - Stress difference.
σ_3 - Confining stress.
ε_a - Axial strain.
ε_t - Transverse strain.
ε_v - Volume strain.

Mechanical behavior categories:
c - Closure of pre-existing cracks.
led - Linear elastic deformation.
mc - Microcracking.

Perlite 3s

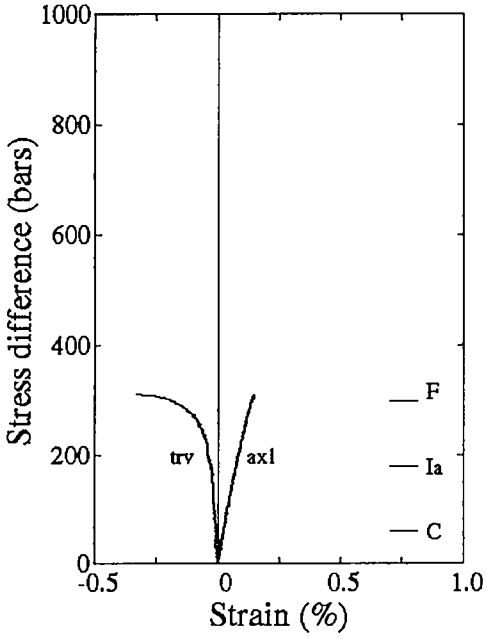

Fig. A3s-1. Mechanical response of specimen to uniaxial compression. Transition stress levels '*C*' and '*Ia*', and the fracture stress '*F*' are defined in Table A3s-3. Axial and transverse strains are identified as 'axl' and 'trv', respectively.

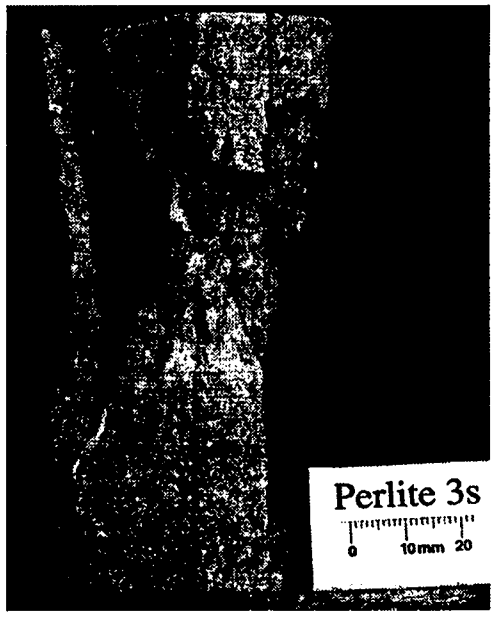

Fig. A3s-2. Post-test photograph of specimen.

Table A3s-1. Summary of physical and mechanical properties.

Specimen type	Perlite
Density, bulk (geometric determination)	1.86 g/cm^3
Density, grain	not determined
Moisture (ASTM D2216)	0.20%
Elastic constants:	
Young's modulus	238.1 kbars
Poisson's ratio	0.419
Mechanical behavior stress levels:	
Closure of pre-existing cracks	0 - 60 bars
Linear elastic deformation	60 - 180 bars
Microcracking	180 - 310 bars
Fracture strength	310 bars
Fracture angle (shear)	65°

Perlite 3s

Specimen Source. Specimen **Perlite 3s** was cored from bulk material retrieved from Grefco's perlite mine operations located off US Highway 60, 3 miles south of Socorro, Socorro County, New Mexico. The quarry is located at coordinates 34°01'32" north latitude and 106°56'14" west longitude. The sample was recovered from the quarry floor in the vicinity of the geophysical array for small - scale explosive experiments. The bulk material was retrieved April, 1993 and not protected from moisture loss. The specimen was tested June, 1993 as a laboratory dry specimen.

Table A3s-2. Test conditions.

Operating procedure	ASTM D3148
Specimen preparation	ASTM D4543
Specimen geometry:	
Shape	cylindrical
Diameter	2.11 inches
Length to diameter ratio	2.02
Specimen orientation (angle between flow banding and plane normal to cylindrical axis)	90° $[\sigma_1 \| \|]$
Strain rate; average	1.7×10^{-6} sec^{-1}

Specimen Description. The test specimen is perlite, a volcanic rock, gray in color with a distinctive "flow banding" structure. The perlite, consisting of highly porous volcanic glass, contains less than 5 volume percent crystals and crystal clusters of feldspar and quartz (?) that are ≤2 mm diameter. Pores of the glassy matrix are sub millimeter in size, and have elongate, flat outlines parallel to the banding structure of the rock. The test specimen was cored such that banding is parallel to the cylindrical axis of the specimen. Narrow, submillimeter wide, open fractures to a length of 1 cm are observed on the test specimen surface but are not abundant. These open fractures are perpendicular to the banding and are prevalent at specific horizons. At a given horizon the fractures may display a regular spacing of 1.0 to 1.3 cm. No displacement is observed across these fractures. They are interpreted as unhealed segments of fractures that originally passed through the specimen.

Characteristics of the Failed Specimen. The failed specimen has both shear and tensile fractures. Geometric relationships between fractures suggests that shear failure preceded tensile splitting and was responsible for specimen failure. The shear failure surface cuts across flow banding at the shallow angle of 25°, forming rough, step-like structures. Roughness of fracture surfaces may partially be due to preferred failure along the periphery of crystals and crystal clusters. Step-like structures are spaced 1 cm or greater and may not recur with consistent spacing. The trace of this fracture forms an angle of 65° to a plane normal to the cylindrical axis. With cylindrical axis as vertical reference, the strike of the shear plane essentially coincides with the strike of banding. Tensile splitting formed an abundance of splintered pieces, which are concentrated along the periphery of the specimen in close proximity to the shear plane. Tensile splitting was also effective at splintering one side of the specimen where the plane of banding is tangent to the circular outline of the specimen. Fracture surfaces resulting from tensile splitting are nearly vertical.

Perlite 3s

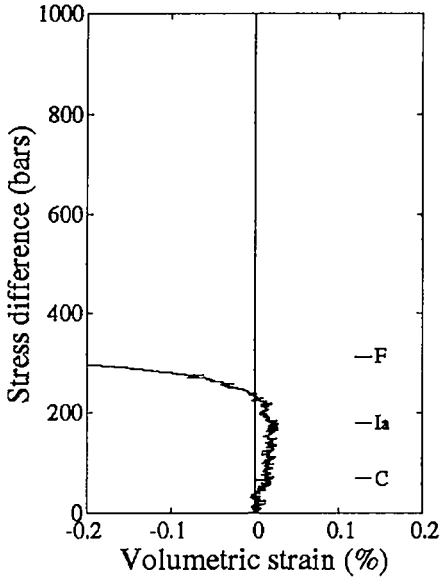

Fig. A3s-3. Volumetric strain resulting from uniaxial compression.

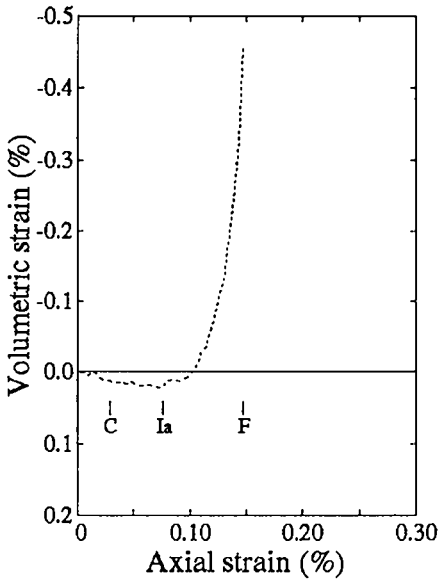

Fig. A3s-4. Relationship between volumetric and axial strain measurements.

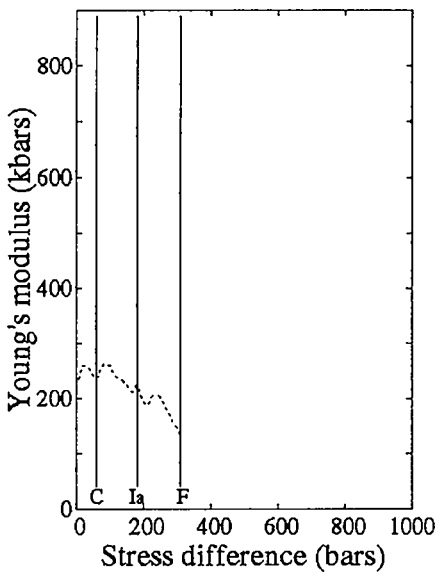

Fig. A3s-5. Young's modulus or, as appropriate, the parameter ($\Delta\sigma_{axl}$ / $\Delta\varepsilon_{axl}$) as a function of stress difference.

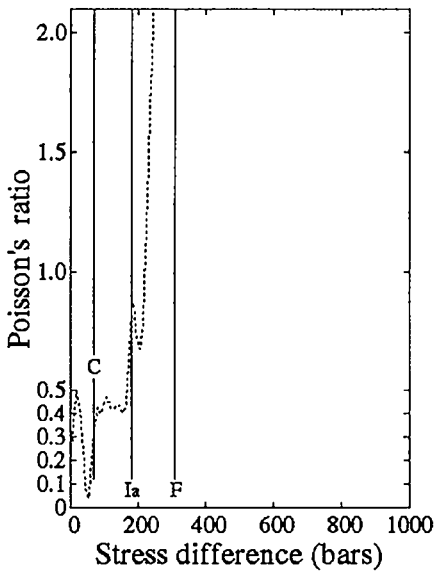

Fig. A3s-6. Poisson's ratio or, as appropriate, the parameter ($-\Delta\varepsilon_{trv}$ / $\Delta\varepsilon_{axl}$) as a function of stress difference.

Note: Transition stress levels '*C*', and '*Ia*', and the fracture stress '*F*' are defined in Table A3s-3. Axial and transverse strains are identified as 'axl' and 'trv', respectively.

Perlite 3s

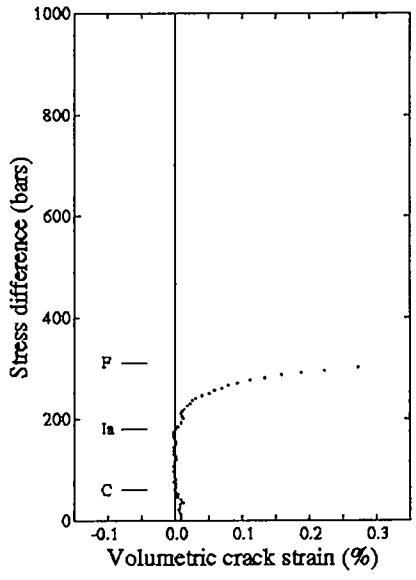

Fig. A3s-7. Volumetric crack strain or "crack porosity" as a function of stress difference in uniaxial compression. Transition stress levels '*C*', and '*Ia*', and the fracture stress '*F*' are defined in Table A3s-3.

Table A3s-3. Mechanical response of **Perlite 3s** at selected values of stress difference.

$\Delta\sigma$ (bars)	σ_3 (bars)	ε_a (%)	ε_t (%)	Mechanical behavior	Notes
50	0	0.02	-0.01	c	
60	0	0.03	-0.01	c→led	Transition stress level '*C*'.
100	0	0.04	-0.01	led	$[(d\varepsilon_v/d\sigma)_{led} = 0.68\times10^{-3}$ kb$^{-1}]$
150	0	0.06	-0.02	led	
180	0	0.08	-0.03	led→mc	Transition stress level '*Ia*'. Const. volume deformation.
200	0	0.09	-0.04	mc	
250	0	0.11	-0.07	mc	
300	0	0.14	-0.19	mc	
310	0	0.15	-0.34	mc	Fracture stress level '*F*'.

$\Delta\sigma$ - Stress difference.
σ_3 - Confining stress.
ε_a - Axial strain.
ε_t - Transverse strain.
ε_v - Volume strain.

Mechanical behavior categories:
c - Closure of pre-existing cracks.
led - Linear elastic deformation.
mc - Microcracking.

Perlite 4s

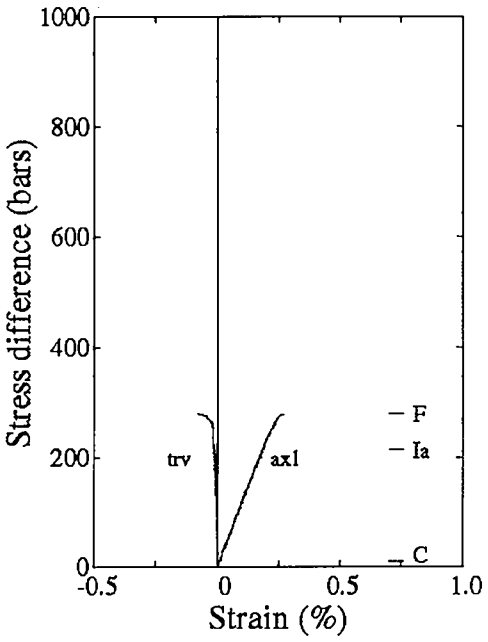

Fig. A4s-1. Mechanical response of specimen to uniaxial compression. Transition stress levels '*C*' and '*Ia*', and the fracture stress '*F*' are defined in Table A4s-3. Axial and transverse strains are identified as 'axl' and 'trv', respectively.

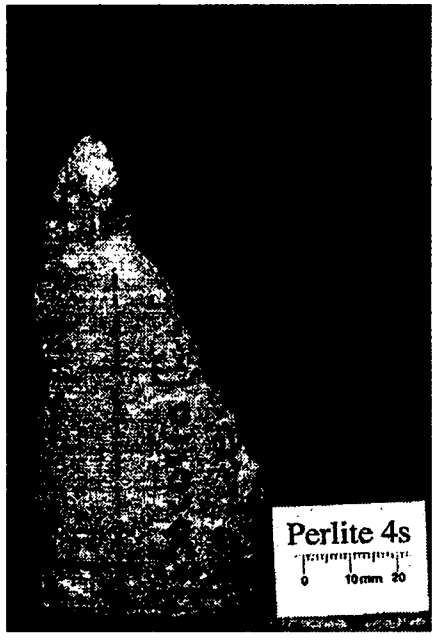

Fig. A4s-2. Post-test photograph of specimen.

Table A4s-1. Summary of physical and mechanical properties.

Specimen type	Perlite
Density, bulk (geometric determination)	1.90 g/cm^3
Density, grain	not determined
Moisture (ASTM D2216)	0.68%
Elastic constants:	
Young's modulus	117.4 kbars
Poisson's ratio	0.080
Mechanical behavior stress levels:	
Closure of pre-existing cracks	0 - 10 bars
Linear elastic deformation	10 - 215 bars
Microcracking	215 - 280 bars
Fracture strength	280 bars
Fracture angle (shear)	64°

Perlite 4s

Specimen Source. Specimen **Perlite 4s** was cored from bulk material retrieved from Grefco's perlite mine operations located off US Highway 60, 3 miles south of Socorro, Socorro County, New Mexico. The quarry is located at coordinates 34°01'32" north latitude and 106°56'14" west longitude. The sample was recovered from the quarry floor in the vicinity of the geophysical array for small - scale explosive experiments. The bulk material was retrieved April, 1993 and not protected from moisture loss. The specimen was tested June, 1993 as a laboratory dry specimen.

Table 2. Test conditions.

Operating procedure	ASTM D3148
Specimen preparation	ASTM D4543
Specimen geometry:	
Shape	cylindrical
Diameter	2.09 inches
Length to diameter ratio	2.08
Specimen orientation (angle between flow banding and plane normal to cylindrical axis)	0° $[\sigma_{1\perp}]$
Strain rate; average	3.6×10^{-6} sec^{-1}

Specimen Description. The test specimen is perlite, a volcanic rock, gray in color with a distinctive "flow banding" structure. The perlite, consisting of highly porous volcanic glass, contains less than 5 volume percent crystals and crystal clusters of feldspar and quartz (?) that are ≤5 mm diameter. Pores of the glassy matrix are submillimeter in size, and have elongate, flat outlines parallel to the banding structure of the rock. The test specimen was cored such that banding is perpendicular to the cylindrical axis of the specimen. Narrow, submillimeter wide, open fractures to a length of 1 cm are observed on the test specimen surface but are not abundant. The fractures form discontinuous linear features oriented at a high angle to the flow banding. No displacement is observed across these fractures. They are interpreted as unhealed segments of fractures that originally passed through the specimen.

Characteristics of the Failed Specimen. The failed specimen has both shear and tensile fractures. Geometric relationships between fractures suggests that shear failure preceded tensile splitting and was responsible for specimen failure. Shear failure created a single steeply inclined fracture passing entirely through the specimen. The surface of this planar feature consists of closely spaced, narrow step-like structures, which are controlled by the flow banding. The measured angle for this fracture is 64° with respect to a plane normal to the cylindrical axis. Tensile splitting formed an abundance of splintered pieces. Fracture surfaces resulting from tensile splitting are nearly vertical. Tensile fractures intersect the shear fracture but do not project into the facing wall. Fine glassy particles, abundant to the point of obscuring the fracture surface, were associated with fractures. There is no record, however, identifying the associated fracture type or that this condition is generally true for all fractures.

Perlite 4s

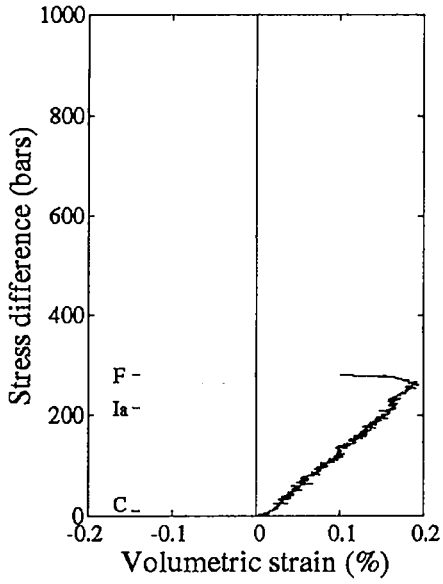

Fig. A4s-3. Volumetric strain resulting from uniaxial compression.

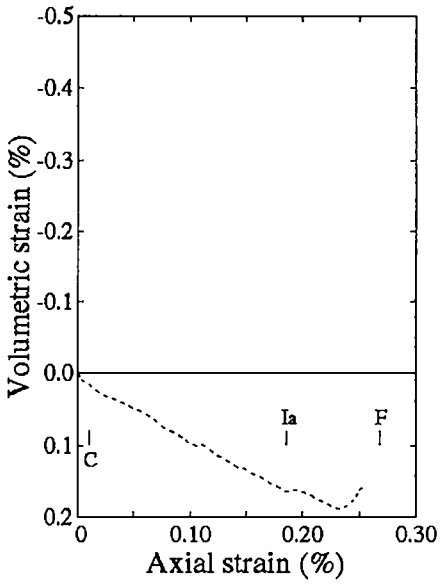

Fig. A4s-4. Relationship between volumetric and axial strain measurements.

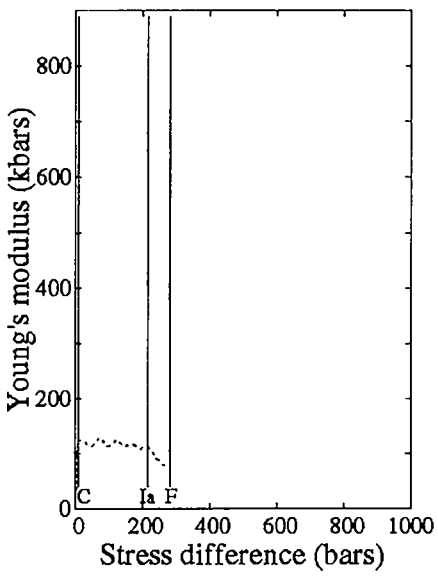

Fig. A4s-5. Young's modulus or, as appropriate, the parameter ($\Delta\sigma_{axl}$ / $\Delta\varepsilon_{axl}$) as a function of stress difference.

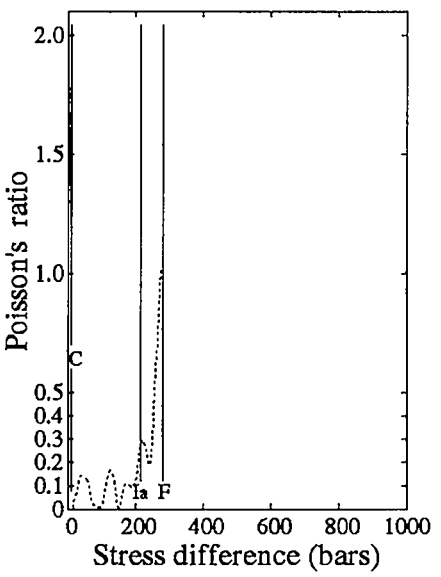

Fig. A4s-6. Poisson's ratio or, as appropriate, the parameter ($-\Delta\varepsilon_{trv}$ / $\Delta\varepsilon_{axl}$) as a function of stress difference.

Note: Transition stress levels '*C*', and '*Ia*', and the fracture stress '*F*' are defined in Table A4s-3. Axial and transverse strains are identified as 'axl' and 'trv', respectively.

Perlite 4s

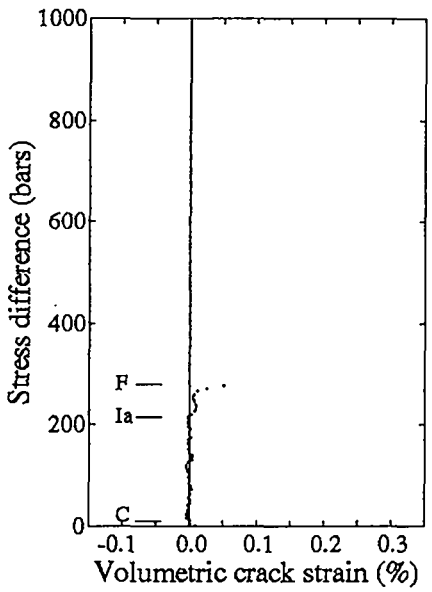

Fig. A4s-7. Volumetric crack strain or "crack porosity" as a function of stress difference in uniaxial compression. Transition stress levels '*C*', and '*Ia*', and the fracture stress '*F*' are defined in Table A4s-3.

Table A4s-3. Mechanical response of **Perlite 4s** at selected values of stress difference.

$\Delta\sigma$ (bars)	σ_3 (bars)	ε_a (%)	ε_t (%)	Mechanical behavior	Notes
10	0	0.01	0.0	c→led	Transition stress level '*C*'.
50	0	0.04	0.0	led	
100	0	0.09	0.0	led	$[(d\varepsilon_v/d\sigma)_{led} = 7.15\times10^{-3}$ kb$^{-1}]$
150	0	0.13	-0.01	led	
200	0	0.17	-0.01	led	
215	0	0.19	-0.01	led→mc	Transition stress level '*Ia*'.
250	0	0.22	-0.02	mc	
265	0	0.24	-0.03	mc	Const. volume deformation.
280	0	0.27	-0.08	mc	Fracture stress level '*F*'.

$\Delta\sigma$ - Stress difference.
σ_3 - Confining stress.
ε_a - Axial strain.
ε_t - Transverse strain.
ε_v - Volume strain.

Mechanical behavior categories:
c - Closure of pre-existing cracks.
led - Linear elastic deformation.
mc - Microcracking.

Perlite 5s

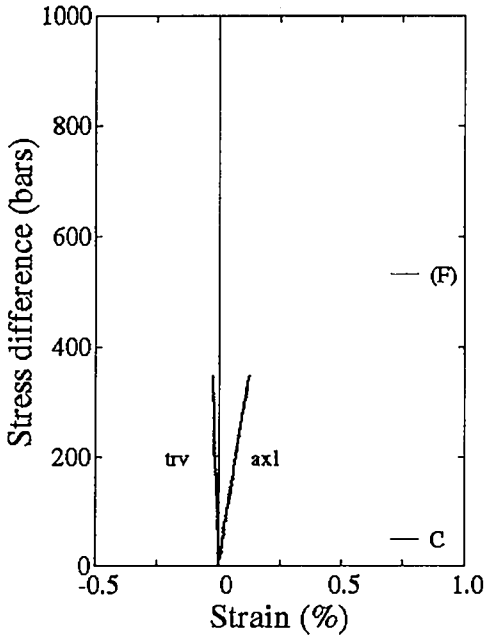

Fig. A5s-1. Mechanical response of specimen to uniaxial compression. Transition stress level '*C*' is defined in Table A5s-3. Fracture stress '*(F)*' was determined from test **Perlite 5s2**. Axial and transverse strains are identified as 'axl' and 'trv', respectively.

No photograph is provided.

====

Test conditions did not result in specimen failure.

Fig. A5s-2. Post-test photograph of specimen.

Table A5s-1. Summary of physical and mechanical properties.

Specimen type	Perlite
Density, bulk (geometric determination)	1.84 g/cm^3
Density, grain	not determined
Moisture (ASTM D2216)	3.0%
Elastic constants:	
Young's modulus	280.3 kbars
Poisson's ratio	0.263
Mechanical behavior stress levels:	
Closure of pre-existing cracks	0 - 50 bars
Linear elastic deformation	50 - ≥350 bars
Microcracking	not determined
Maximum stress difference for load/unload cycle	457 bars
Fracture strength (uniaxial compression test ***Perlite 5s2***)	532 bars
Fracture angles (shear)	(no failure)

Perlite 5s

Specimen Source. Specimen **Perlite 5s** was cored from bulk material retrieved from Grefco's perlite mine operations located off US Highway 60, 3 miles south of Socorro, Socorro County, New Mexico. The quarry is located at coordinates 34°01'32" north latitude and 106°56'14" west longitude. The sample was recovered from the quarry floor in the vicinity of the geophysical array for small - scale explosive experiments. The bulk material was retrieved April, 1993 and not protected from moisture loss. The specimen was tested June, 1993 as a laboratory dry specimen.

Table A5s-2. Test conditions.

Operating procedure	ASTM D3148
Specimen preparation	ASTM D4543
Specimen geometry:	
Shape	cylindrical
Diameter	2.11 inches
Length to diameter ratio	2.00
Specimen orientation (angle between flow banding and plane normal to cylindrical axis)	90° [$\sigma_1 \| \|$]
First load cycle (Specimen was loaded to the maximum force transducer setting without failing. The load rate was then reversed and the test was terminated upon unloading. A second test, "Perlite 5s2," was performed to reach fracture strength.)	
Strain rate; average	1.5×10^{-6} sec^{-1}

Specimen Description. The test specimen is perlite, a volcanic rock, gray in color with a distinctive "flow banding" structure. The perlite, consisting of highly porous volcanic glass, contains less than 5 volume percent crystals and crystal clusters of feldspar and quartz (?) that are ≤3 mm diameter. Pores of the glassy matrix are submillimeter in size, and have elongate, flat outlines parallel to the banding structure of the rock. The test specimen was cored such that banding is parallel to the cylindrical axis of the specimen. Narrow, submillimeter wide, open fractures to a length of 0.5 cm are observed on the test specimen surface but are not abundant. These open fractures are perpendicular to the banding and are prevalent at specific horizons. No displacement is observed across these fractures. They are interpreted as unhealed segments of fractures that originally passed through the specimen.

Post-test Specimen. The physical character of the specimen, post-test, showed no macroscopic changes from the original specimen description. The maximum applied stress was insufficient to cause the perlite to fail. Uniaxial compression test "Perlite 5s2," which was performed on the identical specimen, suggests that the applied stress had reached beyond the linear elastic deformation range. The specimen should have experienced an altering effect due to microcracking.

Limited Data Recovery. Transducer output was recorded for axial stress, and for axial and transverse extensometers for the entire load and unload cycle. However, at stress levels greater than 350 bars a noticeable variance in volumetric strain occurred. This variance is interpreted as an extensometer moving from its reference position on the specimen surface, thereby invalidating the corresponding displacement and strain records. Therefore, no strain data are presented for this uniaxial compression test above 350 bars stress nor for the subsequent unload segment of the stress cycle.

Perlite 5s

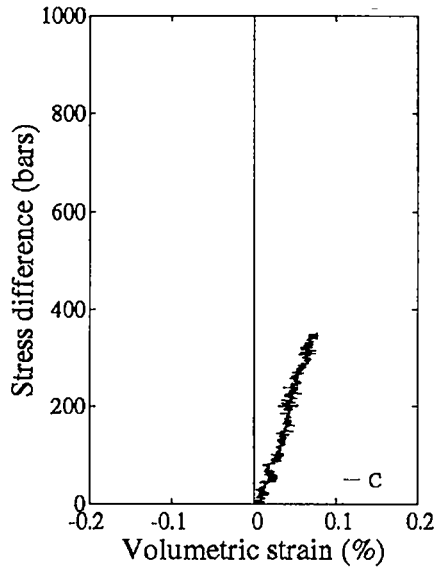

Fig. A5s-3. Volumetric strain resulting from uniaxial compression.

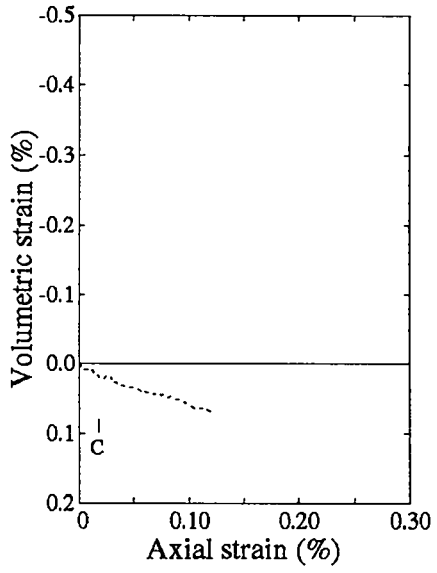

Fig. A5s-4. Relationship between volumetric and axial strain measurements.

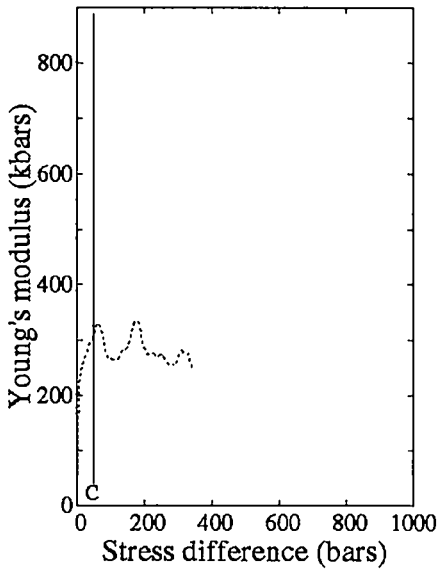

Fig. A5s-5. Young's modulus or, as appropriate, the parameter ($\Delta\sigma_{axl} / \Delta\varepsilon_{axl}$) as a function of stress difference.

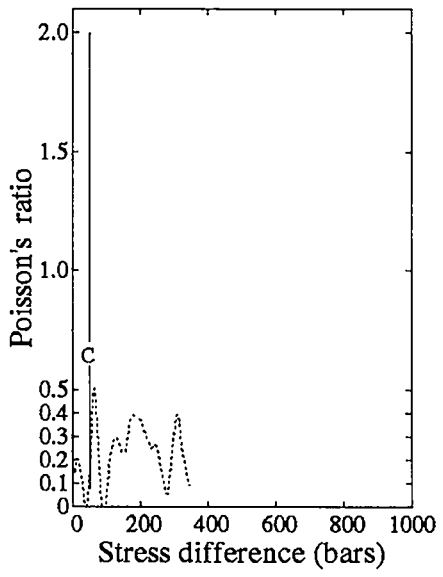

Fig. A5s-6. Poisson's ratio or, as appropriate, the parameter ($-\Delta\varepsilon_{trv} / \Delta\varepsilon_{axl}$) as a function of stress difference.

Note: Transition stress level '*C*' is defined in Table A5s-3. Axial and transverse strains are identified as 'axl' and 'trv', respectively.

Perlite 5s

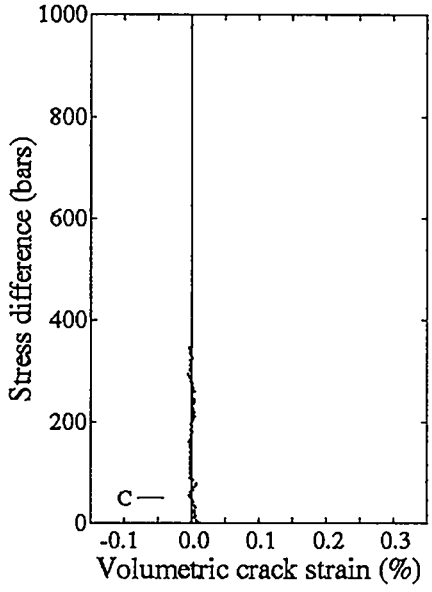

Fig. A5s-7. Volumetric crack strain or "crack porosity" as a function of stress difference in uniaxial compression. Transition stress level '*C*' is defined in Table A5s-3.

Table A5s-3. Mechanical response of **Perlite 5s** at selected values of stress difference.

$\Delta\sigma$ (bars)	σ_3 (bars)	ε_a (%)	ε_t (%)	Mechanical behavior	Notes
50	0	0.02	0.0	c→led	Transition stress level '*C*'.
100	0	0.04	0.0	led	
150	0	0.05	-0.01	led	
200	0	0.07	-0.01	led	$[(d\varepsilon_v/d\sigma)_{led} = 1.69\times10^{-3}$ kb$^{-1}]$
250	0	0.09	-0.02	led	
300	0	0.11	-0.02	led	
350	0	0.13	-0.02	led	

$\Delta\sigma$ - Stress difference.
σ_3 - Confining stress.
ε_a - Axial strain.
ε_t - Transverse strain.
ε_v - Volume strain.

Mechanical behavior categories:
c - Closure of pre-existing cracks.
led - Linear elastic deformation.
mc - Microcracking.

Perlite 5s2

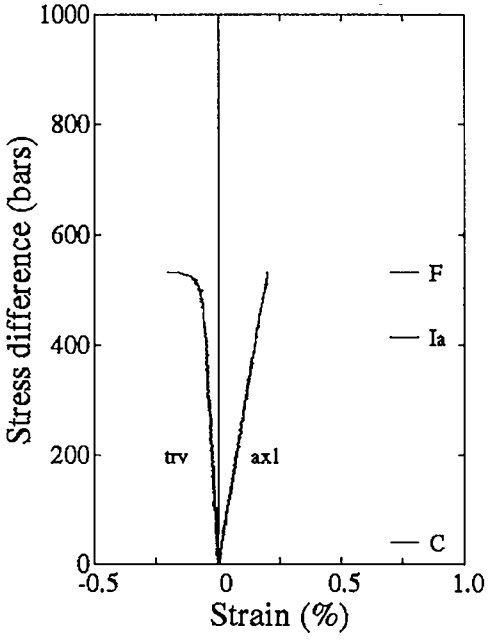

Fig. A5s2-1. Mechanical response of specimen to uniaxial compression. Transition stress levels '*C*' and '*Ia*', and the fracture stress '*F*' are defined in Table A5s2-3. Axial and transverse strains are identified as 'axl' and 'trv', respectively.

Fig. A5s2-2. Post-test photograph of specimen.

Table A5s2-1. Summary of physical and mechanical properties.

Specimen type	Perlite
Density, bulk (geometric determination)	1.84 g/cm^3
Density, grain	not determined
Moisture (ASTM D2216)	3.0%
Elastic constants:	
Young's modulus	273.5 kbars
Poisson's ratio	0.342
Mechanical behavior stress levels:	
Closure of pre-existing cracks	0 - 40 bars
Linear elastic deformation	40 - 415 bars
Microcracking	415 - 532 bars
Fracture strength	532 bars
Fracture angle (shear)	70°

Perlite 5s2

Specimen Source. Specimen **Perlite 5s** was cored from bulk material retrieved from Grefco's perlite mine operations located off US Highway 60, 3 miles south of Socorro, Socorro County, New Mexico. The quarry is located at coordinates 34°01'32" north latitude and 106°56'14" west longitude. The sample was recovered from the quarry floor in the vicinity of the geophysical array for small - scale explosive experiments. The bulk material was retrieved April, 1993 and not protected from moisture loss. The specimen was tested June, 1993 as a laboratory dry specimen.

Table A5s2-2. Test conditions.

Operating procedure	ASTM D3148
Specimen preparation	ASTM D4543
Specimen geometry:	
Shape	cylindrical
Diameter	2.11 inches
Length to diameter ratio	2.00
Specimen orientation (angle between flow banding and plane normal to cylindrical axis)	90° [σ_1||]
Second load cycle (first load cycle reached a peak stress difference of 457 bars; see "Perlite 5s")	
Strain rate; average	1.5×10^{-6} sec^{-1}

Specimen Description. The test specimen is perlite, a volcanic rock, gray in color with a distinctive "flow banding" structure. The perlite, consisting of highly porous volcanic glass, contains less than 5 volume percent crystals and crystal clusters of feldspar and quartz (?) that are ≤3 mm diameter. Pores of the glassy matrix are submillimeter in size, and have elongate, flat outlines parallel to the banding structure of the rock. The test specimen was cored such that banding is parallel to the cylindrical axis of the specimen. Narrow, submillimeter wide, open fractures to a length of 0.5 cm are observed on the test specimen surface but are not abundant. These open fractures are perpendicular to the banding and are prevalent at specific horizons. No displacement is observed across these fractures. They are interpreted as unhealed segments of fractures that originally passed through the specimen.

Characteristics of the Failed Specimen. The failed specimen has both shear and tensile fractures. Geometric relationships between fractures suggests that shear failure preceded tensile splitting and was responsible for specimen failure. Shear failure created a single steeply inclined fracture passing entirely through the specimen. The surface of this planar feature consists of closely spaced, narrow step-like structures, which are controlled by the flow banding. The measured angle for this fracture is 70° to a plane normal to the cylindrical axis. With cylindrical axis as vertical reference, the strike of the shear plane essentially coincides with the strike of banding. Tensile splitting formed an abundance of splintered pieces with tabular and prismatic shapes. These pieces are prominent along the periphery of the specimen where the curved specimen wall is nearly parallel to the flow banding. Fracture surfaces resulting from tensile splitting are nearly vertical.

Perlite 5s2

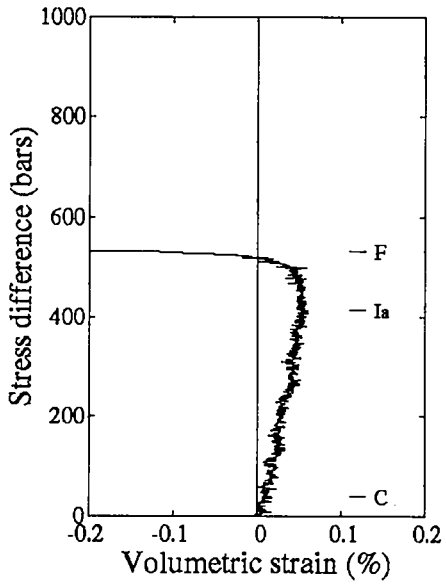

Fig. A5s2-3. Volumetric strain resulting from uniaxial compression.

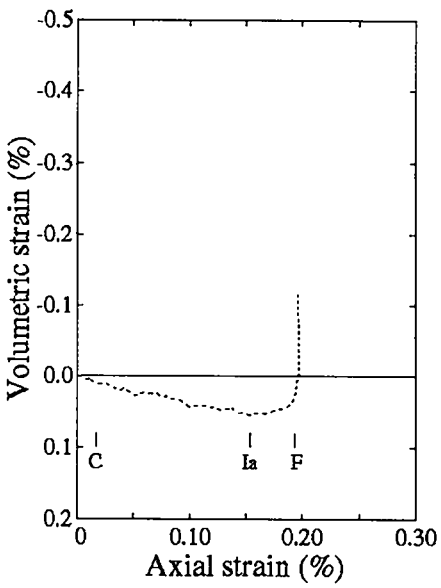

Fig. A5s2-4. Relationship between volumetric and axial strain measurements.

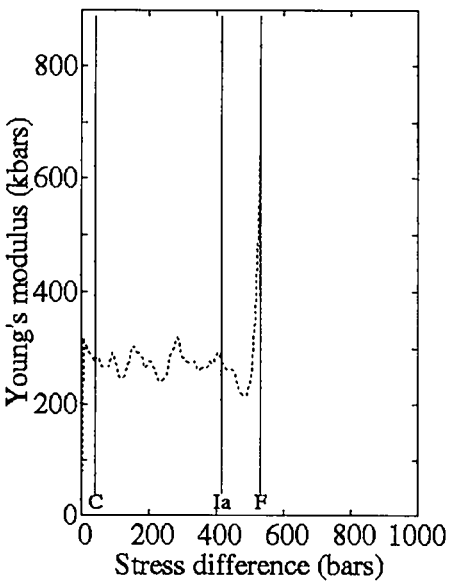

Fig. A5s2-5. Young's modulus or, as appropriate, the parameter ($\Delta\sigma_{axl}$ / $\Delta\varepsilon_{axl}$) as a function of stress difference.

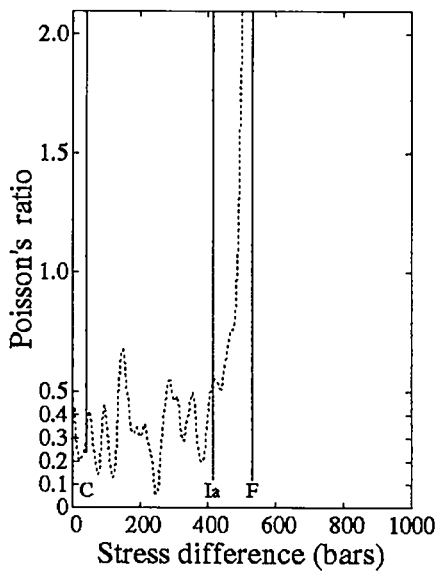

Fig. A5s2-6. Poisson's ratio or, as appropriate, the parameter ($-\Delta\varepsilon_{trv}$ / $\Delta\varepsilon_{axl}$) as a function of stress difference.

Note: Transition stress levels '*C*', and '*Ia*', and the fracture stress '*F*' are defined in Table A5s2-3. Axial and transverse strains are identified as 'axl' and 'trv', respectively.

Perlite 5s2

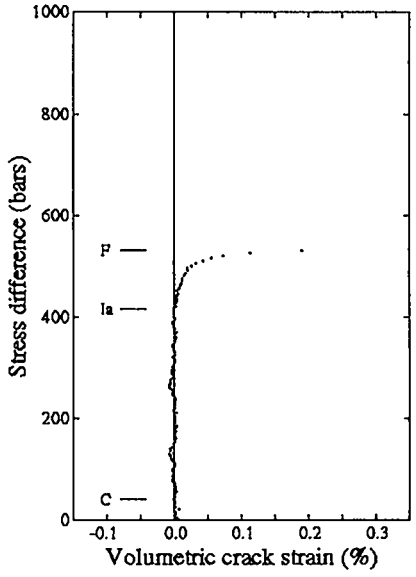

Fig. A5s2-7. Volumetric crack strain or "crack porosity" as a function of stress difference in uniaxial compression. Transition stress levels '*C*', and '*Ia*', and the fracture stress '*F*' are defined in Table A5s2-3.

Table A5s2-3. Mechanical response of **Perlite 5s2** at selected values of stress difference.

$\Delta\sigma$ (bars)	σ_3 (bars)	ε_a (%)	ε_t (%)	Mechanical behavior	Notes
40	0	0.02	0.0	c→led	Transition stress level '*C*'.
50	0	0.02	-0.01	led	
100	0	0.04	-0.01	led	
150	0	0.06	-0.02	led	
200	0	0.08	-0.02	led	$[(d\varepsilon_v/d\sigma)_{led} = 1.16\times10^{-3}$ kb$^{-1}]$
250	0	0.10	-0.03	led	
300	0	0.11	-0.04	led	
350	0	0.13	-0.04	led	
400	0	0.15	-0.05	led	
415	0	0.15	-0.05	led→mc	Transition stress level '*Ia*'.
420	0	0.16	-0.05	mc	Const. volume deformation.
450	0	0.17	-0.06	mc	
500	0	0.19	-0.08	mc	
532	0	0.19	-0.21	mc	Fracture stress level '*F*'.

$\Delta\sigma$ - Stress difference.
σ_3 - Confining stress.
ε_a - Axial strain.
ε_t - Transverse strain.
ε_v - Volume strain.

Mechanical behavior categories:
c - Closure of pre-existing cracks.
led - Linear elastic deformation.
mc - Microcracking.

Perlite 6s

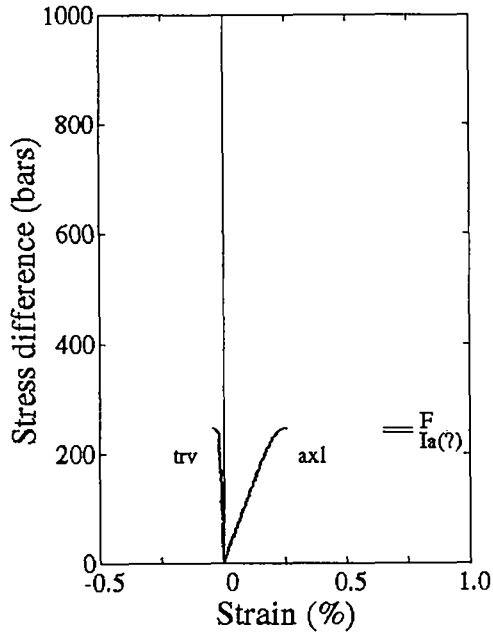

Fig. A6s-1. Mechanical response of specimen to uniaxial compression. Transition stress level '*Ia*', and the fracture stress '*F*' are defined in Table A6s-3. Axial and transverse strains are identified as 'axl' and 'trv', respectively.

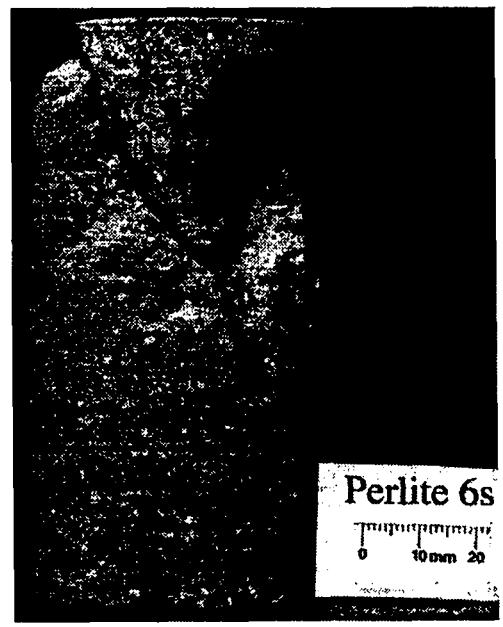

Fig. A6s-2. Post-test photograph of specimen.

Table A6s-1. Summary of physical and mechanical properties.

Specimen type	Perlite
Density, bulk (geometric determination)	1.87 g/cm^3
Density, grain	not determined
Moisture (ASTM D2216)	0.41%
Elastic constants:	
Young's modulus	116.0 kbars
Poisson's ratio	0.089
Mechanical behavior stress levels:	
Linear elastic deformation	0 - 240 (?) bars
Microcracking	240 (?) - 247 bars
Fracture strength	247 bars
Fracture angles (shear)	42°, 58°

Perlite 6s

Specimen Source. Specimen **Perlite 6s** was cored from bulk material retrieved from Grefco's perlite mine operations located off US Highway 60, 3 miles south of Socorro, Socorro County, New Mexico. The quarry is located at coordinates 34°01'32" north latitude and 106°56'14" west longitude. The sample was recovered from the quarry floor in the vicinity of the geophysical array for small - scale explosive experiments. The bulk material was retrieved April, 1993 and not protected from moisture loss. The specimen was tested June, 1993 as a laboratory dry specimen.

Table A6s-2. Test conditions.

Operating procedure	ASTM D3148
Specimen preparation	ASTM D4543
Specimen geometry:	
Shape	cylindrical
Diameter	2.11 inches
Length to diameter ratio	2.03
Specimen orientation (angle between flow banding and plane normal to cylindrical axis)	0° $[\sigma_{1\perp}]$
Strain rate; average	3.6×10^{-6} sec^{-1}

Specimen Description. The test specimen is perlite, a volcanic rock, gray in color with a distinctive "flow banding" structure. The perlite, consisting of highly porous volcanic glass, contains less than 5 volume percent crystals and crystal clusters of feldspar and quartz (?) that are ≤3 mm diameter. Pores of the glassy matrix are sub millimeter in size, and have elongate, flat outlines parallel to the banding structure of the rock. The test specimen was cored such that banding is perpendicular to the cylindrical axis of the specimen. Narrow, submillimeter wide, open fractures to a length of 1 cm are observed on the test specimen surface but are not abundant. These open fractures are perpendicular to the banding and are prevalent at specific horizons. At a given horizon the fractures may display a regular spacing of 1.0 to 1.3 cm. No displacement is observed across these fractures. They are interpreted as unhealed segments of fractures that originally passed through the specimen.

Characteristics of the Failed Specimen. The failed specimen has both shear and tensile fractures. Geometric relationships between fractures suggests that shear failure preceded tensile splitting and was responsible for specimen failure. Shear failure surfaces cut steeply across flow banding, forming rough, step-like structures. The length of the steps are controlled by banding, whereas surface roughness may partially result from preferred failure around the periphery of crystals and crystal clusters. Step-like structures are spaced 1 cm or greater and may not recur with consistent spacing. Shear surfaces are lined with ground glass particles, which may be so abundant as to obstruct surface features along the plane. No single shear fracture cuts entirely across the specimen, instead the two major shear surfaces meet at the apex of a short wedge-shaped end piece above which the fracture is formed by tensile splitting. Measured fracture angles for shear surfaces are 42° and 58° to a plane normal to the cylindrical axis. Tensile splitting is observed as a vertical fracture down the center of the specimen to the apex of the wedge-shaped end piece, and as minor splinters of perlite concentrated along the periphery of the specimen in close proximity to the shear plane. The long tensile fracture has no step-like structures or may be envisioned as a single step. This fracture does not contain ground glass.

Perlite 6s

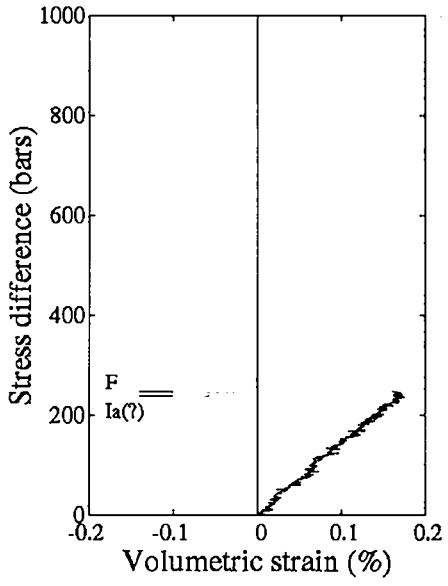

Fig. A6s-3. Volumetric strain resulting from uniaxial compression.

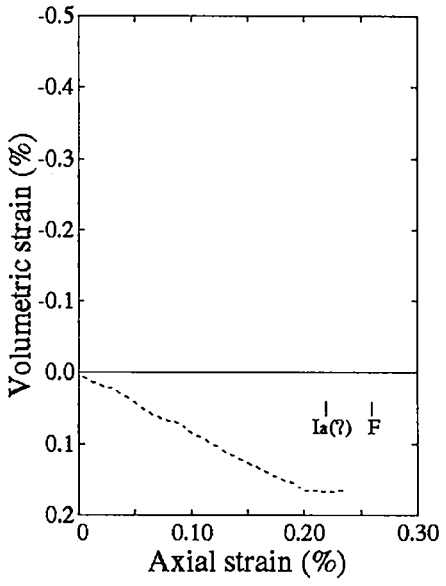

Fig. A6s-4. Relationship between volumetric and axial strain measurements.

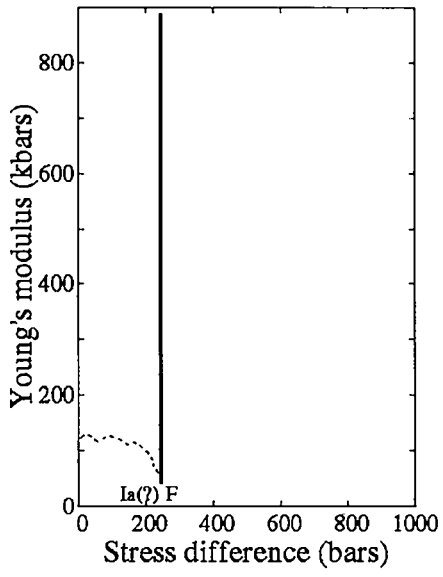

Fig. A6s-5. Young's modulus or, as appropriate, the parameter ($\Delta\sigma_{axl}$ / $\Delta\varepsilon_{axl}$) as a function of stress difference.

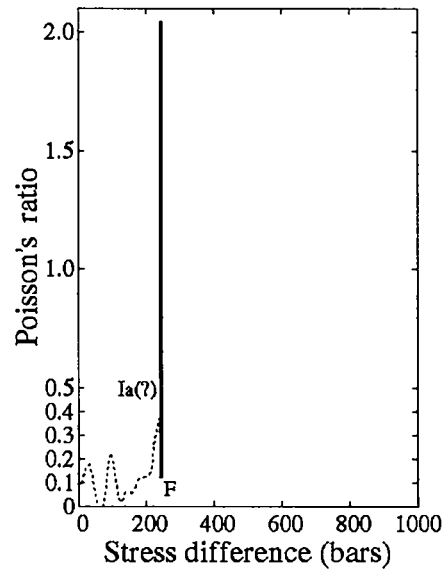

Fig. A6s-6. Poisson's ratio or, as appropriate, the parameter ($-\Delta\varepsilon_{trv}$ / $\Delta\varepsilon_{axl}$) as a function of stress difference.

Note: Transition stress level '*Ia*', and the fracture stress '*F*' are defined in Table A6s-3. Axial and transverse strains are identified as 'axl' and 'trv', respectively.

Perlite 6s

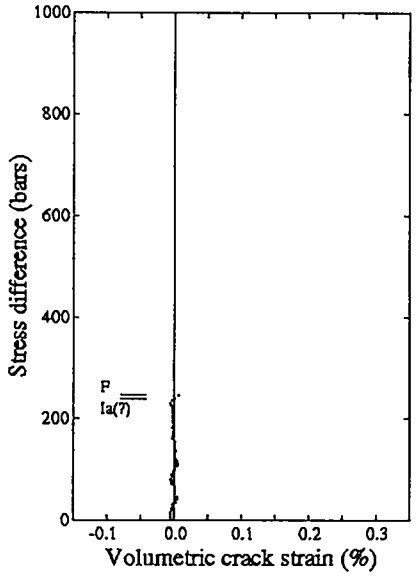

Fig. A6s-7. Volumetric crack strain or "crack porosity" as a function of stress difference in uniaxial compression. Transition stress level '*Ia*', and the fracture stress '*F*' are defined in Table A6s-3.

Table A6s-3. Mechanical response of **Perlite 6s** at selected values of stress difference.

$\Delta\sigma$ (bars)	σ_3 (bars)	ε_a (%)	ε_t (%)	Mechanical behavior	Notes
50	0	0.04	0.0	led	
100	0	0.08	-0.01	led	$[(d\varepsilon_v/d\sigma)_{led} = 7.08\times10^{-3}$ kb$^{-1}]$
150	0	0.12	-0.01	led	
200	0	0.17	-0.01	led	
240 (?)	0	0.22	-0.03	led→mc	Transition stress level '*Ia*'.
245	0	0.24	-0.04	mc	Const. volume deformation.
247	0	0.26	-0.05	mc	Fracture stress level '*F*'.

$\Delta\sigma$ - Stress difference.
σ_3 - Confining stress.
ε_a - Axial strain.
ε_t - Transverse strain.
ε_v - Volume strain.

Mechanical behavior categories:
c - Closure of pre-existing cracks.
led - Linear elastic deformation.
mc - Microcracking.

Perlite 7s

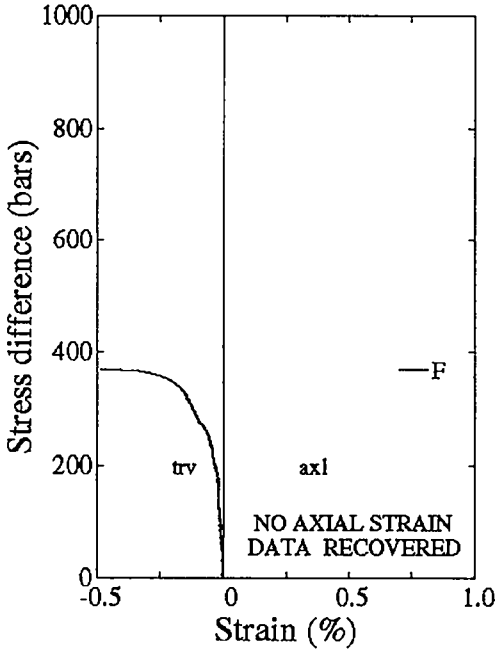

Fig. A7s-1. Mechanical response of specimen to uniaxial compression. Fracture stress '*F*' is defined in Table A7s-1. Axial and transverse strains are identified as 'axl' and 'trv', respectively.

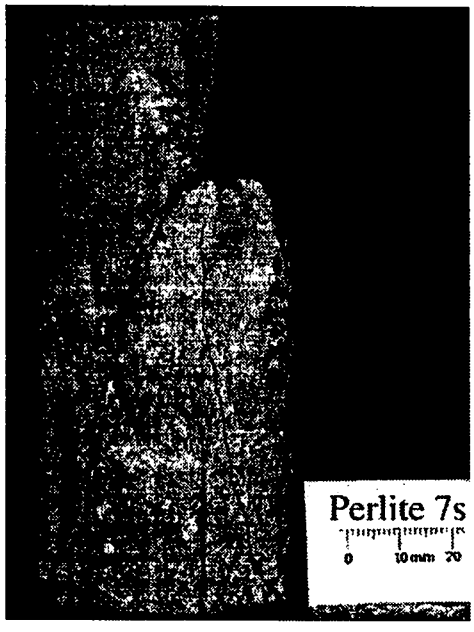

Fig. A7s-2. Post-test photograph of specimen.

Table A7s-1. Summary of physical and mechanical properties.

Specimen type	Perlite
Density, bulk (geometric determination)	1.79 g/cm^3
Density, grain	not determined
Moisture (ASTM D2216)	0.87%
Elastic constants:	
Young's modulus	not determined
Poisson's ratio	not determined
Mechanical behavior stress levels:	
Closure of pre-existing cracks	not determined
Linear elastic deformation	not determined
Microcracking	not determined
Fracture strength ('*F*')	369 bars
Fracture angle (shear)	78°

Perlite 7s

Specimen Source. Specimen **Perlite 7s** was cored from bulk material retrieved from Grefco's perlite mine operations located off US Highway 60, 3 miles south of Socorro, Socorro County, New Mexico. The quarry is located at coordinates 34°01'32" north latitude and 106°56'14" west longitude. The sample was recovered from the quarry floor in the vicinity of the geophysical array for small - scale explosive experiments. The bulk material was retrieved April, 1993 and not protected from moisture loss. The specimen was tested June, 1993 as a laboratory dry specimen.

Table A7s-2. Test conditions.

Operating procedure	ASTM D3148
Specimen preparation	ASTM D4543
Specimen geometry:	
Shape	cylindrical
Diameter	2.11 inches
Length to diameter ratio	2.15
Specimen orientation (angle between flow banding and plane normal to cylindrical axis)	90° $[\sigma_{1\|\|}]$
Strain rate; average; estimated	3.6×10^{-6} sec^{-1}

Specimen Description. The test specimen is perlite, a volcanic rock, gray in color with a distinctive "flow banding" structure. The perlite, consisting of highly porous volcanic glass, contains less than 5 volume percent crystals and crystal clusters of feldspar and quartz (?) that are ≤4 mm diameter. Pores of the glassy matrix are submillimeter in size, and have elongate, flat outlines parallel to the banding structure of the rock. The test specimen was cored such that banding is parallel to the cylindrical axis of the specimen. Narrow, submillimeter wide, open fractures to a length of 0.5 cm are observed on the test specimen surface but are not abundant. The fractures form discontinuous linear features oriented at a high angle to the flow banding. No displacement is observed across these fractures. They are interpreted as unhealed segments of fractures that originally passed through the specimen.

Characteristics of the Failed Specimen. The failed specimen has both shear and tensile fractures. Geometric relationships between fractures suggests that shear failure preceded tensile splitting and was responsible for specimen failure. Shear failure created a single steeply inclined fracture passing entirely through the specimen. The surface of this planar feature consists of wide step-like structures, which are controlled by the flow banding. The trace of this fracture forms an angle of 78° to a plane normal to the cylindrical axis. With cylindrical axis as vertical reference, the strike of the shear plane essentially coincides with the strike of banding. Tensile splitting formed an abundance of splintered and tabular pieces, which are concentrated along the periphery of the specimen in close proximity to the shear plane. These fractures are nearly vertical. Tensile fractures intersect the shear fracture but do not project into the facing wall. Fine glassy particles dust the largest fracture surfaces. There is no record, however, associating glassy particles with fracture type.

Limited Data Recovery. Technical difficulties with the axial extensometer were responsible for the lack of recoverable axial strain data.

Perlite 13s

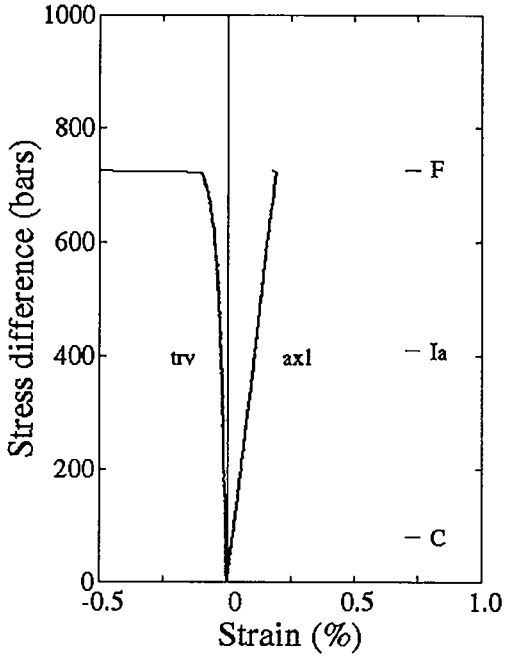

Fig. A13s-1. Mechanical response of specimen to uniaxial compression. Transition stress levels '*C*' and '*Ia*', and the fracture stress '*F*' are defined in Table A13s-3. Axial and transverse strains are identified as 'axl' and 'trv', respectively.

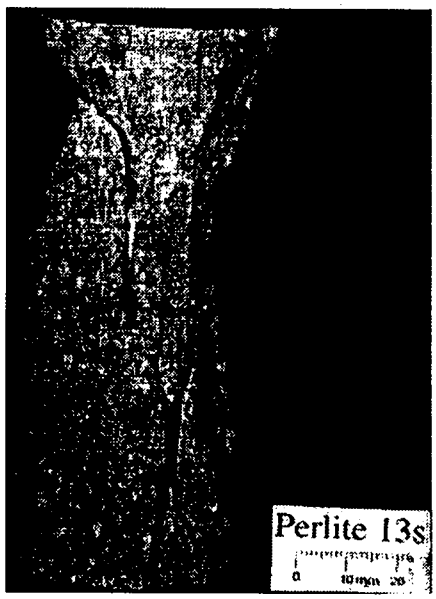

Fig. A13s2. Post-test photograph of specimen.

Table A13s-1. Summary of physical and mechanical properties.

Specimen type	Perlite
Density, bulk (geometric determination)	2.04 g/cm^3
Density, grain	not determined
Moisture (ASTM D2216)	0.57%
Elastic constants:	
Young's modulus	377.1 kbars
Poisson's ratio	0.232
Mechanical behavior stress levels:	
Closure of pre-existing cracks	0 - 80 bars
Linear elastic deformation	80 - 410 bars
Microcracking	410 - 726 bars
Fracture strength	726 bars
Fracture angle (shear)	75°

Perlite 13s

Specimen Source. Specimen **Perlite 13s** was cored from bulk material retrieved from Grefco's perlite mine operations located off US Highway 60, 3 miles south of Socorro, Socorro County, New Mexico. The quarry is located at coordinates 34°01'32" north latitude and 106°56'14" west longitude. The sample was recovered from the quarry floor in the vicinity of the geophysical array for small - scale explosive experiments. The bulk material was retrieved April, 1993 and not protected from moisture loss. The specimen was tested June, 1994 as a laboratory dry specimen.

Table A13s-2. Test conditions.

Operating procedure	ASTM D3148
Specimen preparation	ASTM D4543
Specimen geometry:	
Shape	cylindrical
Diameter	2.08 inches
Length to diameter ratio	2.21
Specimen orientation (angle between flow banding and plane normal to cylindrical axis)	90° $[\sigma_1 \| \|]$
Strain rate; average	1.1×10^{-6} sec^{-1}

Specimen Description. The test specimen is perlite, a volcanic rock, gray in color with a distinctive "flow banding" structure. The perlite, consisting of highly porous volcanic glass, contains less than 5 volume percent crystals and crystal clusters of feldspar and quartz (?) that are ≤5 mm diameter. Pores of the glassy matrix are submillimeter in size, and have elongate, flat outlines parallel to the banding structure of the rock. Narrow, submillimeter wide, open fractures to a length of 0.4 cm are observed on the test specimen surface but are not abundant. The fractures form discontinuous linear features oriented at a high angle to the flow banding. No displacement is observed across these fractures. They are interpreted as unhealed segments of fractures that may originally have passed through the specimen. This test specimen and specimens **14s** and **15s** were extracted from the identical bulk rock. Each of these three specimens were cored such that banding is parallel to the cylindrical axis of the specimen. Specimens **13s** and **14s** were aligned with axes parallel to each other and perpendicular to specimen **15s**.

Characteristics of the Failed Specimen. The failed specimen has both shear and tensile fractures. Geometric relationships between fractures suggests that shear failure preceded tensile splitting and was responsible for specimen failure. Shear failure created a single steeply inclined fracture passing entirely through the specimen. The fracture forms an undulating planar feature locally consisting of closely spaced, narrow step-like structures, which are controlled by the flow banding. The trace of this fracture forms an angle of 75° to a plane normal to the cylindrical axis. With cylindrical axis as vertical reference, the strike of the shear plane essentially coincides with the strike of banding. Tensile splitting formed an abundance of splintered pieces, which are concentrated along the periphery of the specimen in close proximity to the shear plane. Tensile splitting was also effective at splintering one side of the specimen where the plane of banding is tangent to the circular outline of the specimen. Fracture surfaces resulting from tensile splitting are nearly vertical. Tensile splitting parallel to banding created narrow step-like structures. Tensile fractures intersect the shear fracture but do not project into the facing wall.

Perlite 13s

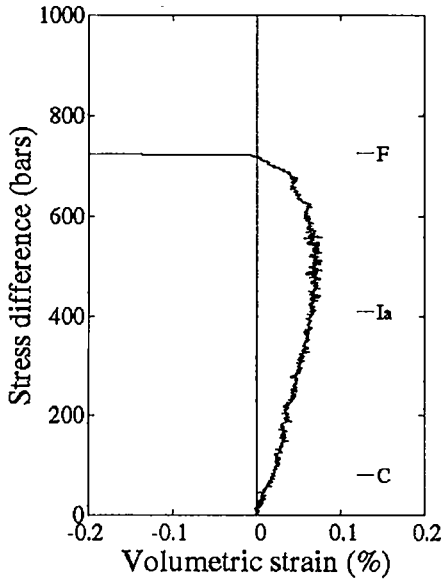

Fig. A13s-3. Volumetric strain resulting from uniaxial compression.

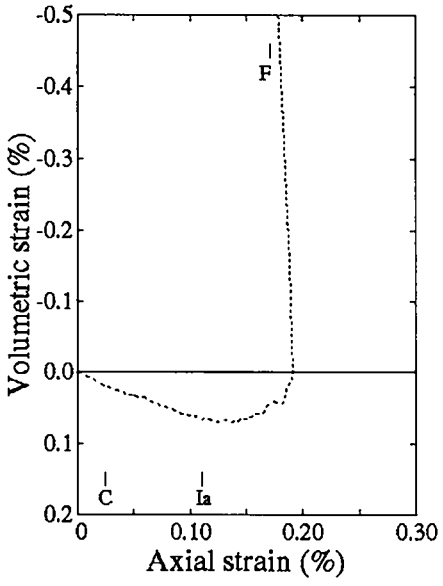

Fig. A13s-4. Relationship between volumetric and axial strain measurements.

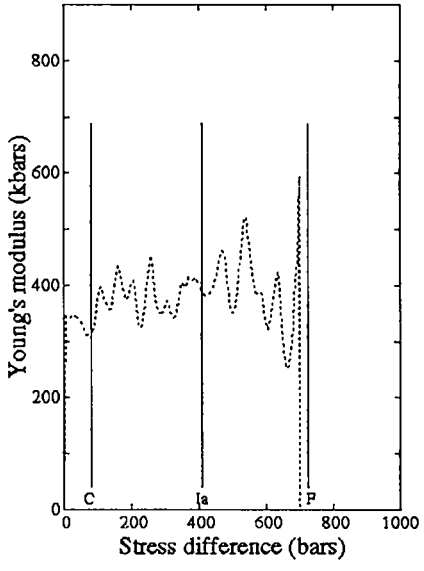

Fig. A13s-5. Young's modulus or, as appropriate, the parameter ($\Delta\sigma_{axl}$ / $\Delta\varepsilon_{axl}$) as a function of stress difference.

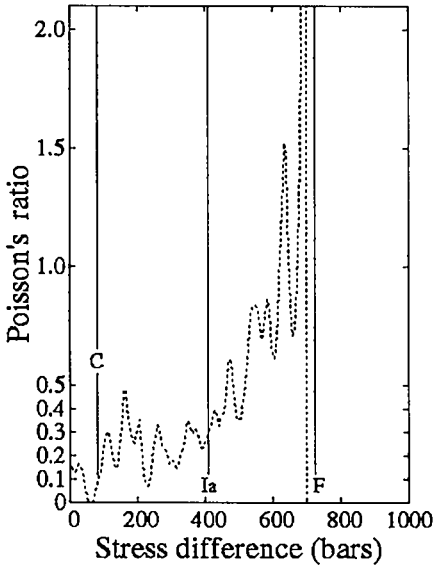

Fig. A13s-6. Poisson's ratio or, as appropriate, the parameter ($-\Delta\varepsilon_{trv}$ / $\Delta\varepsilon_{axl}$) as a function of stress difference.

Note: Transition stress levels '*C*', and '*Ia*', and the fracture stress '*F*' are defined in Table A13s-3. Axial and transverse strains are identified as 'axl' and 'trv', respectively.

Perlite 13s

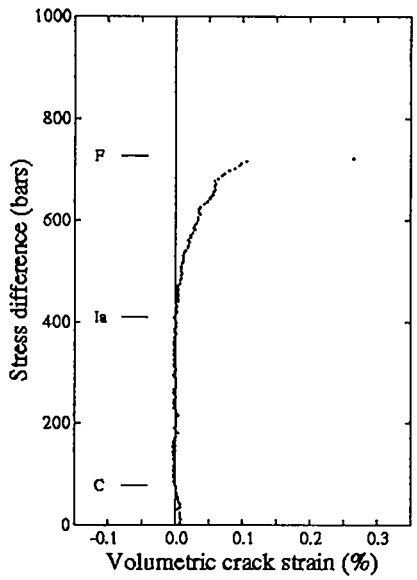

Fig. A13s-7. Volumetric crack strain or "crack porosity" as a function of stress difference in uniaxial compression. Transition stress levels '*C*', and '*Ia*', and the fracture stress '*F*' are defined in Table A13s-3.

Table A13s-3. Mechanical response of **Perlite 13s** at selected values of stress difference.

$\Delta\sigma$ (bars)	σ_3 (bars)	ε_a (%)	ε_t (%)	Mechanical behavior	Notes
50	0	0.01	0.0	c	
80	0	0.02	0.0	c→led	Transition stress level '*C*'.
100	0	0.03	0.0	led	
150	0	0.04	-0.01	led	
200	0	0.06	-0.01	led	
250	0	0.07	-0.01	led	$[(d\varepsilon_v/d\sigma)_{led} = 1.42\times10^{-3}$ kb$^{-1}]$
300	0	0.08	-0.02	led	
350	0	0.10	-0.02	led	
400	0	0.11	-0.02	led	
410	0	0.11	-0.02	led→mc	Transition stress level '*Ia*'.
450	0	0.12	-0.03	mc	
495	0	0.13	-0.03	mc	Const. volume deformation.
500	0	0.13	-0.03	mc	
550	0	0.14	-0.04	mc	
600	0	0.16	-0.05	mc	
650	0	0.17	-0.06	mc	
700	0	0.19	-0.08	mc	
726	0	0.17	-0.57	mc	Fracture stress level '*F*'.

$\Delta\sigma$ - Stress difference. σ_3 - Confining stress.
ε_a - Axial strain. ε_t - Transverse strain.
ε_v - Volume strain.

Mechanical behavior categories:
c - Closure of pre-existing cracks.
led - Linear elastic deformation.
mc - Microcracking.

Perlite 14s

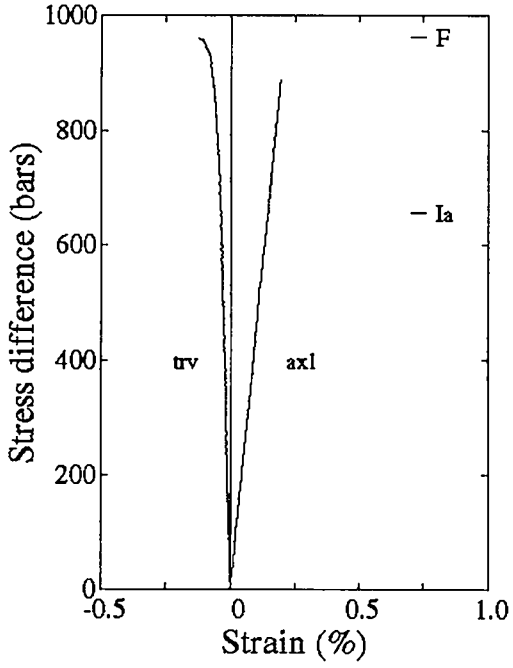

Fig. A14s-1. Mechanical response of specimen to uniaxial compression. Transition stress level '*Ia*', and the fracture stress '*F*' are defined in Table A14s-3. Axial and transverse strains are identified as 'axl' and 'trv', respectively.

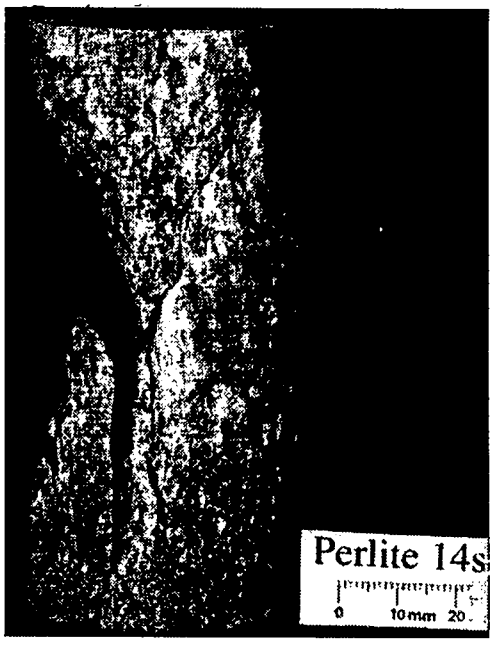

Fig. A14s-2. Post-test photograph of specimen.

Table A14s-1. Summary of physical and mechanical properties.

Specimen type	Perlite
Density, bulk (geometric determination)	2.05 g/cm^3
Density, grain	not determined
Moisture (ASTM D2216)	0.53%
Elastic constants:	
Young's modulus	459.2 kbars
Poisson's ratio	0.257
Mechanical behavior stress levels:	
Linear elastic deformation	0 - 655 bars
Microcracking	655 - 963 bars
Fracture strength	963 bars
Fracture angle (shear)	69°

Perlite 14s

Specimen Source. Specimen **Perlite 14s** was cored from bulk material retrieved from Grefco's perlite mine operations located off US Highway 60, 3 miles south of Socorro, Socorro County, New Mexico. The quarry is located at coordinates 34°01'32" north latitude and 106°56'14" west longitude. The sample was recovered from the quarry floor in the vicinity of the geophysical array for small - scale explosive experiments. The bulk material was retrieved April, 1993 and not protected from moisture loss. The specimen was tested June, 1994 as a laboratory dry specimen.

Table A14s-2. Test conditions.

Operating procedure	ASTM D3148
Specimen preparation	ASTM D4543
Specimen geometry:	
Shape	cylindrical
Diameter	2.05 inches
Length to diameter ratio	2.08
Specimen orientation (angle between flow banding and plane normal to cylindrical axis)	90° $[\sigma_1 \| \|]$
Strain rate; average	3.0×10^{-6} sec^{-1}

Specimen Description. The test specimen is perlite, a volcanic rock, gray in color with a distinctive "flow banding" structure. The perlite, consisting of highly porous volcanic glass, contains less than 5 volume percent crystals and crystal clusters of feldspar and quartz (?) that are ≤5 mm diameter. Pores of the glassy matrix are submillimeter in size, and have elongate, flat outlines parallel to the banding structure of the rock. This test specimen and specimens **13s** and **15s** were extracted from the identical bulk rock. Each of these three specimens was cored such that banding is parallel to the cylindrical axis of the specimen. Specimens **13s** and **14s** were aligned with axes parallel to each other and perpendicular to specimen **15s.**

Characteristics of the Failed Specimen. The failed specimen has both shear and tensile fractures. Geometric relationships between fractures suggests that shear failure preceded tensile splitting and was responsible for specimen failure. Shear failure created a single steeply inclined fracture passing entirely through the specimen. The fracture forms a broad undulating planar feature locally consisting of narrow step-like structures, which are controlled by the flow banding. The fracture forms an angle averaging 69° to a plane normal to the cylindrical axis. With cylindrical axis as vertical reference, the strike of the shear plane is rotated 40° to 45° from the strike of banding. Failure by tensile splitting formed an abundance of splintered pieces, which are concentrated along the periphery of the specimen in close proximity to the shear plane. Fracture surfaces resulting from tensile splitting are nearly vertical. Tensile splitting parallel to banding created narrow step-like structures.

Perlite 14s

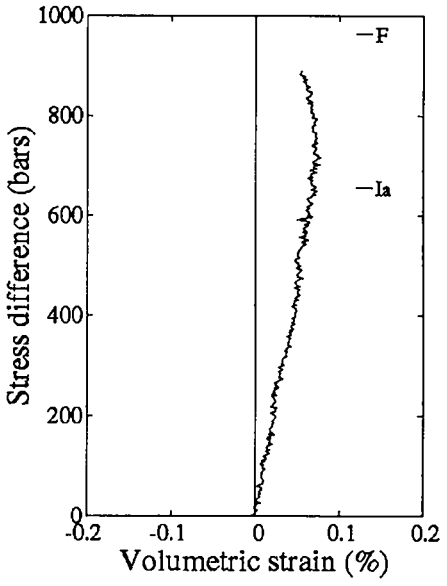

Fig. A14s-3. Volumetric strain resulting from uniaxial compression.

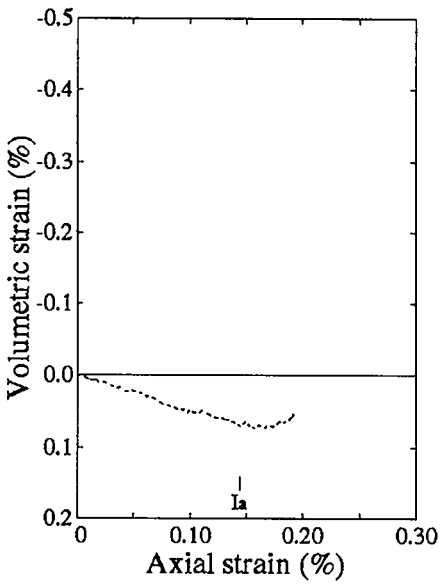

Fig. A14s-4. Relationship between volumetric and axial strain measurements.

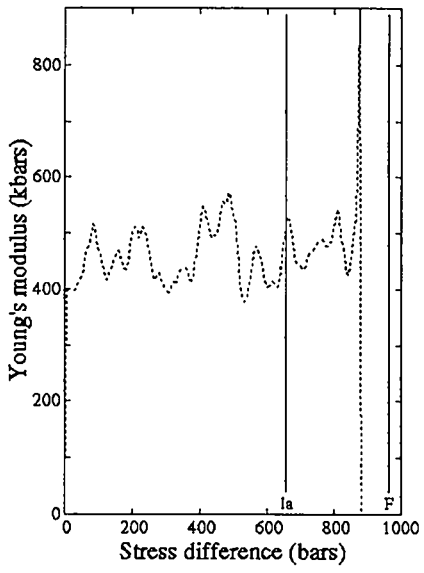

Fig. A14s-5. Young's modulus or, as appropriate, the parameter ($\Delta\sigma_{axl} / \Delta\varepsilon_{axl}$) as a function of stress difference.

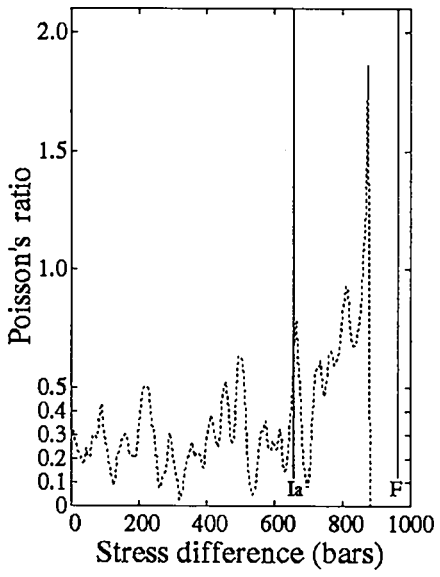

Fig. A14s-6. Poisson's ratio or, as appropriate, the parameter ($-\Delta\varepsilon_{trv} / \Delta\varepsilon_{axl}$) as a function of stress difference.

Note: Transition stress level '*Ia*', and the fracture stress '*F*' are defined in Table A14s-3. Axial and transverse strains are identified as 'axl' and 'trv', respectively.

Perlite 14s

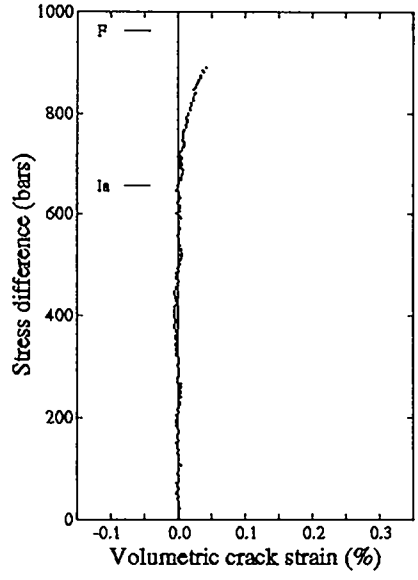

Fig. A14s-7. Volumetric crack strain or "crack porosity" as a function of stress difference in uniaxial compression. Transition stress level '*Ia*', and the fracture stress '*F*' are defined in Table A14s-3.

Table A14s-3. Mechanical response of **Perlite 14s** at selected values of stress difference.

$\Delta\sigma$ (bars)	σ_3 (bars)	ε_a (%)	ε_t (%)	Mechanical behavior	Notes
50	0	0.01	0.0	led	
100	0	0.02	-0.01	led	
150	0	0.03	-0.01	led	
200	0	0.04	-0.01	led	
250	0	0.05	-0.02	led	$[(d\varepsilon_v/d\sigma)_{Ia} = 1.06\times10^{-3}$ kb$^{-1}]$
300	0	0.07	-0.02	led	
350	0	0.08	-0.02	led	
400	0	0.09	-0.02	led	
450	0	0.10	-0.03	led	
500	0	0.11	-0.03	led	
550	0	0.12	-0.03	led	
600	0	0.13	-0.03	led	
650	0	0.14	-0.04	led	
655	0	0.14	-0.04	led→mc	Transition stress level '*Ia*'.
700	0	0.15	-0.04	mc	
735	0	0.16	-0.05	mc	Const. volume deformation.
750	0	0.17	-0.05	mc	
800	0	0.18	-0.05	mc	
850	0	0.19	-0.06	mc	
900	0	n/d	-0.07	mc	
950	0	n/d	-0.10	mc	
963	0	n/d	-0.13	mc	Fracture stress level '*F*'.

$\Delta\sigma$ - Stress difference. σ_3 - Confining stress.
ε_a - Axial strain. ε_t - Transverse strain.
ε_v - Volume strain. n/d - not determined

Mechanical behavior categories:
c - Closure of pre-existing cracks.
led - Linear elastic deformation.
mc - Microcracking.

Perlite 15s

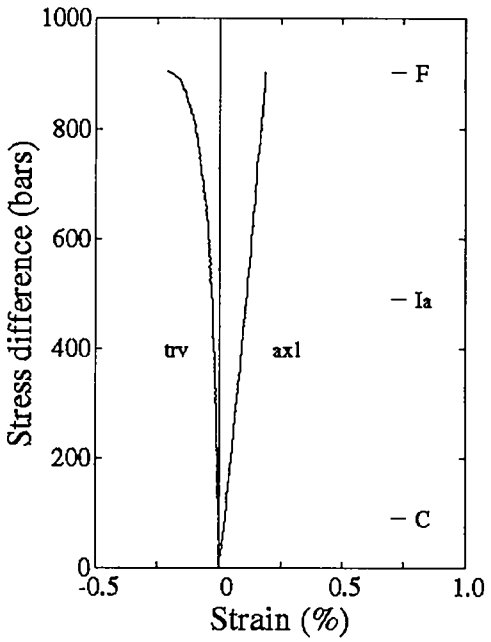

Fig. A15s-1. Mechanical response of specimen to uniaxial compression. Transition stress levels '*C*' and '*Ia*', and the fracture stress '*F*' are defined in Table A15s-3. Axial and transverse strains are identified as 'axl' and 'trv', respectively.

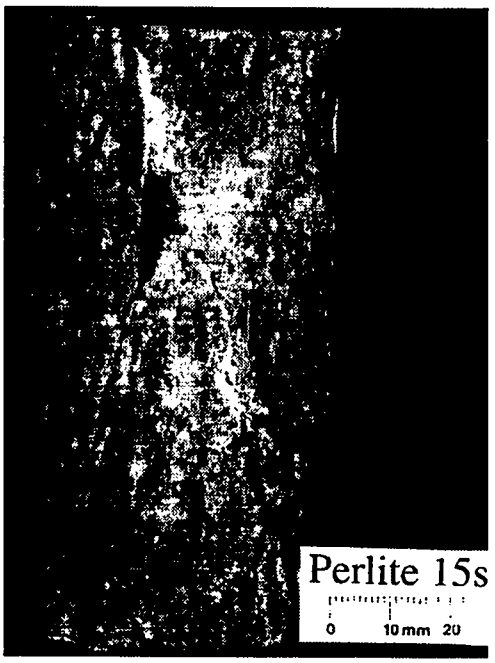

Fig. A15s-2. Post-test photograph of specimen.

Table A15s-1. Summary of physical and mechanical properties.

Specimen type	Perlite
Density, bulk (geometric determination)	2.04 g/cm^3
Density, grain	not determined
Moisture (ASTM D2216)	0.44%
Elastic constants:	
Young's modulus	465.1 kbars
Poisson's ratio	0.296
Mechanical behavior stress levels:	
Closure of pre-existing cracks	0 - 90 bars
Linear elastic deformation	90 - 490 bars
Microcracking	490 - 904 bars
Fracture strength	904 bars
Fracture angles (shear)	76°, 78°

Perlite 15s

Specimen Source. Specimen **Perlite 15s** was cored from bulk material retrieved from Grefco's perlite mine operations located off US Highway 60, 3 miles south of Socorro, Socorro County, New Mexico. The quarry is located at coordinates 34°01'32" north latitude and 106°56'14" west longitude. The sample was recovered from the quarry floor in the vicinity of the geophysical array for small - scale explosive experiments. Bulk material was retrieved April, 1993 and not protected from moisture loss. The specimen was tested June, 1994 as a laboratory dry specimen.

Table A15s-2. Test conditions.

Operating procedure	ASTM D3148
Specimen preparation	ASTM D4543
Specimen geometry:	
Shape	cylindrical
Diameter	2.07 inches
Length to diameter ratio	2.01
Specimen orientation (angle between flow banding and plane normal to cylindrical axis)	90° $[\sigma_1 \| \|]$
Strain rate; average	2.2×10^{-6} sec^{-1}

Specimen Description. The test specimen is perlite, a volcanic rock, gray in color with a distinctive "flow banding" structure. The perlite, consisting of highly porous volcanic glass, contains less than 5 volume percent crystals and crystal clusters of feldspar and quartz (?) that are ≤5 mm diameter. Pores of the glassy matrix are submillimeter in size, and have elongate, flat outlines parallel to the banding structure of the rock. This test specimen and specimens **13s** and **14s** were extracted from the identical bulk rock. Each of these three specimens was cored such that banding is parallel to the cylindrical axis of the specimen. Specimens **13s** and **14s** were aligned with axes parallel to each other and perpendicular to specimen **15s**.

Characteristics of the Failed Specimen. The failed specimen has both shear and tensile fractures. Geometric relationships between fractures suggests that shear failure preceded tensile splitting and was responsible for specimen failure. Shear failure created two steeply inclined fractures. The fractures are inclined 76° and 78° from a plane normal to the cylindrical axis and outline a wedge-shaped piece of perlite at one end of the specimen. Fracture surfaces form broad undulating planar features locally consisting of closely spaced, narrow step-like structures, which are controlled by the flow banding. With cylindrical axis as vertical reference, the strike of the shear planes are rotated no more than 10° from the strike of banding. Failure by tensile splitting formed an abundance of splintered pieces, which are concentrated along the periphery of the specimen in close proximity to shear planes. Fracture surfaces resulting from tensile splitting are nearly vertical. Tensile splitting parallel to banding created narrow step-like structures.

Perlite 15s

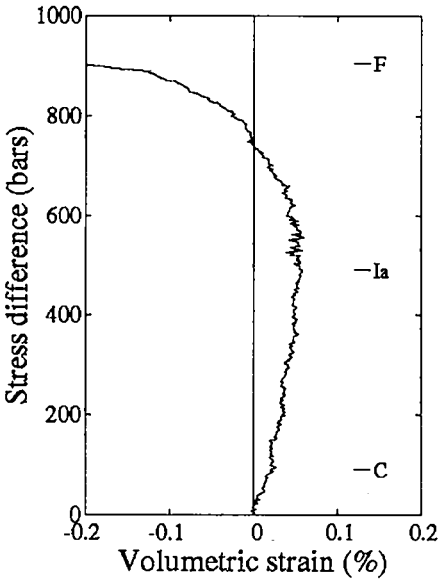

Fig. A15s-3. Volumetric strain resulting from uniaxial compression.

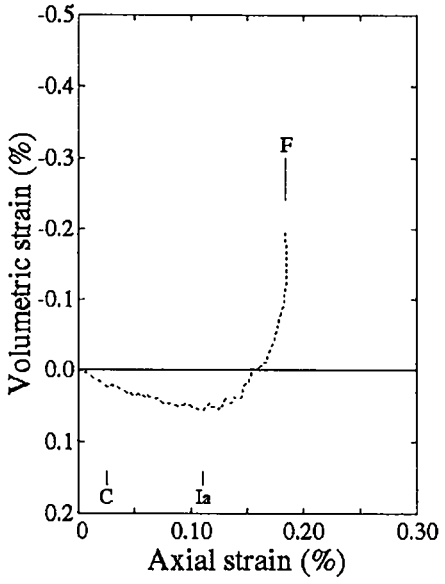

Fig. A15s-4. Relationship between volumetric and axial strain measurements.

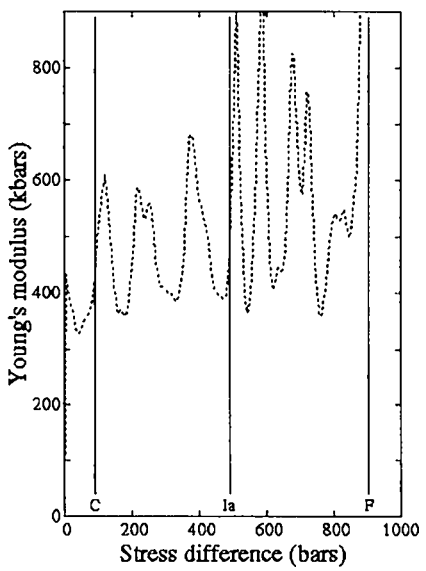

Fig. A15s-5. Young's modulus or, as appropriate, the parameter ($\Delta\sigma_{axl} / \Delta\varepsilon_{axl}$) as a function of stress difference.

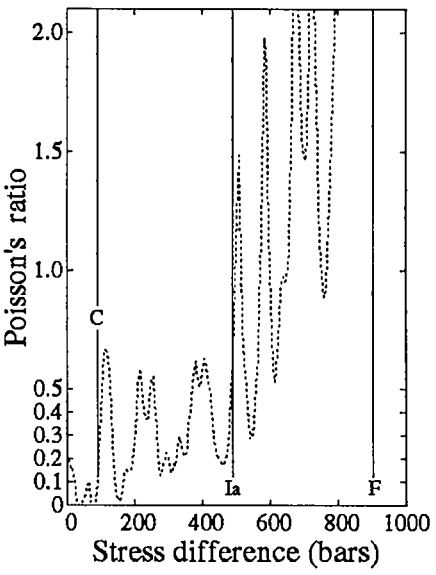

Fig. A15s-6. Poisson's ratio or, as appropriate, the parameter ($-\Delta\varepsilon_{trv} / \Delta\varepsilon_{axl}$) as a function of stress difference.

Note: Transition stress levels '*C*' and '*Ia*', and the fracture stress '*F*' are defined in Table A15s-3. Axial and transverse strains are identified as 'axl' and 'trv', respectively.

Perlite 15s

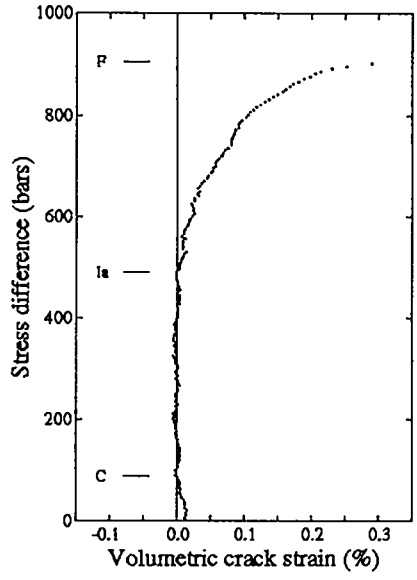

Fig. A15s-7. Volumetric crack strain or "crack porosity" as a function of stress difference in uniaxial compression. Transition stress levels '*C*', and '*Ia*', and the fracture stress '*F*' are defined in Table A15s-3.

Table A15s-3. Mechanical response of **Perlite 15s** at selected values of stress difference.

$\Delta\sigma$ (bars)	σ_3 (bars)	ε_a (%)	ε_t (%)	Mechanical behavior	Notes
50	0	0.01	0.0	c	
90	0	0.03	0.0	c→led	Transition stress level '*C*'.
100	0	0.03	0.0	led	
150	0	0.04	-0.01	led	
200	0	0.05	-0.01	led	
250	0	0.06	-0.01	led	$[(d\varepsilon_v/d\sigma)_{ini} = 0.88\times10^{-3}$ kb$^{-1}]$
300	0	0.07	-0.02	led	
350	0	0.08	-0.02	led	
400	0	0.09	-0.02	led	
450	0	0.10	-0.03	led	
490	0	0.11	-0.03	led→mc	Transition stress level '*Ia*'.
500	0	0.11	-0.03	mc	
510	0	0.11	-0.03	mc	Const. volume deformation.
550	0	0.12	-0.04	mc	
600	0	0.13	-0.04	mc	
650	0	0.14	-0.05	mc	
700	0	0.15	-0.07	mc	
750	0	0.16	-0.08	mc	
800	0	0.17	-0.10	mc	
850	0	0.18	-0.13	mc	
900	0	0.18	-0.19	mc	
904	0	0.18	-0.21	mc	Fracture stress level '*F*'.

$\Delta\sigma$ - Stress difference. σ_3 - Confining stress.
ε_a - Axial strain. ε_t - Transverse strain.
ε_v - Volume strain.

Mechanical behavior categories:
c - Closure of pre-existing cracks.
led - Linear elastic deformation.
mc - Microcracking.

Perlite 16s

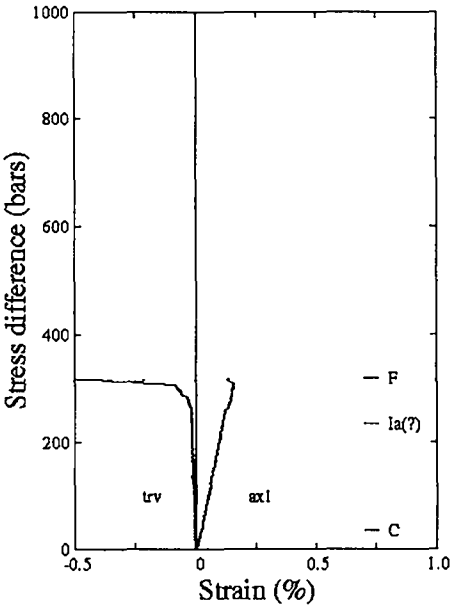

Fig. A16s-1. Mechanical response of specimen to uniaxial compression. Transition stress levels '*C*' and '*Ia*', and the fracture stress '*F*' are defined in Table A16s-3. Axial and transverse strains are identified as 'axl' and 'trv', respectively.

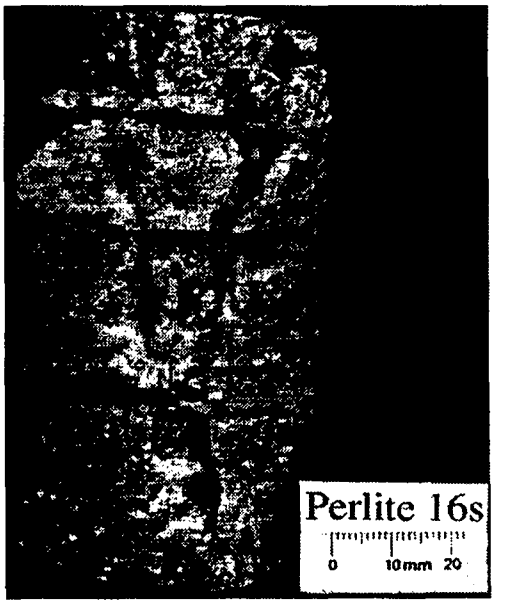

Fig. A16s-2. Post-test photograph of specimen.

Table A16s-1. Summary of physical and mechanical properties.

Specimen type	Perlite
Density, bulk (geometric determination)	2.08 g/cm^3
Density, grain	not determined
Moisture (ASTM D2216)	1.21%
Elastic constants:	
Young's modulus	224.0 kbars
Poisson's ratio	0.131
Mechanical behavior stress levels:	
Closure of pre-existing cracks	0 - 35 bars
Linear elastic deformation	35 - 235 (?) bars
Microcracking	235 (?) - 319 bars
Fracture strength	319 bars
Fracture angle (shear)	not applicable

Perlite 16s

Specimen Source. Specimen **Perlite 16s** was cored from bulk material retrieved from Grefco's perlite mine operations located off US Highway 60, 3 miles south of Socorro, Socorro County, New Mexico. The quarry is located at coordinates 34°01'32" north latitude and 106°56'14" west longitude. The sample was recovered from a portion of the quarry north-northwest of the geophysical array for small - scale explosive experiments. Bulk material was collected from this site because it was known to respond much differently to quarry ripping operations than perlite at the geophysical array. Collected material was previously subjected to a chemical delayed ripple-fire explosion. The bulk material was retrieved June, 1993 and not protected from moisture loss. The specimen was tested June, 1994 as a laboratory dry specimen.

Table A16s-2. Test conditions.

Operating procedure	ASTM D3148
Specimen preparation	ASTM D4543
Specimen geometry:	
Shape	cylindrical
Diameter	2.07 inches
Length to diameter ratio	1.93‡
[‡ not in strict agreement with ASTM D4543.]	
Specimen orientation (angle between flow banding and plane normal to cylindrical axis)	0° $[\sigma_{1\perp}]$
Strain rate; average	4.4×10^{-6} sec^{-1}

Specimen Description. The test specimen is perlite, a volcanic rock, gray in color with a distinctive "flow banding" structure. The perlite, consisting primarily of volcanic glass, contains less than 5 volume percent crystals and crystal clusters of feldspar and quartz (?) that are ≤4 mm diameter. Unlike perlite collected in the vicinity of the geophysical array for intermediate scale source experiments, **Perlite 16s** has a dense glass matrix. Microscopic examination reveals impure, smoky-colored glass, which may or may not contain visible minute pores. The glass is interlayered with glass consisting of a fine granular texture. Glass with granular texture also appears as elliptical features embedded in dense glass. A bulk density of 2.08 g/cm^3 for this specimen (Table A16s-1), although relatively high compared to other perlite specimens, is not significantly different than **Perlite 13s, 14s** and **15s.** Compared to the descriptive nature of the glass matrix, the bulk density should expectedly be greater. The low measured value for bulk density is due to the specimen's numerous partially open fractures. Exposed fracture traces have lengths measuring to 4.4 cm. Most fractures are steeply inclined to the flow banding, however, fractures parallel to banding are also present. No displacement is observed across fractures.

Characteristics of the Failed Specimen. The failed specimen is dominated with fractures created by tensile splitting, which appears to be responsible for failure. Little evidence exists for a shear failure surface other than a segment that was controlled by a preexisting fracture. The specimen was fractured such that one-half the circular cross-section was rubbled and the other half remained intact. Fracture surfaces resulting from tensile splitting are nearly vertical, creating long splinters or tabular pieces of rock. Fracture surfaces are uneven to blocky owing to the flow banding structure and to the subconchoidal fracture of dense glass.

Perlite 16s

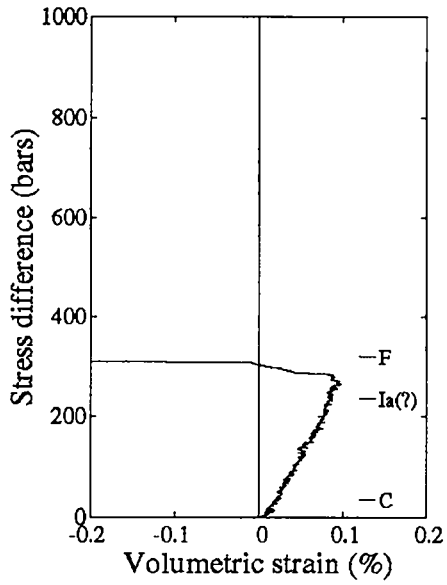

Fig. A16s-3. Volumetric strain resulting from uniaxial compression.

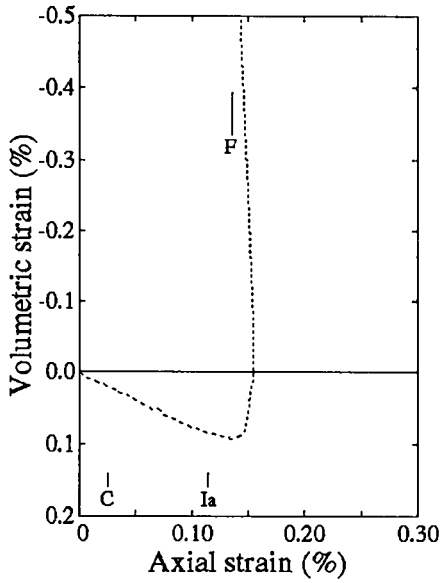

Fig. A16s-4. Relationship between volumetric and axial strain measurements.

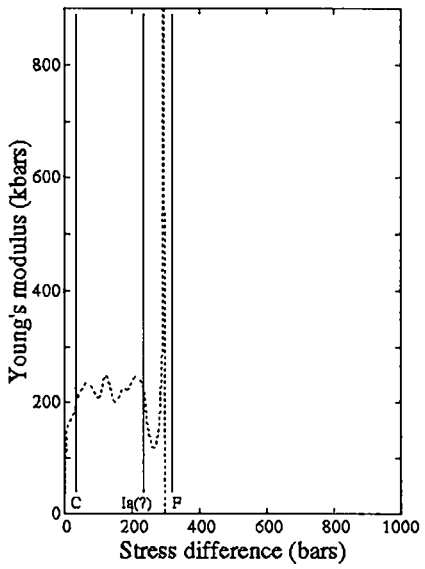

Fig. A16s-5. Young's modulus or, as appropriate, the parameter ($\Delta\sigma_{axl} / \Delta\varepsilon_{axl}$) as a function of stress difference.

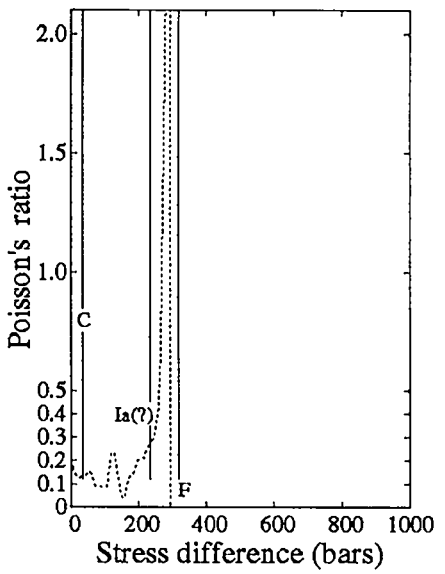

Fig. A16s-6. Poisson's ratio or, as appropriate, the parameter ($-\Delta\varepsilon_{trv} / \Delta\varepsilon_{axl}$) as a function of stress difference.

Note: Transition stress levels '*C*', and '*Ia*', and the fracture stress '*F*' are defined in Table A16s-3. Axial and transverse strains are identified as 'axl' and 'trv', respectively.

Perlite 16s

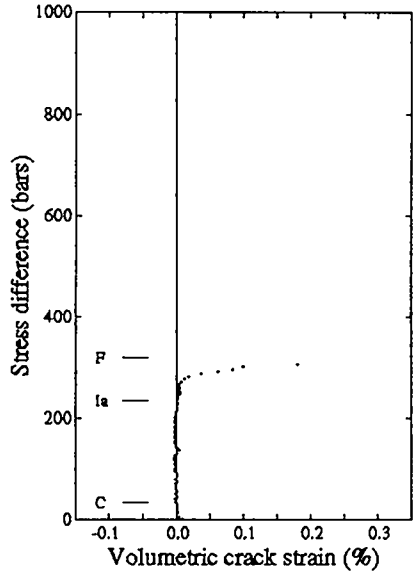

Fig. A16s-7. Volumetric crack strain or "crack porosity" as a function of stress difference in uniaxial compression. Transition stress levels '*C*', and '*Ia*', and the fracture stress '*F*' are defined in Table A16s-3.

Table A16s-3. Mechanical response of **Perlite 16s** at selected values of stress difference.

$\Delta\sigma$ (bars)	σ_3 (bars)	ε_a (%)	ε_t (%)	Mechanical behavior	Notes
35	0	0.03	0.0	c→led	Transition stress level '*C*'.
50	0	0.03	0.0	led	
100	0	0.05	-0.01	led	
150	0	0.08	-0.01	led	$[(d\varepsilon_v/d\sigma)_{kd} = 3.30\times10^{-3}$ kb$^{-1}]$
200	0	0.10	-0.01	led	
235 (?)	0	0.11	-0.01	led→mc	Transition stress level '*Ia*'.
250	0	0.12	-0.02	mc	
265	0	0.14	-0.02	mc	Const. volume deformation.
300	0	0.16	-0.07	mc	
319	0	0.14	-0.59	mc	Fracture stress level '*F*'.

$\Delta\sigma$ - Stress difference.
σ_3 - Confining stress.
ε_a - Axial strain.
ε_t - Transverse strain.
ε_v - Volume strain.

Mechanical behavior categories:
c - Closure of pre-existing cracks.
led - Linear elastic deformation.
mc - Microcracking.

Appendix B. Memoranda Containing Perlite Properties

This section contains three memoranda referenced in the introduction as containing mechanical and physical properties for Dicaperl mine (Socorro) and No Agua mine (Tres Piedras) perlite. The hydrostatic data for No Agua mine perlite and the wave velocity data collected with uncalibrated equipment are not presented or discussed in the main body of this report.

Los Alamos
NATIONAL LABORATORY

memorandum

Geophysics Group
EES - 3

To/MS: James R. Kamm / F659
From/MS: Harry N. Plannerer / C335
Phone/FAX: 7-4895 / 7-4739
Symbol: EES3-93-208
Date: 19. May 1993

SUBJECT: PERLITE MECHANICAL PROPERTIES

While you await the results for mechanical tests on perlite from Grefco's Socorro Mine, I am supplying you with results from earlier tests conducted on perlite that was obtained from Grefco's No Agua Mine located 5 miles north of Tres Piedras, NM. The results are from two mechanical tests, one unconfined compressive strength test and one triaxial test. No moisture content, or bulk and grain density data exist for the test specimens. The mechanical response of perlite as derived form these tests may be a better representation of the Socorro perlite than the previously modeled Merlin alluvium.

Included in the data set are stress - strain responses for hydrostatic loading to 500 bars and for each of the two compression tests; tables listing the elastic properties of the perlite as derived from the stress - strain responses; and, a tentative Mohr diagram differentiating stable and unstable stress fields for the perlite assuming quasi-static conditions.

Please contact me should you need further information on test conditions, the results or the derivation of the elastic parameters.

Att.: a/s

Cy: F. N. App, EES-3, MS F659
W. M. Brunish, EES-3, MS F659
T. N. Dey, P-15, MS D406
C. L. Edwards, EES-3, MS C335
S. R. Taylor, EES-3, MS C335
T. A. Weaver, EES-3, MS C335
EES-3 Files, MS C335
EES3-qsRM Files, MS C335

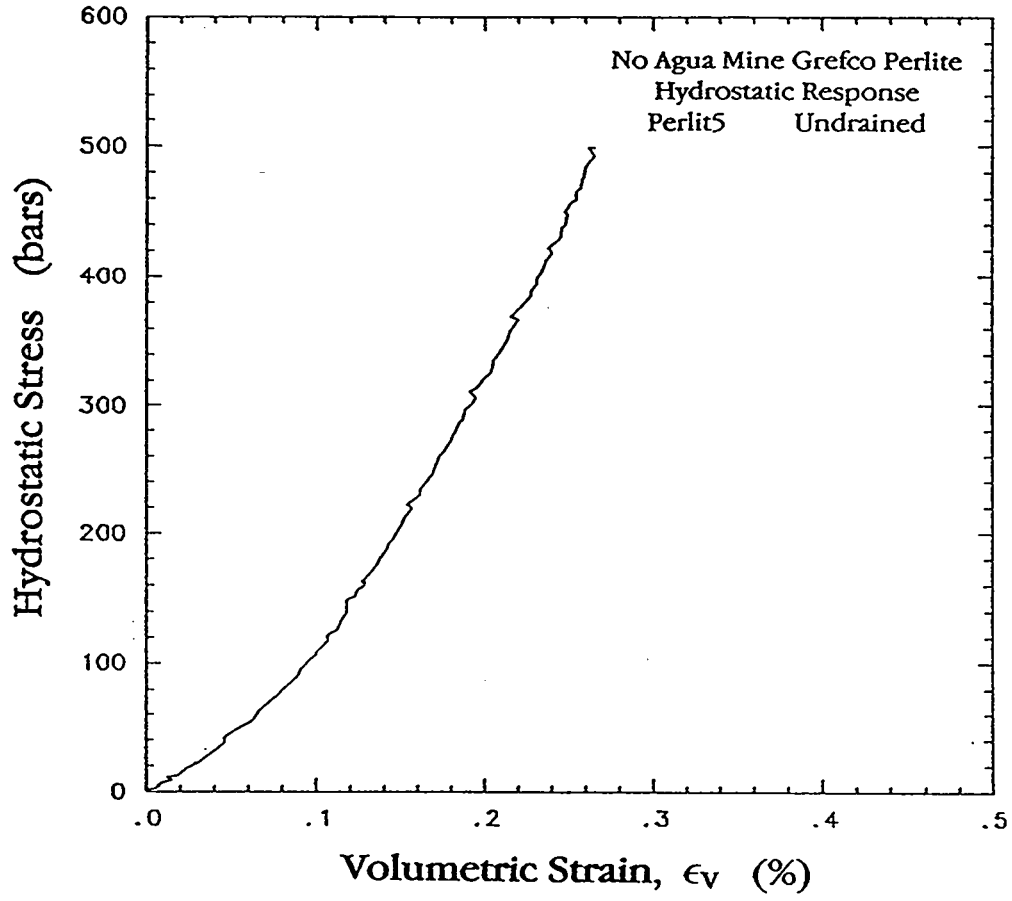

Fig. 1. Hydrostatic response of No Agua Mine perlite on loading to 500 bars stress. Curvature of the response to about 200 bars suggests closure of 0.06% crack porosity (ϵ_V) due to the loading. The more linear response above 200 bars is taken to represent the "elastic" region from which the bulk modulus, $K_{\phi 1}$, has been derived. Hydrostatic loading appears not to have been sufficient to initiate pore reduction in the specimen and, therefore, the yield point and the bulk modulus for the "pore reduction" region are not known.

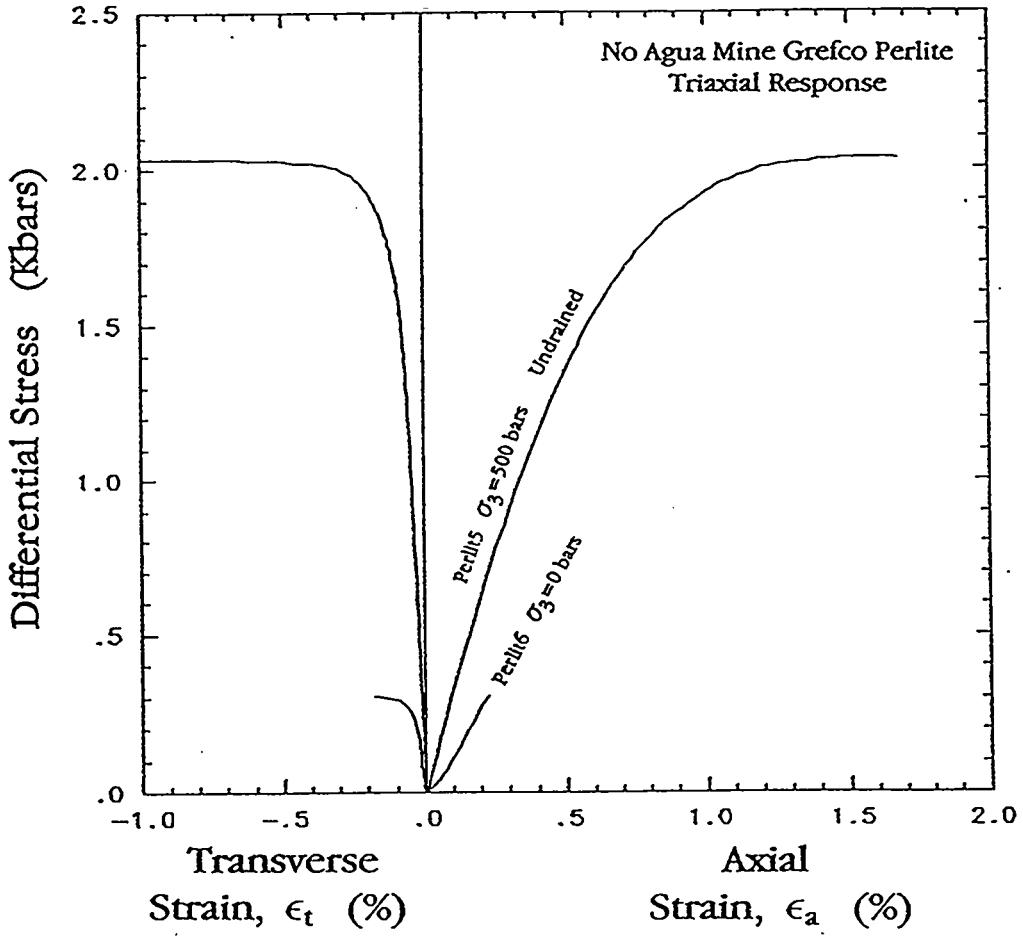

Fig. 2. Response of No Agua Mine perlite to triaxial compression.

Table 1. Bulk Modulus (Incompressibility) for No Agua Mine Grefco Perlite

Specimen	$K_{\phi 1}$ (kbars)	Yield Point (kbars)	$K_{\phi 2}$ (kbars)
Perlit5	196.9	n/d	n/d

$K_{\phi 1}$ - Bulk modulus for the "elastic" region.

$K_{\phi 2}$ - Bulk modulus for the "pore reduction" region.

n/d - not determined.

Table 2. Elastic Properties and Compression Test Parameters for No Agua Mine Grefco Perlite

Specimen	$\Delta\sigma$ (kbars)	σ_3 (kbars)	E (kbars)	ν	Moisture (% tot mass)
Perlit6	0.305	0.0	159.1	0.21	n/d
Perlit5	2.035	0.50	312.5	0.13	n/d

$\Delta\sigma$ - maximum differential stress.

σ_3 - confining stress.

E - Young's modulus.

ν - Poisson's ratio.

n/d - not determined.

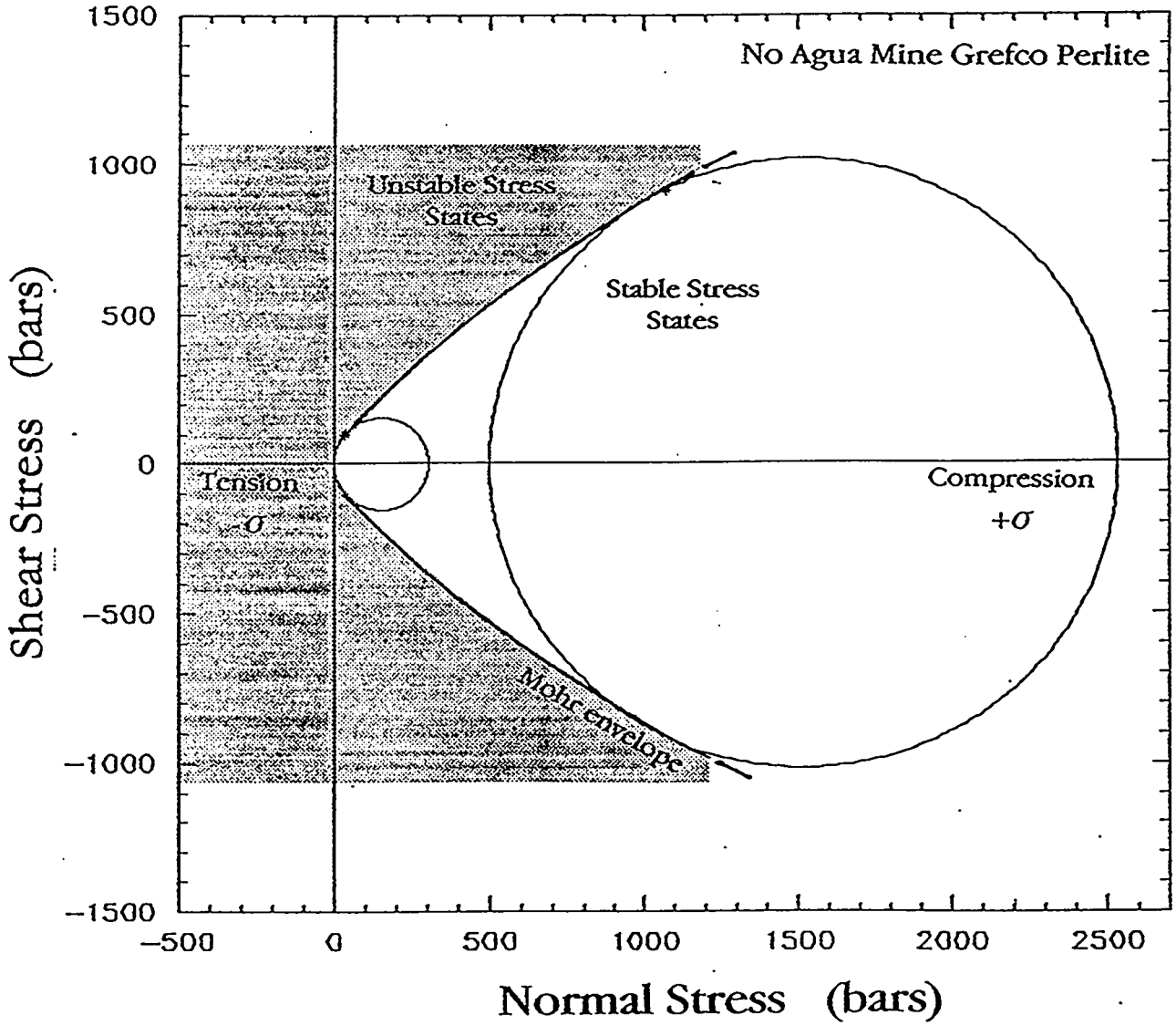

Fig. 3. Mohr stress diagram for Grefco's No Agua Mine Perlite assuming quasi-static conditions. The diagram is constructed based on results from only two mechanical tests and should be considered as tentative.

Los Alamos
NATIONAL LABORATORY

memorandum

Geophysics Group
EES - 3

To/MS: C. L. Edwards / C335
From/MS: Harry N. Plannerer / C335
Phone/FAX: 7-4895 / 7-4739
Symbol: EES3-93-261
Date: 25. June 1993

SUBJECT: PERLITE MECHANICAL PROPERTIES

Attached is a data compilation of physical properties for Grefco's Socorro Mine perlite and the mechanical response of the perlite to uniaxial compression. It is a compilation of available data for the three individual perlite blocks that were supplied to the laboratory in April.

Table 1 of the attachment is a listing of perlite physical properties. Moisture for both crushed and bulk specimens, and the dry bulk and grain densities are measured properties. The total porosity value is a calculated value. The values reported in Table 1 are "as received" perlite. Moisture determinations in Table 2 are the post-test moisture contents for air dried specimens after a preparation process that involved the use of water.

Results for uniaxial compression tests (Table 2) are segregated as to orientation of the maximum principal stress to the characteristic flow banding structure of the perlite. These tests were conducted with the maximum principal stress either perpendicular to the flow banding ($\sigma_{1\perp}$) or in the plane of flow banding ($\sigma_{1\parallel}$). Table 2 shows that the perlite is anisotropic in its mechanical response, having greater strength and larger values for Young's modulus and Poisson's ratio in the orientation ($\sigma_{1\parallel}$) than for ($\sigma_{1\perp}$). The table also shows that an unconfined compressive strength of 264 bars in the ($\sigma_{1\perp}$) orientation is reproducible within a standard deviation of approximately 18 bars. On the other hand, the unconfined compressive strength in the ($\sigma_{1\parallel}$) orientation varies by a magnitude of 240+ bars from 311 bars to 554 bars. From the current suite of specimens, it cannot be ascertained whether this broad spread in ($\sigma_{1\parallel}$) strength values corresponds to spatial inhomogeneities in the rock fabric or to preferred regional orientations.

Please feel free to contact me should you require additional test details. The data shall be presented to you in a final report at a later date.

Att.: a/s

C. L. Edwards 25. June 1993

EES3-93-261. Perlite Mechanical Properties

Cy: F. N. App, EES-3, MS F659
W. M. Brunish, EES-3, MS F659
T. N. Dey, P-15, MS D406
J. R. Kamm, EES-3, MS F659
D. M. Romero, EES-3, MS C335
S. R. Taylor, EES-3, MS C335
T. A. Weaver, EES-3, MS C335
EES-3 Files, MS C335
EES3-qsRM Files, MS C335

Table 1. Physical Property Determinations for the Socorro Mine Grefco Perlite.

Physical Property	Mean	Range	Comments
Moisture (ASTM D2216)	0.27%	0.23% - 0.29%	crushed spec.
Moisture (ASTM D2216)	0.25%	0.16% - 0.37%	bulk specimens
Dry Bulk Density (ASTM C20)	1.86 g/cm^3	1.83 - 1.93 g/cm^3	
Grain Density (He pycnometer)	2.350 g/cm^3	2.341 - 2.359 g/cm^3	
Total Porosity (Calc.)	20.9%		

Table 2. Elastic Properties and Compression Test Parameters for the Socorro Mine Grefco Perlite (ASTM D3148; D2216).

Specimen	$\Delta\sigma$ (kbars)	σ_3 (kbars)	E (kbars)	ν	Moisture (% tot mass)
σ_1 perpendicular to flow banding ($\sigma_{1\perp}$):					
Perlit1S	0.249	0.0	174.3	0.13	0.19
Perlit2S	0.280	0.0	171.3	0.18	0.16
Perlit4S	0.280	0.0	119.3	0.07	0.68
Perlit6S	0.247	0.0	123.3	0.08	TBD
σ_1 in the plane of the flow banding ($\sigma_{1\parallel}$):					
Perlit3S	0.311	0.0	246.9	0.32	0.20
Perlit5S	[0.470]	0.0	240.0	0.20	2.9
Perlit5S#2	0.554	0.0	280.4	0.29	2.9
Perlit7S	0.367	0.0	TBD	TBD	TBD

$\Delta\sigma$ - maximum differential stress. ν - Poisson's ratio.

σ_3 - confining stress. TBD - to be determined.

E - Young's modulus.

[ ] - maximum stress in a load/unload cycle without failure.

Los Alamos
NATIONAL LABORATORY

memorandum
Geophysics Group
EES - 3

To/MS: C. L. Edwards / C335
From/MS: Harry N. Plannerer / C335
Phone/FAX: 7-4895 / 7-4739
Symbol: EES3-93-432
Date: 27. October 1993

SUBJECT: PERLITE COMPRESSIONAL WAVE VELOCITIES

Compressional (longitudinal) wave velocities through Grefco's Socorro mine perlite were determined by laboratory measurement. The determinations were conducted using three each NX-size core segments oriented perpendicular and parallel to the flow banding structure that is visible in the tested specimens. The measurements were made on laboratory air-dried specimens at room temperature and at atmospheric pressure. Please be advised that these measurements were conducted with uncalibrated laboratory instrumentation. I, therefore, cannot confidently express the accuracy associated with these values. Measurements made on materials with published Vp values suggest they are accurate to ±6%.

The compressional wave velocities are found to be highly dependent on path orientation through the perlite. The wave velocity, $Vp_{\perp}$, perpendicular to flow banding was determined as 2.94 - 3.14 km/s and, $Vp_{\parallel}$, parallel to the flow banding was determined as 5.24 - 5.27 km/s. These values compare with a single value of 3.60 km/s obtained for Grefco's No Agua mine perlite for which a path orientation with respect to flow structure could not be determined. The individual velocity measurements are shown in the accompanying table.

Cy: F. N. App, EES-3, MS F659
D. F. Baker, EES-3, MS C335
W. M. Brunish, EES-3, MS F659
T. N. Dey, EES-5, MS F665
J. R. Kamm, EES-3, MS F659
D. M. Romero, EES-3, MS C335
D. C. Pearson, EES-3, MS C335
S. R. Taylor, EES-3, MS C335
T. A. Weaver, EES-3, MS C335
EES-3 Files, MS C335
EES3-qsRM Files, MS C335

Table 1. Laboratory Determinations for the Perlite Compressional Wave Velocity.

Grefco's Socorro Mine Perlite

specimen	path orientation	velocity (km/s)
P4-1	$Vp_{\perp}$	3.08
P4-2	$Vp_{\perp}$	3.14
P4-3	$Vp_{\perp}$	2.94
P8-1	$Vp_{\parallel}$	5.24
P8-2	$Vp_{\parallel}$	5.25
P8-3	$Vp_{\parallel}$	5.27

Grefco's No Agua Mine Perlite

specimen	path orientation	velocity (km/s)
NA9301	not determined	3.60

Path orientations:

$Vp_{\perp}$ - perpendicular to flow banding
$Vp_{\parallel}$ - perpendicular to flow banding

Transducers:

piezoelectric / compression wave energy
1 MHz resonance frequency

Pulse Generator:

rectangular pulse
100 Hz repetition rate
1μs pulse width
100 volt pulse amplitude into 50Ω impedance load